AN ASSESSMENT OF UNCERTAINTIES AND LIMITATIONS IN SIMULATING TROPICAL CYCLONE CLIMATOLOGY AND FUTURE CHANGES

A Thesis
Presented to
The Academic Faculty

by

Asuka Suzuki-Parker

In Partial Fulfillment
of the Requirements for the Degree
Doctor of Philosophy in the
School of Earth and Atmospheric Sciences

Georgia Institute of Technology
August 2011

AN ASSESSMENT OF UNCERTAINTIES AND LIMITATIONS IN SIMULATING TROPICAL CYCLONE CLIMATOLOGY AND FUTURE CHANGES

Approved by:

Dr. Peter J. Webster, Advisor
School of Earth and Atmospheric Sciences
Georgia Institute of Technology

Dr. Yi Deng
School of Earth and Atmospheric Sciences
Georgia Institute of Technology

Dr. Robert X. Black
School of Earth and Atmospheric Sciences
Georgia Institute of Technology

Dr. Gregory J. Holland
NCAR's Earth System Laboratory
National Center for Atmospheric Research

Dr. Judith A. Curry
School of Earth and Atmospheric Sciences
Georgia Institute of Technology

Date Approved: April 22, 2011

To Joe,

いつもそばにいてくれて、ありがとう

ACKNOWLEDGEMENTS

First and foremost, I would like to thank my advisors, Dr. Peter Webster and Dr. Greg Holland, for walking this journey alongside me. I always had doubts in my ability to become a successful researcher and thought about quitting many times, but my advisors never let me go. They gave me challenges to push the limits of my intellect, but at the same time they never forgot to support me along the way. The carefully balanced combination of these challenges and supports is what brought me to where I am today, and I cannot thank them enough. In addition, my advisors provided me the opportunity to be permanently placed at the National Center for Atmospheric Research (NCAR). It was there that I gained real-world experience, which is hard to come by in a traditional graduate school setting. I also would like to thank my thesis committee members: Dr. Judy Curry, Dr. Rob Black, and Dr. Yi Deng for reading my thesis and for their valuable comments.

My heartfelt appreciation goes to the Nested Regional Climate Modeling (NRCM) project team members at NCAR. Dr. James Done, I owe you so much for all the comments and grammatical corrections you made on my thesis. Cindy Bruyere, the numerous conversations I had with you, scientific or non-scientific, were priceless. I also want to thank Dr. Jim Hurrell and Dr. Bill Kuo for initiating and continuing the NRCM project. I was also blessed to have wonderful graduate students and post-docs within the division: Erin Towler, Jonathan Vigh, Clark Evans, and Kevin Mallen. They all provided me casual interactions so I would not be crushed by the overbearing weight of intimidation I felt by being surrounded by experienced researchers at NCAR. I was also

fortunate to have all the fabulous administrative stuff members who always made sure I felt home in the lab. The staff members at the Computational and Information Systems Laboratory also deserve kudos. They provided tremendous amount of computer resources for the NRCM project... and I am sorry I blew up a few parts in the supercomputer *Bluefire*.

Last but not least, I thank my parents for bringing me into this world and sending me over to the United States for my undergraduate and graduate education: 本当にありがとう. And of course, I cannot forget my husband Joe, who supported me throughout this whole process... I love you. You are the best!

TABLE OF CONTENTS

LIST OF TABLES

LIST OF FIGURES

LIST OF ABBREVIATIONS

AEW	African easterly wave
AGCM	atmospheric global circulation model
AMM	Atlantic Meridional Mode
ARW	Advanced Research WRF (Weather Research and Forecasting) Model
CCSM	Community Climate System Model
ECMWF	European Centre for Medium range Weather Forecasting
ENSO	El-Nino southern oscillation
GCM	global atmosphere-ocean coupled model
GEV	general extreme value distribution
GPD	general Pareto distribution
IBTrACs	International Track Archive for Climate Stewardship
IPCC	Intergovernmental Panel on Climate Change
ITCZ	inter-tropical convergence zone
MDR	main development region
MJO	Madden-Julian oscillation
MLE	maximum likelihood estimate
NCAR	National Center for Atmospheric Research
NCEP	National Center for Environmental Prediction
NRCM	Nested Regional Climate Model
PDF	probability distribution function
RCM	regional climate model
RV	relative vorticity

SLP	sea level pressure
SST	sea surface temperature
TC	tropical cyclone

SUMMARY

The recent elevated North Atlantic hurricane activity has generated considerable interests in the interaction between tropical cyclones (TCs) and climate change. The possible connection between TCs and the changing climate has been indicated by observational studies based on historical TC records; they indicate emerging trends in TC frequency and intensity in some TC basins, but the detection of trends has been hotly debated due to TC track data issues. Dynamical climate modeling has also been applied to the problem, but brings its own set of limitations owing to limited model resolution and uncertainties.

The final goal of this study is to project the future changes of North Atlantic TC behavior with global warming for the next 50 years using the Nested Regional Climate Model (NRCM). Throughout the course of reaching this goal, various uncertainties and limitations in simulating TCs by the NRCM are identified and explored.

First we examine the TC tracking algorithm to detect and track simulated TCs from model output. The criteria and thresholds used in the tracking algorithm control the simulated TC climatology, making it difficult to objectively assess the model's ability in simulating TC climatology. Existing tracking algorithms used by previous studies are surveyed and it is found that the criteria and thresholds are very diverse. Sensitivity of varying criteria and thresholds in TC tracking algorithm to simulated TC climatology is very high, especially with the intensity and duration thresholds. It is found that the commonly used criteria may not be strict enough to filter out intense extratropical systems and hybrid systems. We propose that a better distinction between TCs and other low-pressure systems can be achieved by adding the Cyclone Phase technique.

Two sets of NRCM simulations are presented in this dissertation: One in the hindcasting mode, and the other with forcing from the Community Climate System Model (CCSM) to project into the future with global warming. Both of these simulations are assessed using the tracking algorithm with cyclone phase technique.

The NRCM is run in a hindcasting mode for the global tropics in order to assess its ability to simulate the current observed TC climatology. It is found that the NRCM is capable of capturing the general spatial and temporal distributions of TCs, but tends to overproduce TCs particularly in the Northwest Pacific. The overpredction of TCs is associated with the overall convective tendency in the model added with an outstanding theory of wave energy accumulation leading to TC genesis. On the other hand, TC frequency in the tropical North Atlantic is under predicted due to the lack of moist African Easterly Waves. The importance of high-resolution is shown with the additional simulation with two-way nesting.

The NRCM is then forced by the CCSM to project the future changes in North Atlantic TCs. An El Nino-like SST bias in the CCSM induced a high vertical wind shear in tropical North Atlantic, preventing TCs from forming in this region. A simple bias correction method is applied to remove this bias. The model projected an increase both in TC frequency and intensity owing to enhanced TC genesis in the main development region, where the model projects an increased favorability of large-scale environment for TC genesis. However, the model is not capable of explicitly simulating intense (Category 3-5) storms due to the limited model resolution. To extrapolate the prediction to intense storms, we propose a hybrid approach that combines the model results and a statistical modeling using extreme value theory. Specifically, the current observed TC intensity is

statistically modeled with the General Pareto distribution, and the simulated intensity changes from the NRCM are applied to the statistical model to project the changes in intense storms. The results suggest that the occurrence of Category 5 storms may be increased by approximately 50% by 2055.

CHAPTER I

INTRODUCTION

Tropical cyclones (TCs) are of the most extreme and dangerous weather phenomena on Earth. In the United States, landfalling TCs account for an average of $10 billion in damages annually (Pielke et al. 2008). Hurricane Katrina (2005) alone caused $81 billion[1] in damages and took more than 1,800 lives. In developing countries, TC landfalls can be especially detrimental to society. For example, the death toll for Cyclone Nargis (2008) was more than 130,000 in Myanmar (Burma)[2]. Due to the catastrophic nature of TCs, substantial efforts have been devoted to improving short-term predictions of TC track and intensity in an effort to minimize the damages and casualties.

In recent years, the relationship between TC activity and climate change has attracted strong attention in the atmospheric research community. There are a number of evidences suggesting that regional TC activity is going though a substantial shift that may be a response to changing climate. As discussed later in the chapter, however, there is considerable controversy over detection and association of trends in TC activity resulting from climate change due to uncertainties in the observed data and the difficulty in separating natural variability and anthropogenic forcing. Projections of future TC activity also vary considerably. The sources of uncertainties are still being identified and tested for their relative effects on projections of TC activity. However, reliable projections for TC activities are critical for planning by governmental organizations and industries

[1] From Pielke et al. (2008), adjusted to 2005 inflation level.
[2] From the article entitled "Preliminary Swiss Re sigma estimates that over 238,000 people were killed by catastrophes in 2008, insured losses soar to USD 50 billion", Swiss Reinsurance Company Ltd, 2008

located near impacted coastlines. Therefore, identifying the source of uncertainties in future projections of TC activity and developing a mechanism to reduce the uncertainties is of considerable societal importance.

This work examines potential future changes in North Atlantic TC activity that may accompany with increasing greenhouse gases using the Nested Regional Climate Model (NRCM, Holland et al. 2010). Attention will be given to identifying inherent limitations and uncertainties in simulating TC climatology. Approaches to reduce some of these limitations and uncertainties will be proposed. First, we review the current understanding of the TC-climate relationships, detection and attribution of shifts in the observed TC records, and model projections of future TC activity. We conclude this chapter with an outline of the thesis.

Research on TC and climate relationships has a long history. The pioneering work by Gray (1968) presented a comprehensive analysis of the characteristics of the large-scale environment in which TC formation occurs, namely: high sea surface temperature (SST), high low-tropospheric moisture content, a background large-scale cyclonic vorticity, conditional convective instability, and low vertical wind shear. Although these factors are based on their correlation with seasonal TC formation, they have also been used to explain the TC formation variation at interannual to decadal time scales, as outlined below.

The major contributor to TC formation variation at interannual time scales is the El Nino Southern Oscillation (ENSO). For example, it is well known that North Atlantic TCs are active and Northwest Pacific TCs are suppressed during La Nina years, and vise versa during El Nino years (e.g., Gray 1984, Chan 1985). The modulation of TC activity

in these regions by ENSO is largely related to lateral changes in the Pacific and Atlantic Walker circulation, which modulate regional vertical wind shear (e.g., Gray 1984, Chan 1985). There are suggestions that the impact of ENSO events may have changed during the last two decades with the prevalence of central Pacific over eastern Pacific warming events. Kim et al. (2009) show that TCs in the North Atlantic actually increases beyond normal El Nino levels similarly to La Nina. There are a number of other modes of interannual variabilities that modulate regional TC activities, though some of these are controversial. For example: there is some evidence linking modulation of North Atlantic TC activity by the Atlantic Multidecadal Oscillation (e.g., Goldenberg et al. 2001) and the Atlantic Meridional Mode (e.g., Kossin and Vimont, 2007). In the western North Pacific, the Pacific Decadal Oscillation has been shown to potentially impact TC intensity and track (Chan 2008, Liu and Chan 2008). On intraseasonal (30-90 day) scales, the Madden-Julian Oscillation (MJO, Madden and Julian 1972) impacts regional TC activity in multiple basins; Indian Ocean (Hall et al. 2001, Bessafi and Wheeler 2006), western North Pacific (e.g., Liebmann et al. 1994), eastern North Pacific (e.g., Maloney and Hartmann 2000a), and Gulf of Mexico (Maloney and Hartmann 2000b). Association of these modes of variability to TC activity has contributed to the understanding of long-term variation of TC activities in different regions. Unfortunately, these high-amplitude seasonal to interannual modulations of TC activity complicate the separation of natural variability and the climate change signal.

Recent studies have identified some emerging trends in regional TC activities. Using observed TC track data, Webster et al. (2005) reported an increasing trend in intense (Category 4+ in the Saffir-Simpson Hurricane Scale) TCs in all TC basins.

Identifying trends in North Atlantic TC activity (frequency and intensity) over the past 40-years has attracted strong interest in part due to the availability of more reliable observed TC track data (discussed later in the chapter). Emanuel (2005) found a distinct trend in the overall destructiveness of hurricanes, as measured by the intensity-based Power Dissipation Index. A detailed analysis of the observed TC track data by Elsner et al. (2008) supported the findings by Webster et al. (2005) showing that the net North Atlantic TC frequency has increased, and the upper quartile of intensity increased rapidly during the last four decades. Collectively, these studies lead to an agreement in the overall increase in the most intense storms. Holland and Webster (2007) suggested that the increasing trend of TC frequency in North Atlantic has occurred over three stable regimes with rapid changes in between, rather than a smooth linear increase.

The trends noted in North Atlantic TC frequency and intensity has been associated with SST changes. Many studies have attributed the increasing frequency and intensities of TCs to a local SST trend (Webster et al. 2005, Hoyos et al. 2005, Emanuel 2005, Holland and Webster 2007, Saunders and Lea 2008), while atmospheric factors (such as vertical wind shear and low-level moisture) appear to have little contribution (Hoyos et al. 2005). The cause of local SST increase is controversial. Some studies attribute it to anthropogenic forcing (Mann and Emanuel 2006, Gillet et al. 2008), others to natural variability, especially to internal oceanic variation similar to the Atlantic Multidecadal Oscillation (e.g., Zhang and Delworth 2009). Other work has suggested a contribution of remote SST changes to the increasing frequency and intensities of North Atlantic TCs (Vecchi and Soden 2007, Swanson 2008, Wu et al. 2010, Kossin and Vimont 2007), whereby changes between differences in tropical North Atlantic SST and

the tropical mean SST impacts TC-modulating large-scale environmental factors.

Detection of trends in TC frequency is complicated by the short period of reliable observed TC track data that poses a challenge in separating trends from multi-decadal oscillations. Individual records of TCs date back to the 1840's (Knapp et al. 2010). However, track data from the pre-satellite (before 1970's) era is generally less reliable due to inconsistent and/or insufficient observing technology. Thus, detection of trends from the observed TC track data is generally limited to the past 40-years, which makes it difficult to separate trends from multi-decadal oscillation signals (e.g., Goldernberg et al. 2001, Chan 2006). Efforts have been made to reconstruct the tracks of potentially missed TCs for the pre-satellite era based on the reporting-ship track density (Landsea 2007, Chang and Guo 2007, Vecchi et al. 2008). After adjustments are made based on these studies, an increasing trend of TC frequency was substantially reduced (Vecchi and Knutson 2008). An alternative approach is to rely solely on the landfall data since this is the most trusted source. It has been concluded that there is no trend in landfall TC frequency (Landsea 2007, Chan and Xu 2009). However, these two approaches have been criticized because they assume stationarity in TC track density, and do not necessarily represent the basin wide TC activity (Holland 2007).

Detection of trends in TC intensity also suffers from uncertainty in the observed TC track data. In operational forecasting and observations of TCs, the Dvorak technique (Dvorak 1984) has served as the benchmark in estimating the intensity of TCs, even in the North Atlantic, which has a long period of aircraft reconnaissance (Holland 2008). The shortcoming of the Dvorak technique is its subjectivity, in that the estimate of TC intensity relies on visual cloud pattern recognition made by trained analysts. Recently,

Kossin and Velden (2004) suggested that the historical Dvorak technique has a pronounced bias in estimating the central minimum pressure. Further, different agencies have adopted varying standards in implementing the Dvorak technique (Knapp and Kruk 2009), contributing to inter-agency differences in TC trend (Wu et al. 2006). The subjectivity in Dvorak thus contributes to less reliability in the observed TC track data that complicates detection of trends. Similar issues are also found in modeling studies as discussed later in this section.

While detection and attribution of observed TC trends remain controversial, models have produced a relatively more consistent picture with regard to the projected changes of global mean TC frequency and intensity under increasing greenhouse gases. Course-resolution (namely horizontal grid spacing greater than 50km) global atmosphere-ocean coupled models (GCMs) have been shown to be capable of producing TC-like vortices (Manabe et al. 1970, Bengtsson et al. 1982) and they have been used to examine the impact of global warming on TC frequency (e.g., Broccoli and Manabe 1990, Bengstsson et al. 2007, and Tsutsui 2002). In general, these course-resolution GCM studies have found a global reduction of TC frequency under global warming. However, the use of GCMs for simulating TCs has been criticized due to their incapacity to resolve some key features of TCs at fine scales (McBride 1984, Lighthill et al. 1994). Moreover, course-resolution GCMs are not capable of simulating the intense TCs at all. Bengttssn et al. (2007) showed that a relatively high-resolution model projected a significant increase in intense TCs in a warmed climate, but no such increase was seen with a course-resolution (~200km) model simulation. Murakami and Sugi (2010) also found a similar result. Thus, projection of TC intensity change is highly sensitive to the model resolution.

With increasing computeing capacity, studies are now employing high-resolution atmospheric general circulation models (AGCMs) and regional climate models (RCMs). In agreement with GCM studies, AGCMs generally indicate reduced global TC frequency with global warming (Bengtsson et al. 2007, Oouchi et al. 2006, Sugi et al. 2009, Zhao et al. 2009). This reduction is hypothesized to be associated with increasing dry static stability as the atmosphere becomes more stable with greenhouse warming. (e.g., Knutson and Manabe 1995). There is also a general consensus for an increase in mean TC intensity from high-resolution AGCM (Oouchi et al. 2006, Bengtsson et al. 2007) and RCM experiments (Knutson et al. 1998, 2008, Walsh et al. 2004). This is in line with the maximum potential intensity theory (Emanuel 1988, Holland 1997), whereby higher SST provides more favorable conditions for TCs to intensity once they are formed. Thus, there is a general consensus for a future reduction of global TC frequency and an increase of TC intensity. For regional changes, however, there is considerable disagreement. For North Atlantic TC frequency, in particular, some models project an increase (Oouchi et al. 2006), others a decrease (Knutson et al. 2007), yet others no significant change (Murakami and Wang 2010).

These differing conclusions can be attributed to a range of factors. For example, with RCMs the horizontal boundary condition has a considerable impact on modulating the simulated TC climatology. Landman et al. (2005) showed that the simulated TC climatology is sensitive to the model domain size and location of the lateral boundaries. Further, spectral nudging also has a strong impact on the simulated TC climatology. For example, Knutson et al (2007) found that spectral nudging from global analyses markedly reduced an over-production of TCs in their model. Many AGCM and RCM experiments

have adopted a pseudo-global warming approach, whereby the future SST forcing (and lateral boundary forcing for the RCMs) is applied as the sum of current climate variability and a mean climate trend (e.g., Oouchi et al. 2006, Knutson et al. 2007). All GCM projections submitted to the 4th assessment report of the Intergovernmental Panel on Climate Change (IPCC AR4) found an increase of global mean SST. However, the spatial SST patterns increase varied considerably from model to model, contributing perhaps to the inconsistent projections of regional TC frequency based on the AGCM and RCM simulations (Chauvin et al. 2006, Sugi et al. 2009, Zhao et al. 2009). The importance of inhomogeneous spatial patterns of SST change has also been emphasized by Villarini et al. (2011), who successfully reproduced the AGCM and RCM experiments results with a conditional Poisson model using the differences between tropical mean and North Atlantic SST.

In addition to these issues with boundary conditions, there are other limitations with simulating TC climatology by dynamical models. First, explicit simulation of very intense storms (e.g., Category 4-5 storms) is not possible even with high-resolution RCM models. Horizontal resolution of around 1km is recommended for simulating Category 5 storms (Davis et al. 2010) but running a global or regional model at such high-resolution over climate timescales is beyond current computing capacities. Second, the simulated TC climatology is sensitive to the TC detection methodology that is applied. A benchmark for more objectively determined criteria for TC tracking and detection is available (Walsh 2007). However, TC detection and tracking methods, and their uncertainties, are often poorly explained in existing studies. A majority of the high-resolution model studies tune their TC detection criteria so that the resulting TC

frequency matches observations (e.g. Oouchi et al. 2006, Bengtsson et al. 2007, Murakami and Wang 2010). Unfortunately, this may simply cover up other model deficiencies that may result in considerable errors in future projections. The evaluation method for simulated TC climatology also varies considerably. Although the vast majority of studies present the full array of TC climatological variables (e.g., frequency, intensity, storm days), some restrict their discussions only to the simulated storm days (Tsutsui 2002), or focus on hurricane-strength storms (Zhao et al. 2009) in order to minimize the sensitivity to TC tracking criteria. Thus, it is important to take the TC detection method sensitivity and errors into account when evaluating simulated TC projections. This should be accompanied by physical explanations in support of projected changes, such as the simulated large-scale conditions.

Therefore, the specific goals for this work are to;

1. Develop a new method for identifying TCs in climate models and quantify the range of sensitivity of the simulated TC climatology to the TC tracking criteria (Chapter II);
2. Identify model biases in the simulated TC climatology that are independent of TC tracking sensitivity (Chapter III), as well as new sources of uncertainties and inherent limitations in simulating TC climatology (Chapters III and IV);
3. Increase robustness of future TC activity projection to the inherent TC tracking sensitivity (Chapter IV); and
4. Present an alternative approach to address the limitation of TC intensity projection with the dynamical model using a statistical model (Chapter V).

A summary and discussion of the wider implications of the results can be found in

Chapter VI.

CHAPTER II

TROPICAL CYCLONE DETECTION AND TRACKING METHOD

2.1 Introduction

As described in Chapter I, detection of TCs in operational practice may be subjective and sometimes controversial. That is also the case for detection of simulated TCs from model outputs. Research groups around the world have adopted TC tracking schemes using various techniques and threshold criteria. However, they are often not well explained (Walsh et al. 2007). Generally speaking, numerical tracking of TCs starts by locating a localized minimum in sea level pressure (SLP) or maximum in vorticity field to define the center of a potential TC. Then tracks are filtered by maximum wind speed, magnitude of vorticity, a measure of warm-core, and duration for which these criteria are met. Hereafter, for convenience, tracking schemes using these four parameters shall be referred to as *base* tracking. In addition to the base tracking parameters, some studies, especially those with high-resolution models, have adopted some measure of vertical variation of tangentional maximum wind speeds and horizontal temperature anomalies (referred to as *structure* criteria), genesis location criteria, and SLP anomaly thresholds.

One of the first studies to evaluate the skill of numerical models in reproducing the global TC climatology is Bengtsson et al. (1982) using European Centre for Medium range Weather Forecasting (ECMWF) operational global forecasting model at ~200km resolution. They used only wind speed (>25 m s^{-1} at 850hPa) and 850hPa vorticity (>7.0x$10^{-5}s^{-1}$) criteria for detection of simulated TCs. A little over a decade later, as model resolution increased and started to resolve the thermal structure of TCs better,

Bengtsson et al (1995) introduced warm-core and structure criteria to provide a more accurate separation of simulated TCs from extratropical low pressure systems. Parameters and thresholds used for TC tracking have not been changed much since then, even though the resolution has markedly increased. At resolutions coarser than 100km, numerical models can only produce TC-like vortices. But it is generally considered that models with 50km horizontal resolution or less can resolve the major characteristics of TCs adequately; namely the eye, warm-core, axisymmetric wind circulation, and spiral bands, although not the maximum winds or other core details (e.g., Oouchi et al. 2006, Stowasser et al. 2007). Thus the TC tracking scheme should vary to reflect the model resolution difference. However, when studies with T42 (~300km) resolution and 20km resolution use a comparable TC tracking criteria, as represented by Krishnamurti et al. (1998) and Oouch et al. (2006), respectively, them both producing reasonable global TC climatologies raises questions of how this could occur.

Table 2.1 compares TC detection and threshold criteria from recent regional and global climate modeling studies using horizontal resolutions of 50km or less. Even though model resolutions are similar, TC detection criteria exhibits a large variation between the different studies. All of them use maximum wind speed, relative vorticity, warm-core measure, and duration criteria. But the usage of structure criteria and SLP anomaly between the different studies is not universal. Variability in threshold values in each parameter is quite large, especially for maximum wind speed (ranging from 14 m s^{-1} at 850hPa to 17 m s^{-1} at 10m above the surface). Measures of warm-core are also quite diverse. Some use the vertical mean of horizontal temperature anomalies, while others

Table 2.1: TC tracking criteria and threshold used by past global/regional climate modeling studies with horizontal model resolutions of approximately 50km or less. T'xxx refers to horizontal temperature anomaly at xxxhPa, and Vxxx refers to maximum wind seed at xxxhPa.

	Model resolution (km)	Wind speed (m/s)	Vorticity at 850mb ($x10^{-5}$ s-1)	Temp. anomaly (K)	Structure, location	SLP anomaly (hPa)	Duration (days)
Walsh et al. (2004)	30	17 at 10m	1	T'300+T'500+T'700>0	T'300>T'850 V850>V300	-	1
Chauvin et al. (2006)	~50	15 at 850hPa	14	mean(T'300~T'700)>3	T'300>T'850 V850>V300	-	1.5
Oouchi et al. (2006)	20	15 at 850hPa	3.5	T'300+T'500+T'700>2.0	V300<V850 or <35° latitude	2	1.5
Knutson et al. (2007)	18	17 at lowest model level	1.6	mean(T'300~T'500)>0.8	-	4	2
Stowasser et al. (2007)	~50	17 at lowest model level	2.5	mean(T'300~T'850)>0	V850>V300	-	2
Murakami and Wang (2010)	20	14 at 850hPa	3	T'300+T'500+T'700>1.2	V850-V300>2.5, and <45° latitude[*1]	2	1.5

[*1] V850>V300 at genesis

take the sum of multiple levels. Interestingly, simulated frequencies of TCs from these studies are all comparable to each other. Some studies use a strict/strong threshold criterion in one parameter (limiting towards detecting more warm-core-like and/or intense storms, e.g., higher wind speed) although often compensated by relaxing other criteria. Consider the two studies of Chauvin et al. (2006) and Stowasser et al. (2007), for example. Their model resolutions are the same at ~50km (0.5°), but in Chauvin et al., wind speed criteria is much less strict, but all other base tracking parameters are stricter than Stowasser et al.. All of the studies listed in Table 2.1 are global warming experiments and the TC tracking criteria and thresholds are chosen so that the detected number of storms matches those observed in the current era. This may be a sensible procedure for global warming experiments, when the major concern is for the determination of future changes. But subjectively tuning the TC tracking method

parameters does not allow for an objective assessment of the model's performance, leaves uncertainty in the simulated TC frequency, and potentially impacts the changes in future climate.

This chapter assesses the TC tracking scheme in attempt to answering the following two questions;

1) What is the range of uncertainty associated with varying tracking parameters and their thresholds in TC tracking schemes?

2) Are the commonly used criteria strict enough to distinguish TCs from other low-pressure systems?

The first point is examined through a series of sensitivity experiments. First, the base tracking parameters are varied within the range of commonly used values, and second, structure criteria are applied. To our best knowledge, the latter point has not been discussed in literature. It is clear that the significance of addressing these issues becomes more important as models are now able to simulate mesoscale systems with greater detail, potentially making it more difficult to distinguish TCs from other systems such as intense extratropical storms. To aid in this differentiation, the *cyclone phase* technique developed by Hart (2001) is introduced into the tracking criteria.

2.2 Description of cyclone phase technique

As shown in Table 2.1, structure criteria consist of either one or both of the conditions, V850>V300 and/or T'300>T'850, where V denotes maximum tangentional wind and T' is the horizontal temperature anomaly. The first condition is based on the observed vertical variation of tangentional wind speeds, which maximizes near the top of

boundary layer (e.g., Franklin et al., 1993 and 2003). The second condition is also based on the observed vertical variation of horizontal temperature anomalies, which maximizes in the upper-troposphere in mature TCs. Both are physically sound conditions for TCs but they only take two different levels and do not represent the whole vertical variation of thermal structure of low-pressure systems.

The cyclone phase technique (Hart 2001, Evans and Hart 2003, and Hart 2004) provides a more comprehensive measure of the vertical thermal structure of low-pressure systems. It consists of the following three parameters:

i. B term: a measure of axisymmetricity, defined as the difference of 600-900hPa thickness, calculated within 500km radius of the storm center, to the right and left of the storm center with respect to the direction of storm movement;

$$B = h(\overline{Z_{600hPa} - Z_{900hPa}}|_R - \overline{Z_{600hPa} - Z_{900hPa}}|_L),$$

where $h=+1$ for Northern hemisphere, and $h=-1$ for southern hemisphere and Z denotes geopotential height. Tropical systems are axisymmetric and typically have values of B close to zero, whereas mid-latitudinal systems are non-axisymmetric due to their baroclinic frontal nature and are typically associated with B > 10 (Hart 2003).

ii. -VTL term: a measure of the vertical thermal structure in the lower-troposphere, defined as vertical derivative of horizontal height perturbation from 900 to 600hPa;

$$-|VTL| = \left.\frac{\partial(\Delta Z)}{\partial \ln p}\right|_{900hPa}^{600hPa}$$

iii. -VTU term: similar to –VTL but for the upper-troposphere;

$$-|VTU| = \frac{\partial(\Delta Z)}{\partial \ln p}\Bigg|_{600hPa}^{300hPa}$$

-VTL and -VTU terms represent the vertical variation of thermal wind. For deep warm-cored TCs, both terms are positive as the height perturbation (and hence the tangential wind) is maximized near the top of the boundary layer. For mid-latitudinal systems the horizontal geopotential height perturbation is maximized in the upper troposphere. As a result, –VTL and –VTU terms are negative. Occasionally –VTL and –VTU terms may have different signs for a system that is transitioning from cold-core to warm-core (or vise versa), as represented by Hurricane Olga (2001) (Hart 2003).

Values of B<10, –VTL>0 and –VTU>0 are recommended to classify low-pressure systems as pure tropical warm-core systems (Hart 2004).

2.3 Sensitivity experiment design

Sensitivity to varying parameters and their thresholds in TC detection criteria is explored using January-December 2005 data from the Nested Regional Climate Model (NRCM) tropical channel simulation (described in Chapter III). These data cover the global tropics at 36km resolution with 51 vertical levels archived at 6 hourly intervals. We choose this dataset over reanalysis because of the horizontal resolution. The shortfall of using the channel simulation data is that there is no "correct TC frequency" with which to compare the number of TCs detected from TC tracking. Even though this simulation is driven by reanalysis, it is not appropriate to assume that the model produces TCs at the

observed frequency. Hence, the results from the sensitivity tests are given in a relative sense; for parameters with variable thresholds (e.g., wind speed), variations of the number of detected TC tracks by varying the threshold values from a standard threshold will be given, and for parameters that are either binary (e.g., structure criteria) the difference of the number of detected TC tracks by turning the parameter on or off are presented.

Table 2.2 summarizes parameters and their threshold ranges for the sensitivity study. For base criteria, the maximum wind speed threshold is set to 17 m s^{-1} but the vertical level at which the wind speed is measured is allowed to vary between 850hPa, 1000hPa, and 10m above the surface. This approximately corresponds to varying the maximum wind speed from 13 to 17 m s^{-1} at 10m (Franklin et al. 2003). The relative vorticity (RV, measured at 850hPa) threshold is varied from 1.0 $x10^{-5}$ to 5.0$x10^{-5}$ s^{-1}. A warm-core is defined by the sum of horizontal temperature anomalies at 300, 500, and 700hPa and its threshold is varied from 0 to 3 K. Finally, the duration threshold is varied from 1 to 3 days.

Table 2.2: Summary of tracking parameters and their threshold ranges used for the sensitivity experiment.

	Parameter	Threshold Range
Base tracking	Maximum wind level	850mb, 1000mb, or 10m surface
	Relative vorticity (s-1)	1.0 to 5.0x10-5
	T'300+T'500+T'700 (K)	0.0 to 2.0
	Duration (days)	1 to 3
Structure criteria	V850>V300 and T'300>T'850	Yes or no
Cyclone phase	B	-20 to 50
	-VTL	-100 to 200
	-VTU	-100 to 200

Specific steps of base tracking are as follows:

- First, the sea level pressure (SLP) field is scanned to locate all local minima, which are marked as potential centers of TCs. There is no requirement on the minimum SLP value, or the difference from the environmental SLP value;
- Next the maximum wind speed and the magnitude of 850hPa RV are found within a box ±1° latitude/longitude from the SLP minimum location;
- Horizontal temperature anomalies are calculated as the difference between the average in the TC core area (within 1° from the center) and the surrounding environment (1-10° from the center);
- Once the tracker finds a feature that satisfies the base criteria of 850hPa wind speed > 17 m s^{-1}, cyclonic RV > $1.0x10^{-5}s^{-1}$, and T'>0, it searches for the location of the same feature at the next time step within 5° of the previous location. If there exists more than two systems within the search box, then the closest one to the last location is chosen.
- A successful track must retain the base parameter thresholds for at least 1 day.

After base tracking is completed, values of V850-V300, T'300-T'850 and cyclone phase parameters are calculated along each of the tracks at each time step. Tracks resulting from base tracking are then further filtered based on the satisfaction of all of the base parameters, structure and cyclone phase criteria. As defined in Section 2.2, the thresholds for the cyclone phase of pure tropical warm-core systems are B<10, -VTL>0 and –VTU>0. The sensitivity of these criteria to varying these cyclone phase thresholds (as described in Table 2.2) is tested in the next section.

2.4 Results

Table 2.3 shows the changes in the number of detected tracks (per year) by adding structure and cyclone phase criteria for the strongest (maximum wind level at 10m, RV = $5.0x10^{-5}s^{-1}$, T' = 2K, and duration = 3 days) and the weakest (maximum wind level at 850hPa, RV = $1.0x10^{-5}s^{-1}$, T' = 0K, and duration = 1 day) base parameter combinations. Only the results from the strongest and the weakest base combinations are presented here because the numbers of detected tracks from all other combination lie between the two. For simplicity, cyclone phase parameters are set to those recommended by Hart (2004) for TCs. Without structure or cyclone phase filtering, the numbers of detected tracks vary by an order or magnitude, from 155 to 1467 (Table 2.3, first row). With the weakest base combination, the TC tracker detects numerous small-scale systems such as mesoscale convective systems and orographically-induced systems in high terrain. The extremely high count of 1476 per year using the weakest base criteria without structure or cyclone phase filtering is due to inclusion of such erroneous systems. If the maximum wind measurement level is at 10m and duration is increased to 3 days, the inclusion of

Table 2.3: Number of detected tracks (per year) from base tracking only (top), from base tracking with structure criteria (middle), and from base tracking with both structure and cyclone phase criteria (bottom). Left column is the strongest base case where all of parameters within base tracking are set to be the most strict value. Right column is the weakest base case.

	Strongest base (win.lev.=10m, T'=2, RV=5.0, duration=3)	Weakest base (win.lev.=850mb, T'=0, RV=1.0, duration=1)
Base only	155	1467
Base+structure	106	691
Base+structure+basic CP[*1]	62	363

[*1] basic CP = recommended threshold by Hart (2004) (B<10, -VTL&-VTU>0)

mesoscale convective systems is reduced significantly. But this is not sufficient to exclude some orographically induced systems and subtropical cyclones in the Southeast Pacific (Figure 2.1a).

Adding the structure filtering decreases the number of tracks for both the strongest and the weakest base cases (Table 2.3, second row). Structure filtering halves the number of detected tracks for the weakest base case and by ~30% for the strongest base case. Although the base parameters alone could not exclude orographically induced and subtropical cyclones, the addition of structure criteria appears to filter out these erroneous systems (Figure 2.1b).

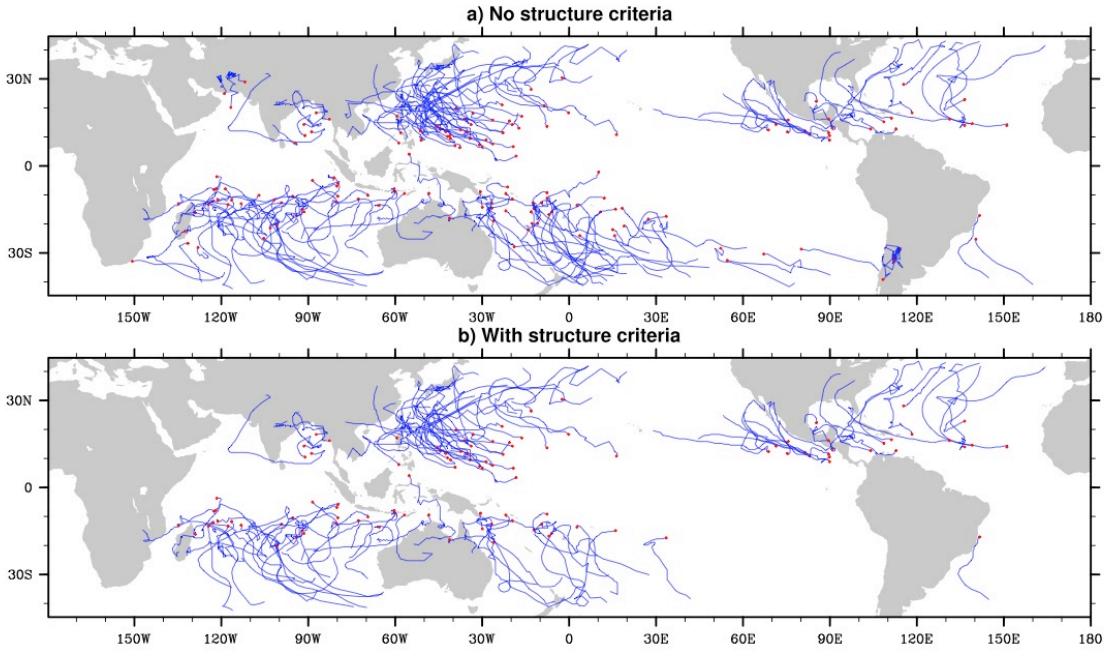

Figure 2.1: Tracks from the strongest base case without structure criteria (top) and with structure criteria (bottom). Red dots are track start points, and blue lines are tracks.

Adding cyclone phase filtering reduces the number of detected tracks further (Table 2.3, third row). This suggests that the cyclone phase filtering is excluding some of the systems that satisfy structure criteria and only more-TC-like systems are allowed to pass the filtering. This will be discussed in detail later in this chapter.

Table 2.4 summarizes the sensitivity to varying individual base parameters when structure filtering is also applied. These changes are shown both as absolute numbers and percentage changes from the standard case (note that % changes are not applicable for the maximum wind measurement level which provides the base). Here, the standard case is arbitrarily set to T'=2, RV=5.0 and duration = 1. Considerable sensitivity to variations in all parameters is found when the other parameters are set at the weakest base criteria. However, the sensitivity is considerably reduced for the strongest base criteria, where changes to relative vorticity or temperature anomaly criteria make no difference. The highest sensitivity is to the maximum-wind measurement level (or wind speed at a particular vertical level) and duration, as these are the only terms for which there is any sensitivity for the strongest base case. Of course, this conclusion holds only within the range of parameter thresholds tested here. Outside this range the conclusion may well change.

As mentioned before, cyclone phase criteria are stricter than structure criteria in such a way that adding cyclone phase criteria on top of structure criteria further reduces the number of detected TC tracks (Table 2.3). This point is further investigated here. Figure 2.2 compares the composite plots of zonal vertical cross section of horizontal temperature anomaly for 50 cases chosen randomly where only structure criteria are satisfied (a) and instances where both structure criteria and cyclone phase criteria (using

Table 2.4: Summary of detected number of tracks (per year) for base tracking sensitivity for a) varying maximum wind measurement level, b) varying temperature anomaly, c) varying relative vorticity, and d) track duration.

a) Vary wind level

	Strongest (T'=2, RV=5.0, duration=3)	Weakest (dt=0, RV=1.0, duration=1)
	# Tracks	# Tracks
850hPa	133	691
1000hPa	115	272
10m	106	223

b) Vary temperature anomaly

		Strongest (win.lev.=10m, RV=5.0, duration=3)		Weakest (win.lev.=850mb, RV=1.0, duration=1)	
T' (K)	%change T' from T'=2	# Tracks	%change from T'=2 count	# Tracks	%change from T'=2 count
0	-100	106	0	691	155.93
0.5	-75	106	0	569	110.74
1	-50	106	0	436	61.48
1.5	-25	106	0	337	24.81
2	-	106	-	270	-

c) Vary relative vorticity

		Strongest (win.lev.=10m, T'=2, duration=3)		Weakest (win.lev.=850mb,T'=0,duration=1)	
RV (x10^{-5}s^{-1})	%change RV from RV=5	# Tracks	%change from RV=5.0	# Tracks	%change from RV=5.0
1	-80	106	0	691	53.22
2	-60	106	0	634	40.58
3	-40	106	0	564	25.06
4	-20	106	0	503	11.53
5	-	106	-	451	-

d) Vary duration

		Strongest (win.lev.=10m, T'=2, RV=5.0)		Weakest (win.lev.=850mb,T'=0,RV=0.0)	
Duration (days)	%change duration from duration=1	# Tracks	%change from duration=1	# Tracks	%change from duration=1
1	-66.67	195	83.96	691	177.51
1.5	-50.00	160	50.94	573	130.12
2	-33.33	140	32.08	455	82.73
2.5	-16.67	117	10.38	323	29.72
3	-	106	-	249	-

parameter threshold recommended by Hart 2004) are satisfied (b). The composite using only structure filtering shows a clear sign of warm-core structure, but is weaker when compared to the composite using both structure and cyclone phase criteria.

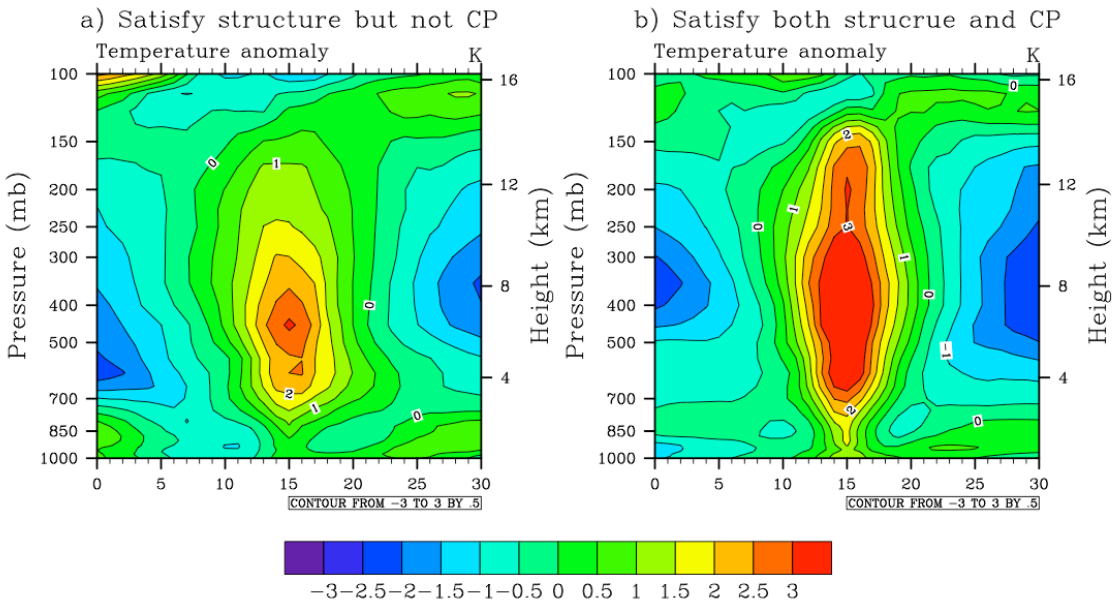

Figure 2.2: Composite plots of vertical cross-section of horizontal temperature anomaly for 50 randomly chosen instances where only structure criteria is satisfied (left) and both structure and basic (B<10, -VTL>0, and -VTU>0) cyclone phase criteria are satisfied (right). Both cases are using the strongest base parameter combination.

However, composite analysis can be contaminated by a small number of extreme cases, so it is instructive to examine some individual cases. Figure 2.3 shows the zonal vertical cross section of temperature anomaly for twelve randomly chosen instances that satisfy structure criteria but fail cyclone phase criteria. Most of the cases presented in Figure 2.3 show a clear warm-core. However, many are not well vertically aligned, and a few (especially the case second to the left in the middle row) show very weak or no sign of warm-core at all. The addition of the cyclone phase criteria (Figure 2.4), selects a

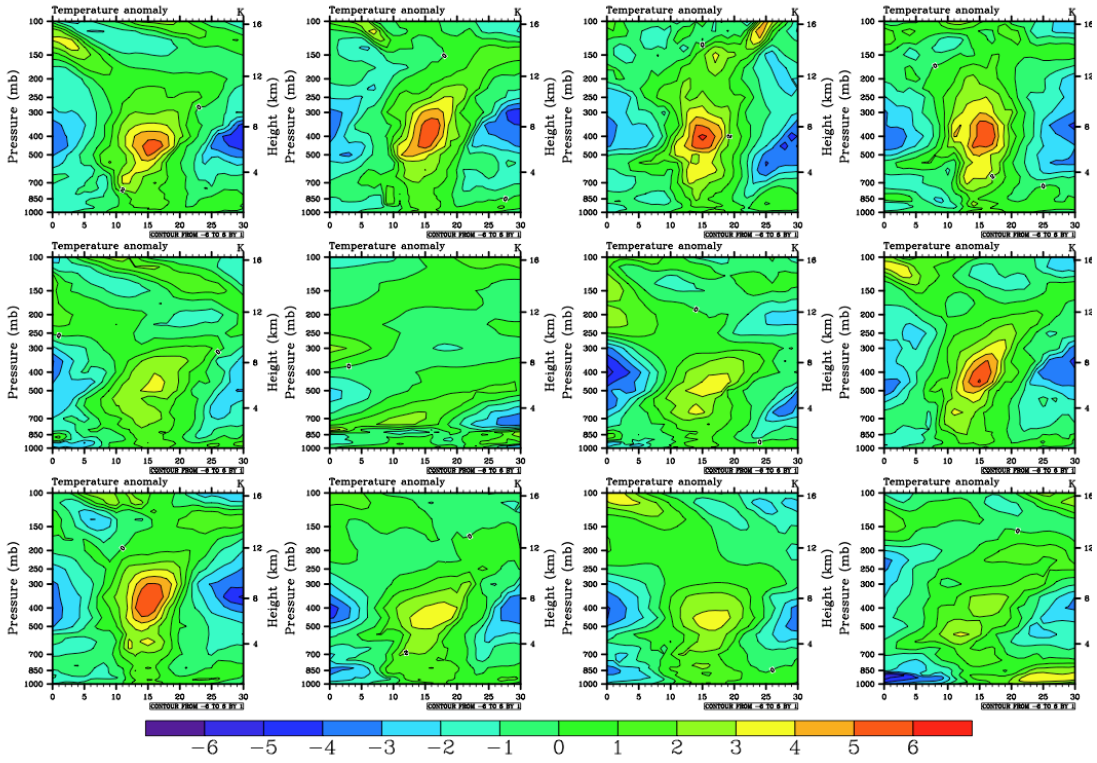

Figure 2.3: Vertical cross-section of horizontal temperature anomaly for 12 randomly chosen instances where structure criteria is satisfied but not cyclone phase. Base parameters are set to be the strongest combination.

warm core that is much more comparable with typical TC structures. All of the cases in Figures 2.3 and 2.4 use the strongest combination of base tracking, which includes T'>2. Thus, the combination of traditional warm-core definition (as in the sum of horizontal temperature anomalies) and structure criteria may not be sufficient to differentiate tropical warm-core systems from other cyclonic systems. This conclusion is supported by the scatter plot of T' and –VTL and –VTU values in Figure 2.5. T'>0 does not necessarily mean –VTL>0 and –VTU>0 (Figure 2.5a and b). This is also the case even when structure criteria are applied (Figure 2.5c and d). T'>0 only assures the existence of warm-core but not the vertical variation or the location of vertical maximum.

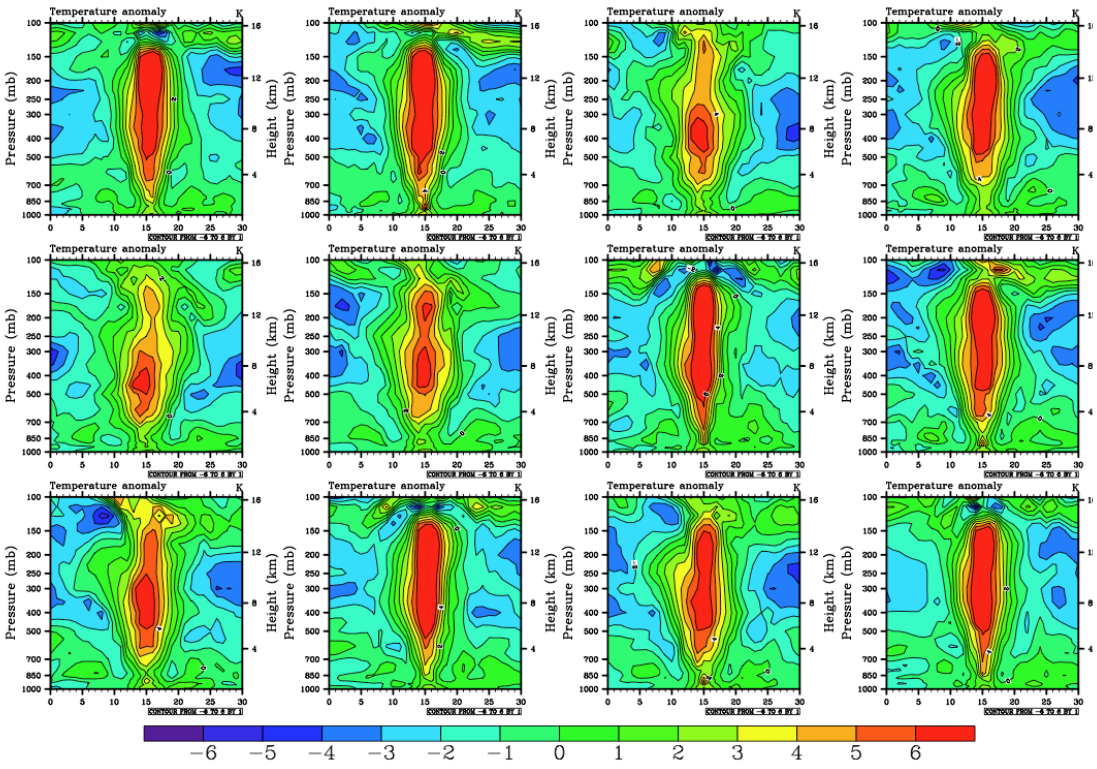

Figure 2.4: Similar to Figure 2.3, but for cases where both structure and cyclone phase criteria are satisfied.

It appears that simply taking a difference at 300 and 850hPa is not sufficient to capture the vertical thermal profile throughout the troposphere.

The threshold of –VTU and –VTL at 0 is determined theoretically and is therefore set for an objective TC tracking. However, setting the threshold for B at 10 is debatable. Hart (2001) and Evans and Hart (2003) justify the B<10 cut-off because no major hurricane has and associated value of B that exceeded 10 based on ECMWF reanalysis. However, weaker TCs (tropical storms and category 1-2 hurricanes) can have B values exceeding 10, often times greater than 20 (Evans and Hart 2003). As the aim of objective TC tracking is to detect hurricane strength systems and tropical cyclones (with maximum wind speeds >17 m s^{-1}), setting B<10 may be too strict. As shown in Figure

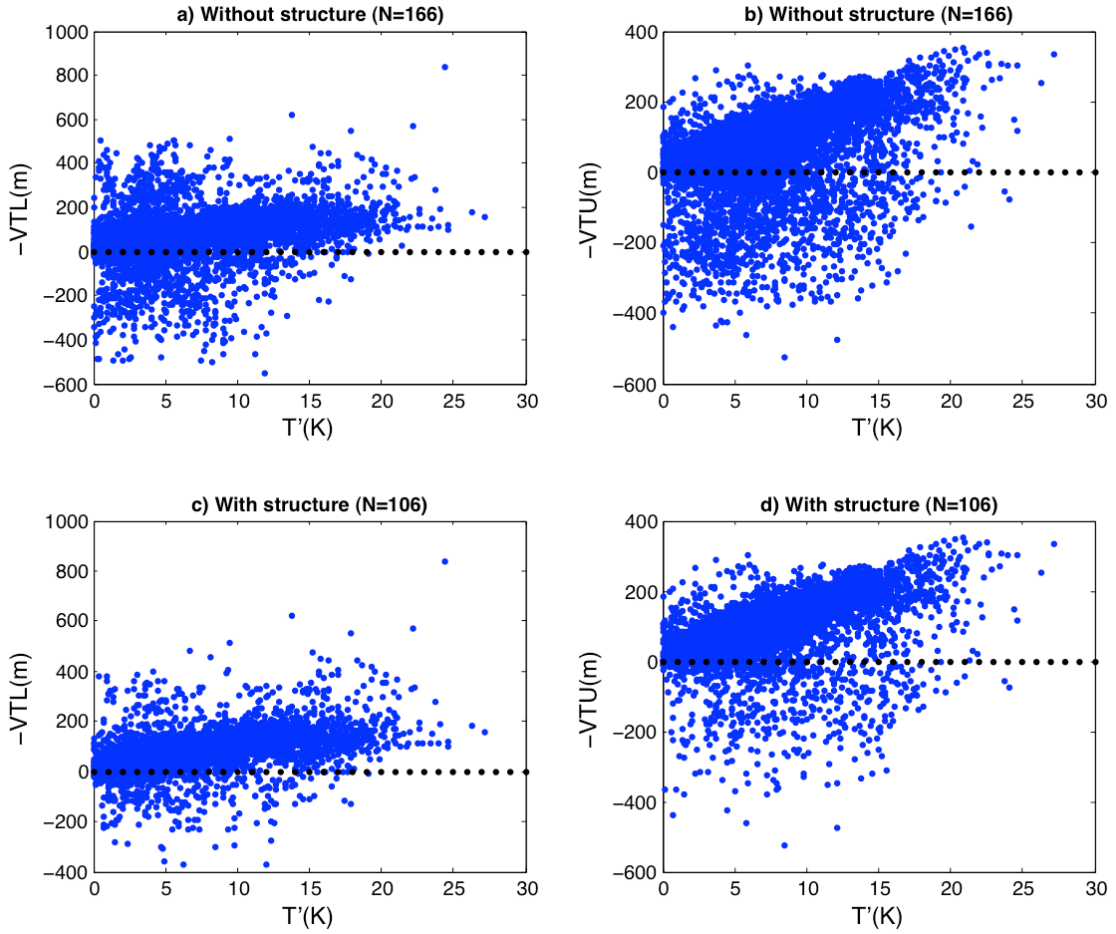

Figure 2.5: Scatter plots of traditional warm-core definition value (sum of horizontal temperature anomalies at 300, 500, and 700hPa) versus -VTL (left column) and -VTU (right column) terms without (top) and with structure criteria (bottom). N is sample population.

2.6, the sensitivity to parameter B disappears for B>20, and there is no significant difference in the composite of vertical structure when 10<B<20 or 20≤B (Figure 2.7). From these results, the threshold for B term may be increased to (or beyond) 20 as long as the conditions –VTL>0 and –VTU>0 are satisfied for TC detection.

Next, the base tracking sensitivity experiments are repeated with cyclone phase filtering included, in order to assess its impact (Table 2.5). This time only maximum

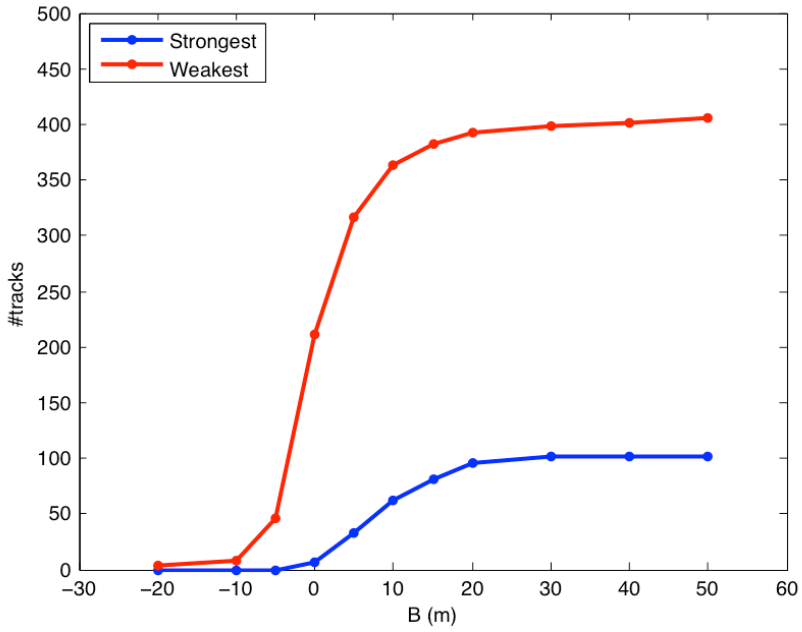

Figure 2.6: Number of detected tracks (per year) as a function of B term for the strongest (red) and the weakest (blue) base parameter combinations, when structure criteria, as well as conditions -VTL>0 and -VTU>0 are satisfied.

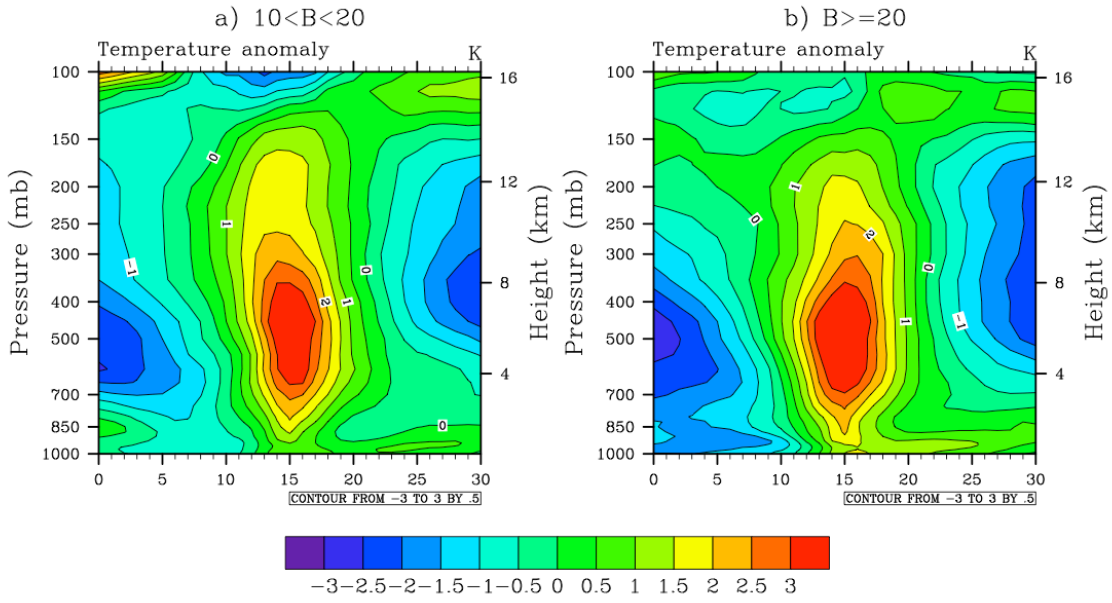

Figure 2.7: Composite plots of vertical cross section of horizontal temperature anomaly of 50 randomly chosen instances satisfying the strongest combination of base criteria, structure criteria, and -VTU>0 and -VTL>0, with a) 10<B<20, and b) B≥20.

wind measurement level and durations are varied and tested. The sensitivity to maximum wind measurement level is about the same with and without cyclone phase filtering when the other three base parameters are set to be the strongest level (though the total number has changed: compare Tables 2.4a and 2.5a). For the weakest base case, the sensitivity to maximum winds increases from 50% to 68% with cyclone phase filtering. This implies that the addition of cyclone phase filtering causes minimal alteration to sensitivity to varying the intensity threshold. However, sensitivity to duration threshold changes is magnified when cyclone phase filtering is applied. For the weakest base case, as an example, the maximum change increases from 177% to 274% (Tables 2.4d and 2.5b). Satisfaction of the cyclone phase criteria for TCs requires the presence of a robust and vertically aligned warm-core; such warm-cores can be short-lived. This is considered to be the primary reason why sensitivity of duration threshold increases when cyclone phase filtering is applied.

Table 2.5: Similar to Table 2.4 but with basic cyclone phase criteria, and only for a) varying maximum wind speed measurement level and b) varying duration.

a) Vary wind level

	Strongest (T'=2, RV=5.0, duration=3)	Weakest (dt=0, RV=1.0, duration=1)
	# Tracks	# Tracks
850hPa	78	363
1000hPa	69	213
10m	62	179

b) Vary duration

		Strongest (win.lev.=10m, T'=2, RV=5.0)			Weakest (win.lev.=850mb,T'=0,RV=0.0)		
Duration (days)	%change duration from duration=1	# Tracks	%change from duration=1	%change ratio	# Tracks	%change from duration=1	%change ratio
1	-66.67	160	158.06	-2.37	363	274.23	-4.11
1.5	-50.00	124	100.00	-2.00	267	175.26	-3.51
2	-33.33	94	51.61	-1.55	182	87.63	-2.63
2.5	-16.67	80	29.03	-1.74	128	31.96	-1.92
3	-	62	-	-	97	-	-

Finally, the sensitivity of intensity distributions to the tracking criteria is examined. Here we compare the distributions of lifetime maximum intensity (measured as wind speed at 10m above surface) from the weakest and the strongest base cases. Here both cases satisfy structure and cyclone phase filtering. Observed intensity probability is maximized at tropical cyclone (17-33 m s^{-1}) strength and quickly decays towards higher intensity (Figure 2.8). Distribution from the weakest base case shows a similar distribution shape, but the distribution from the strongest base case is more normal-shaped with maximum probability in Category 1 (33-42 m s^{-1}) strength. Note the truncation of the NRCM intensity distributions at approximately 60 m s^{-1} is due to the model resolution. Once again, intensity distribution is the most sensitive to maximum wind speed and duration thresholds. The other two base parameters (RV and warm-core) do not have a significant impact. This shows that relaxing tracking criteria can capture a broader range of intensity, but at the cost of capturing spurious systems. The number of tracks for the strongest base case is 62 (per year) but the weakest base case is 363 as it picks up more orographically induced tracks.

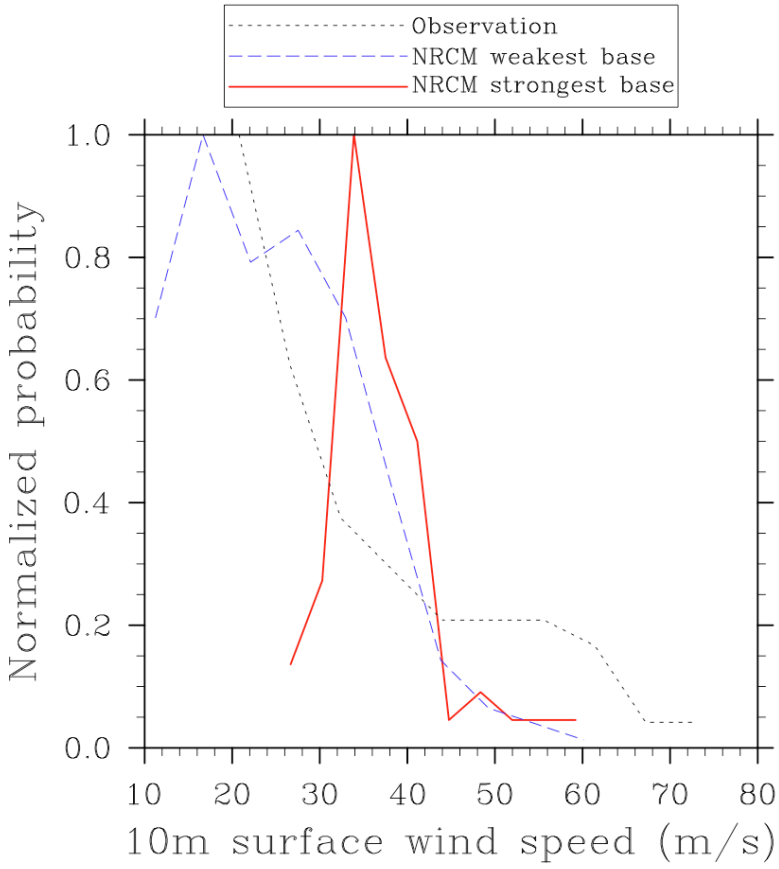

Figure 2.8: Normalized probability (normalized by the maximum population) of lifetime maximum intensity of TCs satisfying the weakest (blue) and strongest (red) base criteria combinations, and of the observed TCs (black).

2.5 Summary and concluding remarks

A survey of recent global/regional modeling studies of TC climatology reveals a large variability among TC detection and tracking criteria and thresholds, even when model horizontal resolutions are similar. Further, many of these studies do not examine the TC detection sensitivity of their underlying parameters. Despite such diversity in TC detection scheme, the resulting TC frequencies among the different studies closely follow observations as the criteria are tuned to ensure that this occurs. Potential risks of

deliberate tuning of the TC tracking criteria include 1) lack of proper assessment of model biases; and, 2) biasing future TC changes due to changes in TC characteristics that are incorrectly represented in the TC trackers.

This study has examined the inherent sensitivity of TC detection to each TC tracking parameter. Parameter thresholds are varied across a reasonable range and tested for their relative impacts on the number of detected tracks. For an improved distinction of TCs from other low-pressure systems, the cyclone phase technique (Hart 2001) is introduced to the TC tracking. The base data are the NRCM tropical channel simulation (Chapter III).

The number of detected TCs can vary from none to more than 1000 per year depending on the parameter configuration. Within the base tracking component, wind measurement level (equivalent to intensity) and duration provide the highest TC detection sensitivity. It is further shown that base tracking alone may not be enough to exclude orographically induced tracks and subtropical cyclones in South Pacific within the range of commonly used parameter values. Addition of structure criteria helps reduce detection of these erroneous TC. Further, vertical cross sections of horizontal temperature anomaly indicated that structure criteria can be satisfied even though there is no clear warm-core. Including cyclone phase parameters provides a more robust approach to detecting valid TCs with vertically aligned warm-cores. However, this also increases the detection sensitivity to cyclone maximum winds and duration parameters. It is also shown that the intensity distribution is sensitive to the TC tracking criteria. The stricter the intensity criteria, the more normal-shaped the distribution becomes.

In the subsequent analysis for the NRCM channel simulation (Chapter III) and North Atlantic climate change experiment (Chapter IV), the following thresholds and criteria are used;

- Maximum wind speed measured at 10m surface > 17 m s^{-1}
- RV > $1.0x10^{-5}$ s^{-1}
- Sum of horizontal temperature anomaly at 300, 500, and 700mb > 2.0K
- Structure criteria satisfied
- B<10, -VTL>0 and –VTU>0
- Duration > 2 days

Maximum wind speed threshold is based on the recommendation by Walsh et al. (2007), who developed an objective framework for resolution-dependent intensity cut-off for numerical detection of simulated TCs. Structure criteria is kept to reduce erroneous tracks associated with orographically induced phenomena and to accelerate the track filtering process. The cyclone phase technique, even though treatment of B term may still be an issue, is adopted in order to detect only tropical warm-core systems. Other parameters are chosen to match the visual examinations of cyclone development using movie loops of 850mb wind speed, OLR, and precipitable water.

The level of uncertainty in the number of detected tracks associated with TC tracking is infinite in the sense that one may tune the tracking parameters to detect no TCs or as many as thousands per year. While quantifying the level of uncertainty associated with TC tracking criteria is not possible, it is still helpful to set a sensible level of uncertainty. To do this, we arbitrarily choose to apply the level of uncertainty in the observed TC track data to the TC tracking. Unfortunately there is no established level of

uncertainty in observed TC track data. A reasonable assumption is that the level of uncertainty in the observed data is proportional to the data resolution. Intensity is usually recorded in 5 knot (~2.5 m s^{-1}) increments, and the temporal resolution is 6-hourly. These increments are applied to TC tracking intensity and duration thresholds to test the inherent uncertainty, as summarized in Table 2.6. These provide a first order estimate of the level of uncertainty associated with TC tracking criteria.

Table 2.6: Number of detected tracks and % changes by varying both intensity (10m surface wind by 2.5 m s^{-1}) and duration (by 6-hours) thresholds from the standard set (intensity: 17 m s^{-1} at 10m surface, duration: 48-hours.

	19.5m/s, 54 hours		17m/s, 48 hours	14.5m/s, 42 hours	
	# of tracks	% change	# of tracks	# of tracks	% change
North Atlantic	10	-16.7	12	14	16.7
East Pacific	8	-11.1	9	14	55.6
West Pacific	23	-11.5	26	33	26.9
Southeast Pacific	3	-40.0	5	7	40.0
Southwest Pacific	5	-44.4	9	15	66.7
Western Australia	5	0.0	5	10	100.0
North Indian	2	-60.0	5	6	20.0
South Indian	18	-18.2	22	26	18.2
Global	**73**	**-21.5**	**93**	**125**	**34.4**

CHAPTER III

SIMULATED TROPICAL CYCLONE CLIMATOLOGY IN THE TROPICAL CHANNEL EXPERIMENTS

3.1 Introduction

As described in Chapter I, coarse resolution GCMs are capable of producing hurricane-like vortices. However, they cannot resolve the hurricane core or the intensity of the hurricane. In addition, they cannot resolve the mesoscale processes that contribute to genesis (Lighthill et al. 1994). Coarse-resolution GCMs also have high tropical biases that generally underestimate precipitation (Randal et al. 2007, Collins et al. 2006), and also poorly simulate tropical modes such as monsoons and convectively coupled waves (e.g. Lin et al. 2006). Capturing these tropical modes is important to simulating TC genesis and development (e.g., Flank 1969, Holland 1995, Ritchie and Holland 1997, Hall et al. 2001, Bassafi and Wheeler, 2006, Done et al. 2010). Since current computing capacity is not sufficient to run global models at very high resolution over decadal time scales, an alternative is to nest a high-resolution mesoscale model within a GCM over a region of interest. This approach has been shown to improve the simulation of TC frequency and structure compared to those in GCMs (Walsh et al. 2004, Knutson et al. 2007) and it is the general approach adopted here. The Advanced Research WRF model version 3 (ARW, Skamarock et al. 2008) has been adapted and nested within either reanalysis or a GCM to simulate regional climate as the Nested Regional Climate Model (NRCM, Holland et al. 2010). Such regional climate modeling is still in its infancy and there remains much to understand about simulating regional climate at high resolution

(Leung et al. 2006). This work is an attempt to contribute to the understanding of high-resolution climate projection.

Two sets of hindcasting experiments are made with the NRCM: a tropical channel configuration with one-way nesting from analysis boundary conditions and a second, a North Atlantic nest within the channel model at higher resolution and with two-way horizontal boundary conditions. This chapter evaluates the simulated TC climatology of these NRCM hindcasting experiments with emphasis on the robustness between the "simulated" (detected) TC frequency from TC tracker and the model biases. TC tracking criteria are tuned to match the visual examination best (Chapter II) but at the cost of increased influence of subjectivity. So the aim is to increase the objectivity in the simulated TC climatology evaluation by mirroring the TC tracking results to the simulated large-scale characteristics.

A number of recent papers have examined tropical variability in the same simulation presented here, such as the Madden-Julian Oscillation (MJO), convectively coupled waves, and the mean climate simulated by the regional model (Tulich et al 2009, Done et al 2010, Caron 2010). These studies are referred to throughout the chapter.

3.2 Model description and observational data

The domain of the tropical channel version of NRCM spans 45ºS to 45ºN with a periodic boundary at the Greenwich meridian (Figure 3.1). Horizontal resolution is 36km with 51 vertical levels up to 10hPa. The NCEP/NCAR reanalysis (Kalnay et al. 1996) is used to provide northern and southern boundary conditions at 6 hourly intervals. Monthly AMIP SST (Hurrell et al. 2008), interpolated to 6-hour increments, provides lower

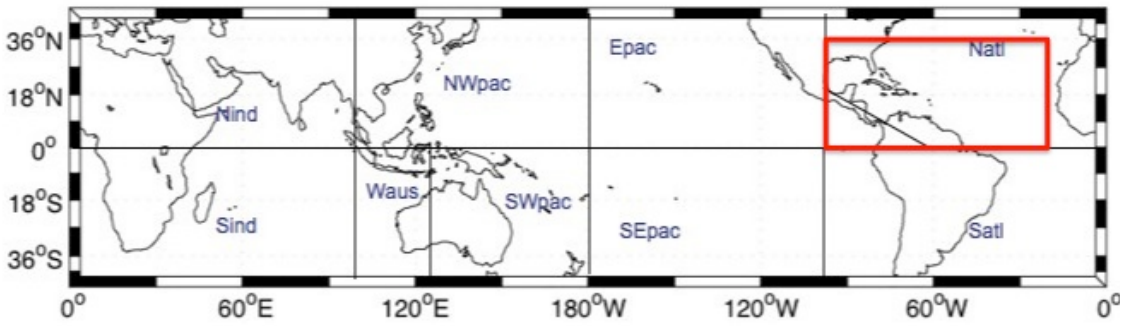

Figure 3.1: The NRCM tropical channel domain. Black solid lines are TC basin boundaries. The red box indicates the 12km child domain for two-way nested simulation.

boundary forcing. The following parameterizations are used: Kain-Fritsch convective parameterization (Kain and Fritsch 1993); the Community Atmospheric Model 3 (CAM3) radiation scheme for short- and long-wave radiation (Collins et al. 2004); the Yonsei University (YSU) planetary boundary layer scheme (Hong et al. 2006); the WRF Single-Moment 6-Class Microphysics Scheme (WSM6) for explicit precipitation processes (Hong and Lim 2006); and the Community Noah Land Surface Model (LSM, Ek et al. 2003). These physics options were chosen following extensive testing of long-term simulations with NRCM over the continental U.S. (Done et al. 2005).

Two simulations are examined in this chapter: a full channel simulation from 2000-2005 with 36 km horizontal resolution, and a second simulation from 1 May 2005 through 1 December 2005 incorporating a 12 km resolution regional domain over the North Atlantic (0-35°N and 20-100°W, solid red box in Figure 3.1), which is two-way nested within the 36km tropical channel domain. Parameterizations and forcing are the same for both simulations except that the SSTs are derived from weekly AMIP SST for

the nested domain. A more detailed description of the two-way nesting is provided in Section 3.3.2.

Simulated TCs are extracted from the simulations using the tracking method described in section 5 of Chapter II. Observed TC statistics are obtained from the International Best Track Archive for Climate Stewardship (IBTrACs, Knapp et al. 2010) version v01cor-r01. IBTrACs contains all tropical systems recorded by at least one agency around the world including non-named tropical depressions. So to be consistent with the TC tracking method used in this study, storm tracks with lifetime maximum wind speed of 17 m s^{-1} or less are excluded from the observed TC statistics. This filtering excludes about 20% of archived tracks from IBTrACs, resulting in 611 tracks for 2000-2005. It also removes most of the storm tracks with duration of less than 48 hours, such that only six out of 611 tracks have a duration of 48 hours or less. Removing these six tracks from the observed data makes little difference in the overall statistics. TxP/NCAR reanalysis is used as the observational base when comparing the simulated large-scale patterns.

3.3 Simulated TC climatology

3.3.1 Channel 6-year simulation (2000-2005)

As shown in Figure 3.2, the overall spatial pattern of TC genesis locations is well captured in the NRCM, although there is a tendency to overproduce TCs particularly in the Northwest Pacific and in the Southern Hemisphere. Figure 3.3 compares simulated and observed annual TC frequency in each of the TC basins defined in Figure 3.1. In the Northwest Pacific (Figure 3.3c), simulated annual TC frequency is higher than

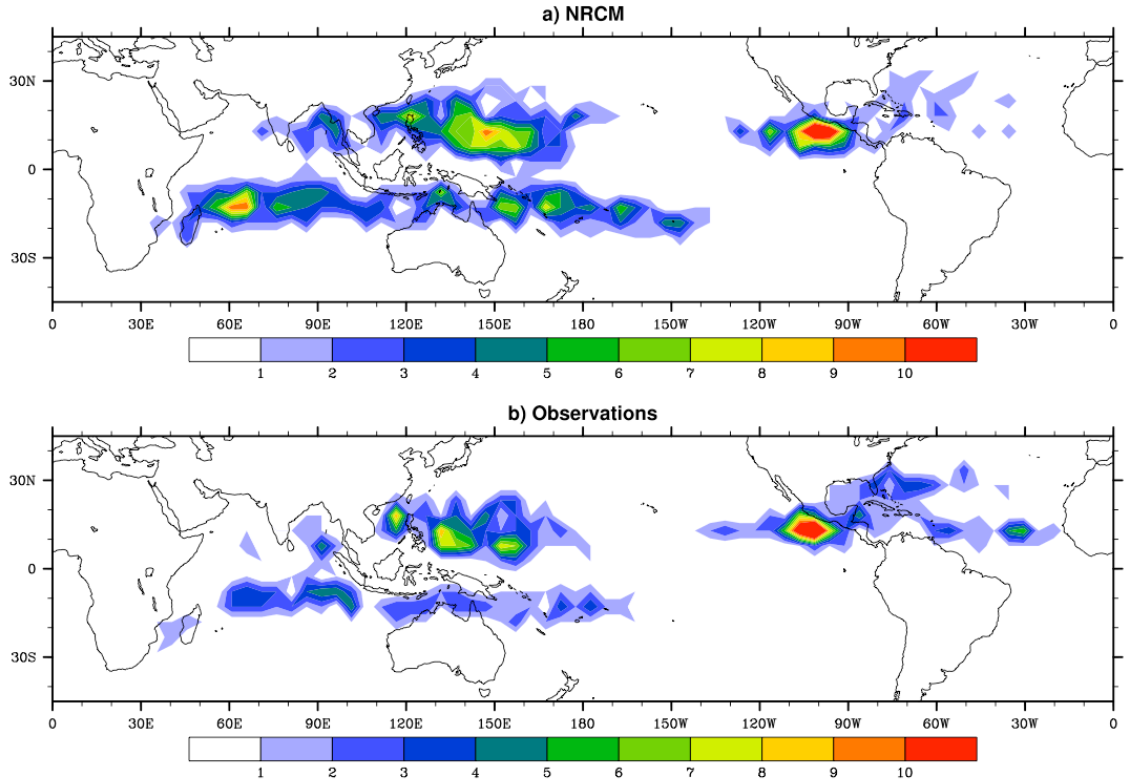

Figure 3.2: Density plots of TC genesis locations from a) the NRCM simulation and b) observations. Genesis occurrence is cumulated for 6-years (2000-2005) for every 5 degree grid boxes.

observations with the exception of year 2000. For 2001-2005, the observed annual TC frequency is consistently outside of the level of uncertainty associated with TC tracking criteria (the definition of the level of uncertainty associated with TC tracking criteria is found in Chapter II Section 5), indicating that over prediction of TCs in NRCM for the Northwest Pacific is likely a systematic bias. A similar over production occurs in the South Indian Ocean (Figure 3.3h). Indications of over production of TCs are noted in other basins, but the bias is less than those in the Northwest Pacific and the South Indian Ocean. The only exception is in the North Atlantic, where NRCM lacks TC genesis in the Main Development Region (MDR, tropical North Atlantic west of the African coast)

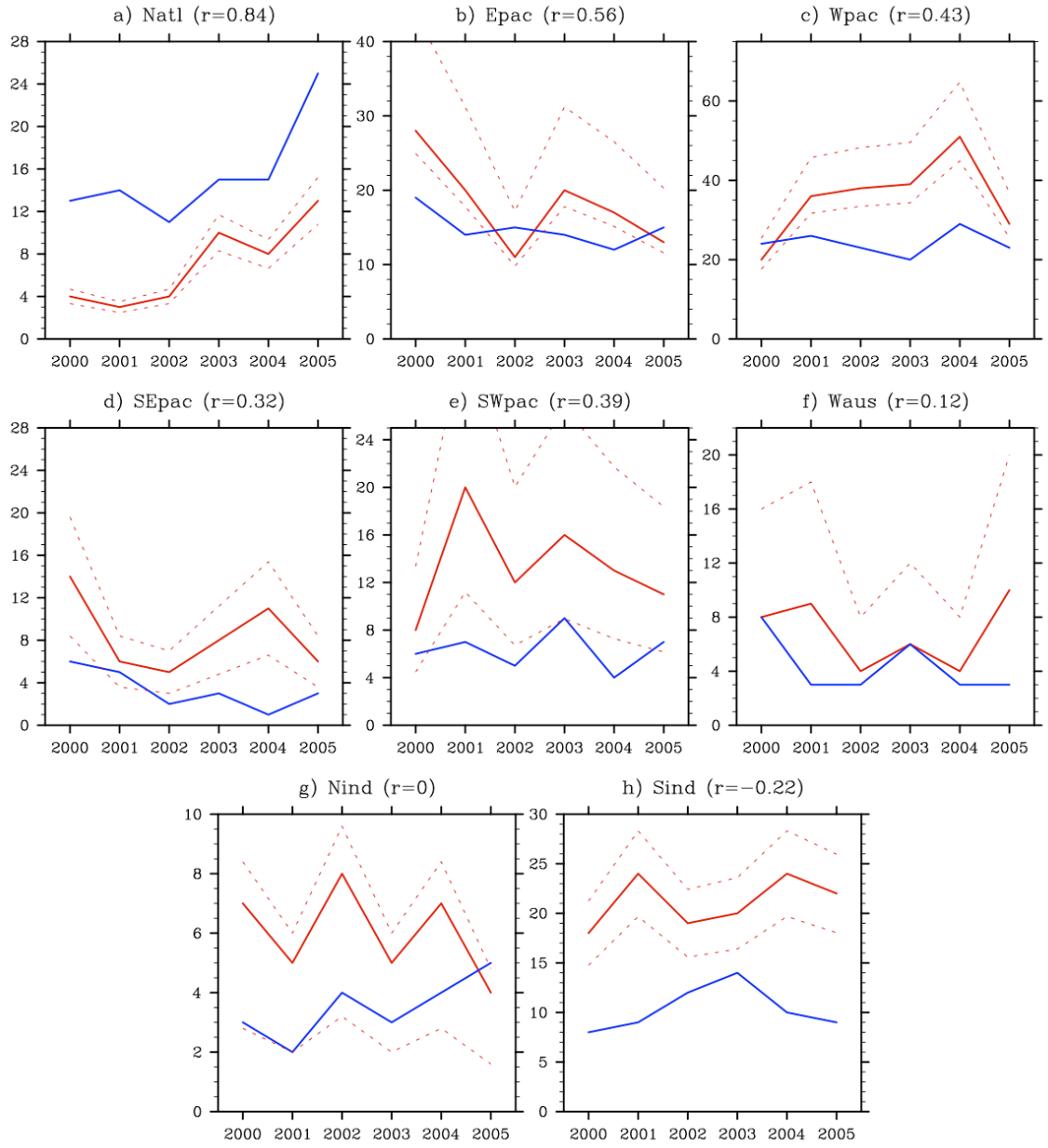

Figure 3.3: Annual frequency of TCs simulated by the NRCM (solid red lines) and the level of uncertainty associated with TC tracking criteria (dotted red lines), and the observed TC frequency (blue lines) for each of TC basins: a) North Atlantic, b) East Pacific, c) Northwest Pacific, d) Southeast Pacific, e) Southwest Pacific, f) Western Australia, g) North Indian Ocean, and h) South Indian Ocean. TC basin boundaries are as shown in Figure 3.1. Values r are the correlation between the simulated and the observed TC frequencies.

(Figure 3.2) and annual TC frequency is significantly underestimated (Figure 3.3a). The overall tendency of over production of TCs contributes to the global overestimate of TCs compared to observations (Figure 3.4). Although the choice of TC tracking criteria largely controls these statistics, there are also some dynamical reasons for the biases in simulated TC frequency.

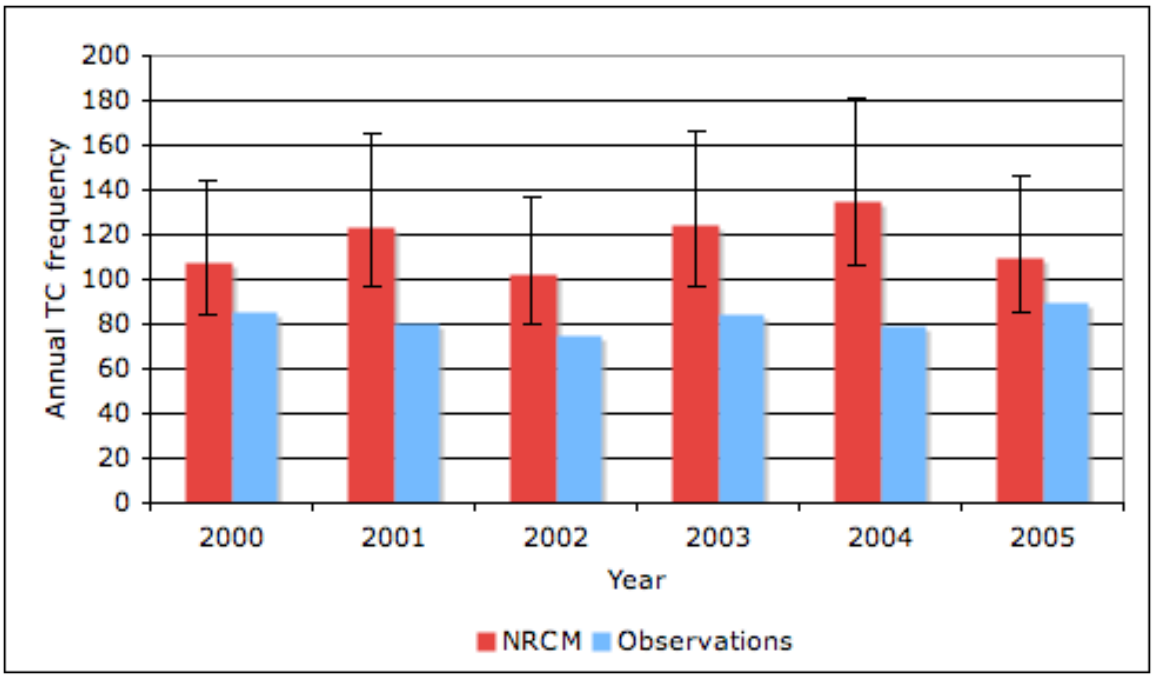

Figure 3.4: Annual TC frequency simulated by the NRCM for the whole tropical channel domain (red bars) with the level of uncertainty associated with TC tracking criteria (black error bars), and the observations (blue bars).

Figure 3.5 shows the simulated and observed large-scale factors that are known to affect TC genesis (Gray 1968) and Figure 3.6 shows the model bias (model minus observations). The general low-tropospheric wind pattern is well captured in the NRCM but the magnitude of the zonal flow is enhanced in the tropical North Pacific and so is the westerly flow in Indian Ocean (Figure 3.5a and 3.6a). Zonal confluence is especially

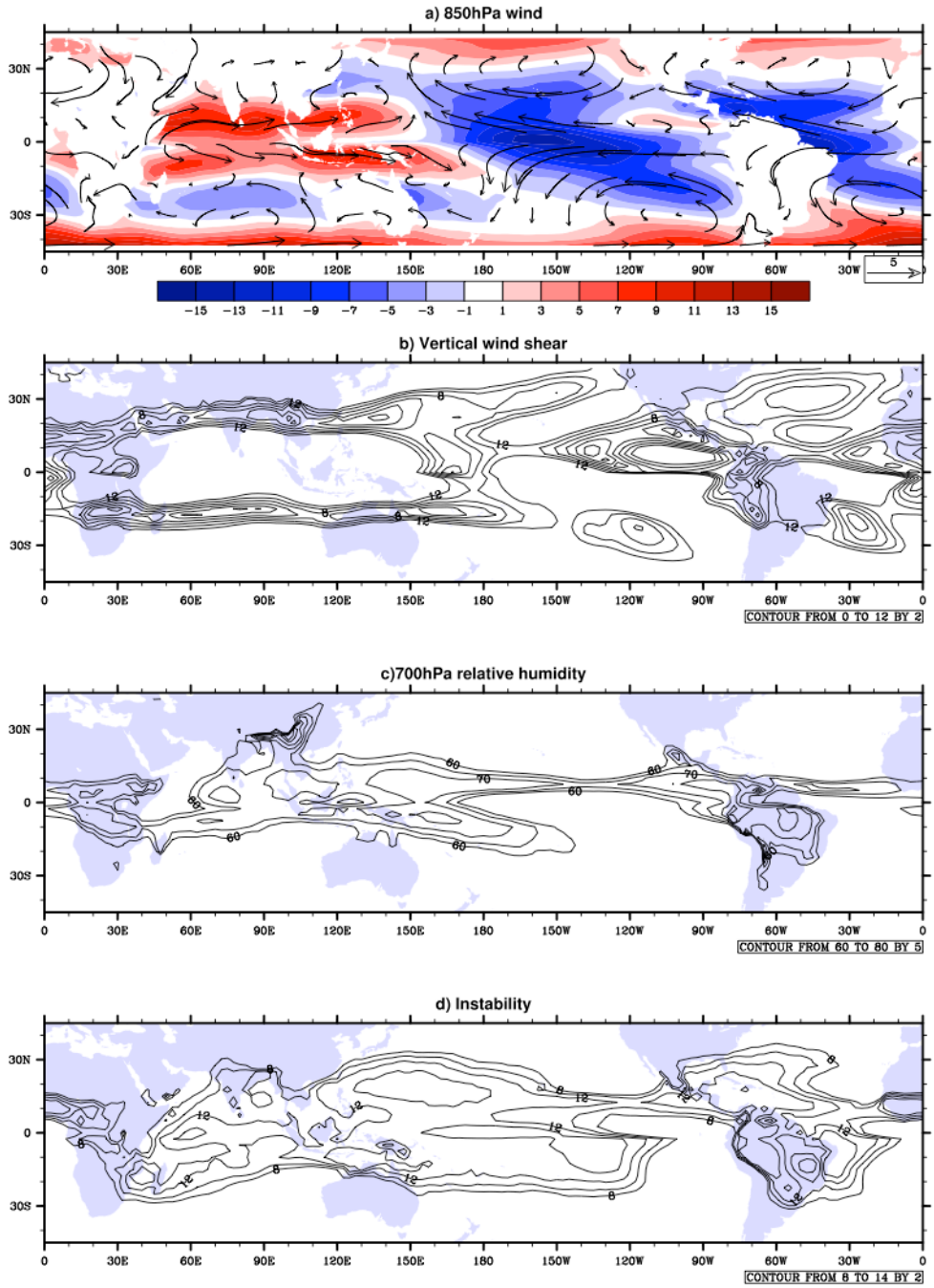

Figure 3.5: Simulated seasonal mean fields of TC-modulating environmental factors averaged over the TC season (August-October for Northern Hemisphere, and December-February for Southern Hemisphere). From top, a) 850hPa wind vectors and zonal wind speed (colored contours, m s^{-1}), b) 200-850hPa vertical wind shear (m s^{-1}), c) 700hPa relative humidity (percent), and d) moist inertial instability defined as the difference of equivalent potential temperatures at 600hPa and surface levels (K).

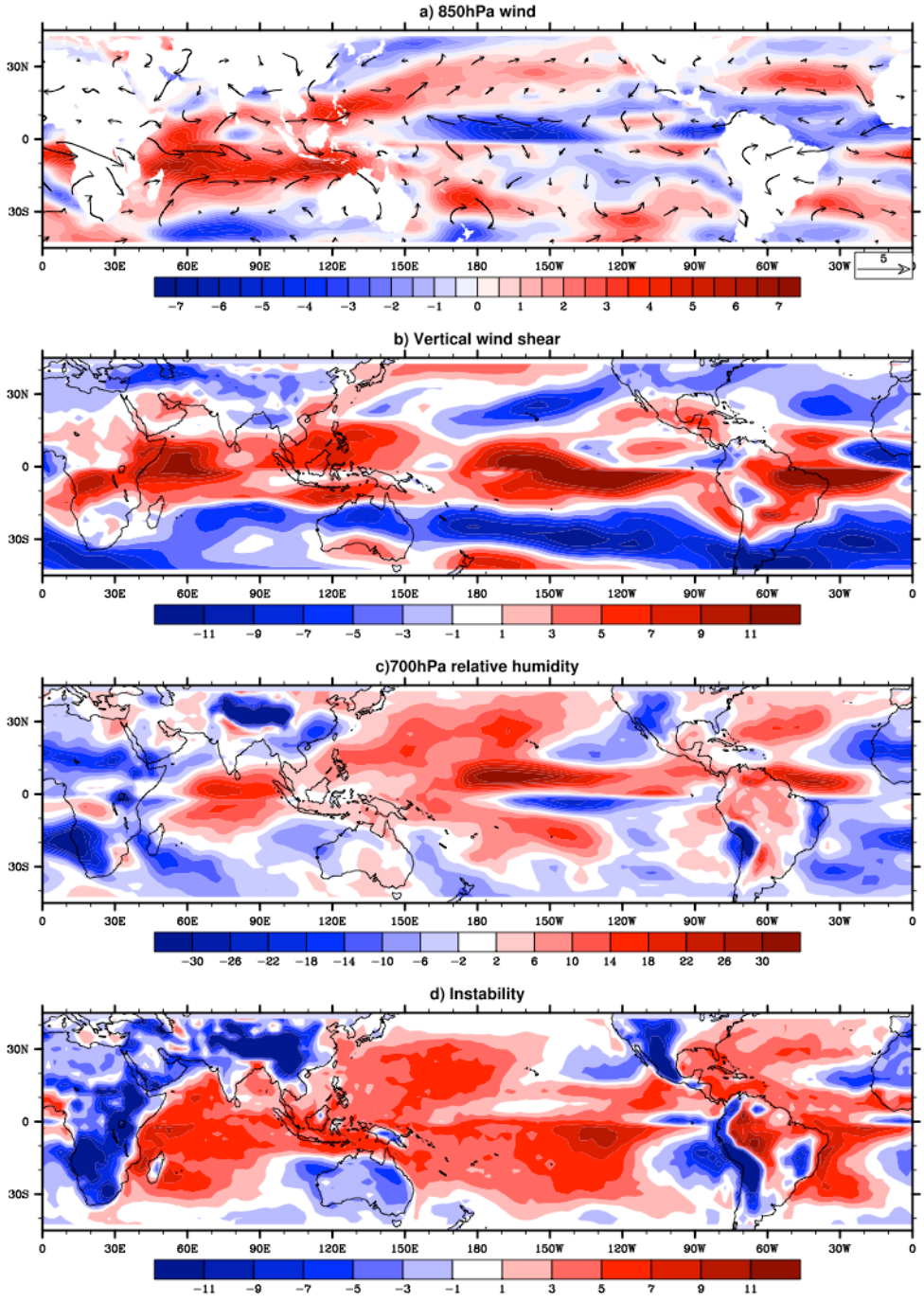

Figure 3.6: Similar to Figure 3.5, but the difference between the NRCM and observations (model minus observations).

intensified in the tropical Northwest Pacific where most of the TCs form (Figure 3.6a). Vertical wind shear is positively biased along the equator (Figure 3.6b) but nonetheless sufficiently low (less than 12 m s^{-1}) for TC genesis in most of the active TC basins (Figure 3.5b). However, 700hPa humidity and moist static instability are also overestimated in most of the TC basins (Figure 3.6c and d).

There is some evidence for the NRCM being too convective overall in the current tropical channel simulation. First, Tulich et al. (2009) analyzed the same simulation and found that there is a high bias in the annual mean precipitation over much of the tropical ocean except for the tropical Atlantic (Figure 3.7). Second, Caron (2011) showed that there is too much variance in daily OLR, which is indicative of frequent intransient convective system passages (Figure 3.8). The exact cause of this over-active convection is not known, but the convective parameterization appears to be a contributing factor (Tulich et al. 2009). Having too much convection does not necessarily lead to more TC genesis, because numerous scattered short-lived convections would distribute low- and mid-level heating across the area and would not allow for an organization of convective systems. A spectrum analysis of precipitation shows that the NRCM underestimates short-lived convective systems, and over-predicts long-lived (> 6 days) convective systems, especially the Rossby-type easterly waves (Tulich et al. 2009). Excessive TC genesis in the NRCM is driven by a combination of low simulated vertical wind, enhanced long-lived convective systems, high moisture content and enhanced instability.

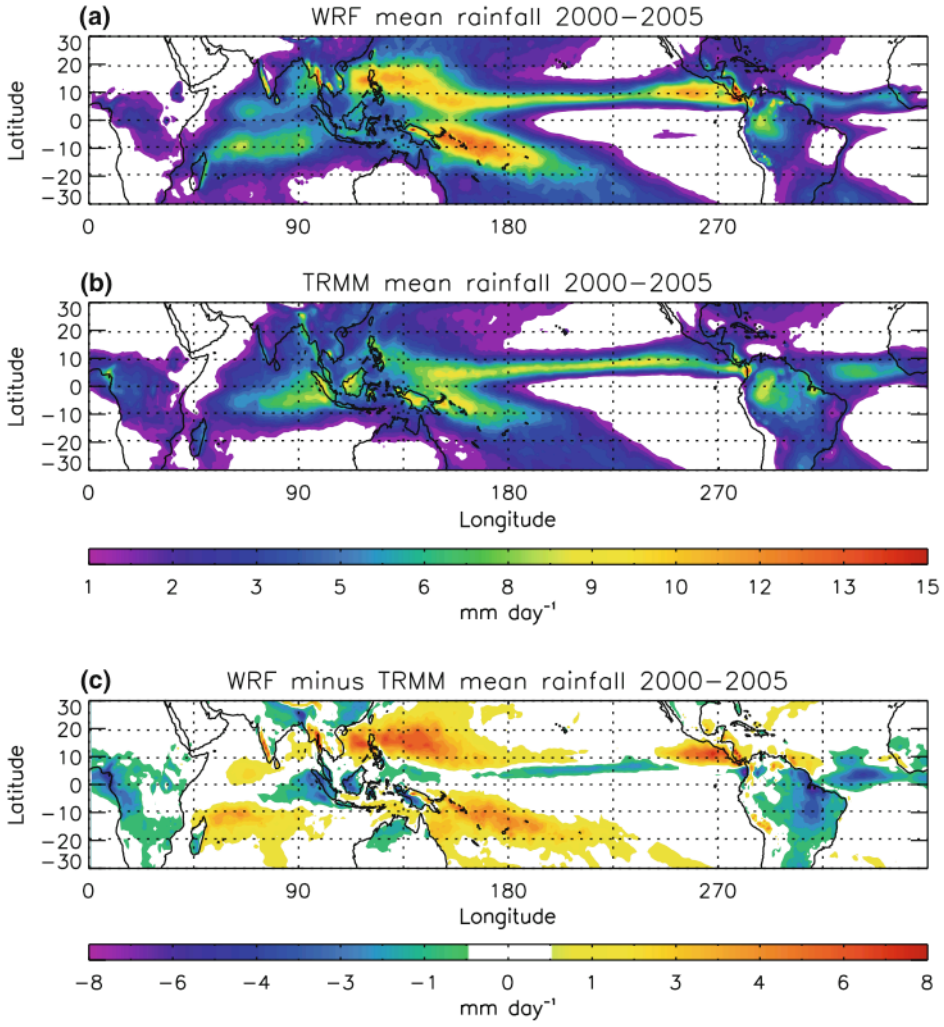

Figure 3.7: Comparison of a) simulated versus b) the Tropical Rainfall Measuring Mission (TRMM, Huffman et al. 2007) annual mean rainfall (mm day^{-1}) during 2000-2005, along with c) the difference between the two (applied from Tulich et al. 2009).

In addition, there are some notable regional biases that could have contributed to the local biases in TC genesis. The overestimate of Northwest Pacific TCs may be partly driven by the anomalously high Asian monsoon flow in the NRCM. Here, there is a region of zonal confluence associated with the exit of low-level easterlies and the eastern end of the Asian monsoon (Figure 3.9b). Easterly waves entering this confluence are

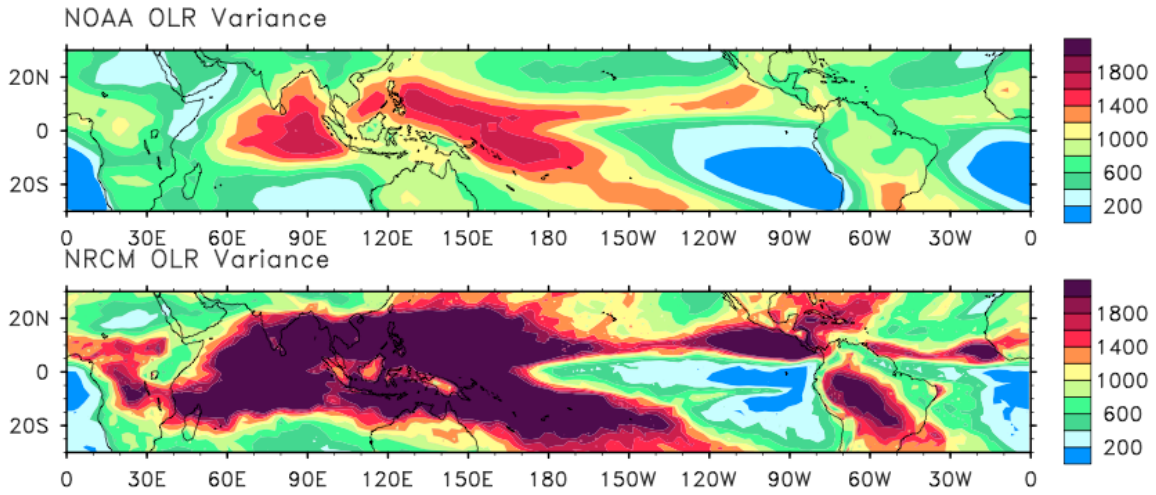

Figure 3.8: The daily variance of outgoing longwave radiation (W m^{-2}) for NOAA (Liebmann and Smith 1996, top) and for NRCM (bottom) (applied from Caron 2011).

thought to form TCs by wave energy accumulation processes (Holland 1995, Webster and Chang 1997, Done et al. 2010). In the NRCM, the magnitude of zonal confluence is stronger compared to observations (Figure 3.9a), and is primarily driven by the anomalous westerly flow associated with the Asian monsoon (Figure 3.9c). Enhanced wave accumulation processes, combined with the model's over-convective tendency, potentially contributed to the over prediction of TCs in this region. Our analysis is consistent with Tulich et al. (2009), who found excessive wave-induced TC genesis in the Northwest Pacific region in the same NRCM simulation.

The underestimation of TCs in the North Atlantic appears to be associated with a lack of moist African Easterly Waves (AEWs, Frank 1969) in the model. Mesoscale convection embedded in AEWs often becomes precursor to TC genesis (e.g., Avila and Pasch 1992). The NRCM simulates the dry, large-scale components of AEWs quite well; a spectrum of meridional wind variance in Figure 3.10 clearly shows a 2-6 day

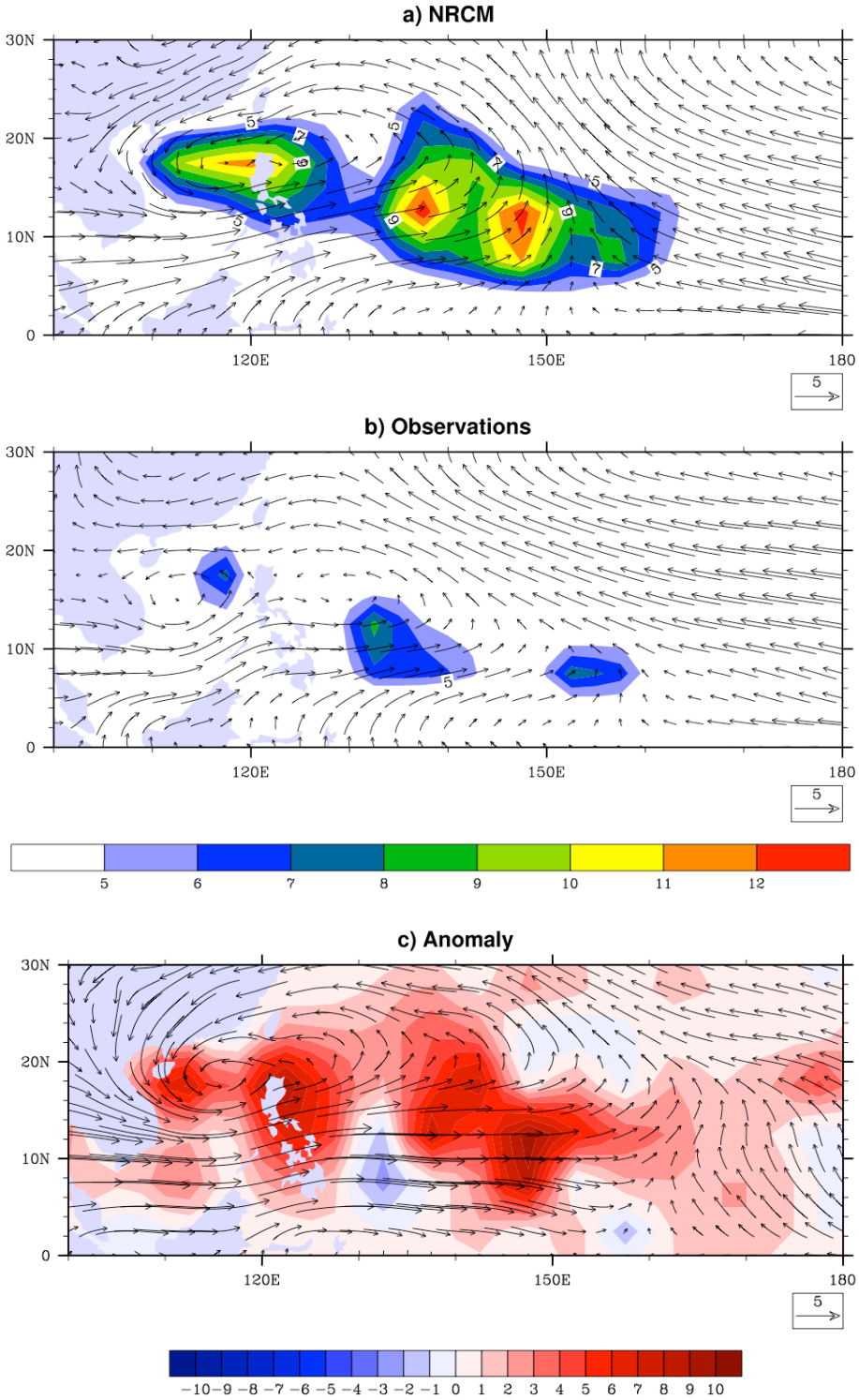

Figure 3.9: Vector plots of August-October 2000-2005 averaged 850hPa winds (m s^{-1}) and TC genesis location density (color contours) from a) the NRCM, b) observations, and c) the difference of the two (model minus observations).

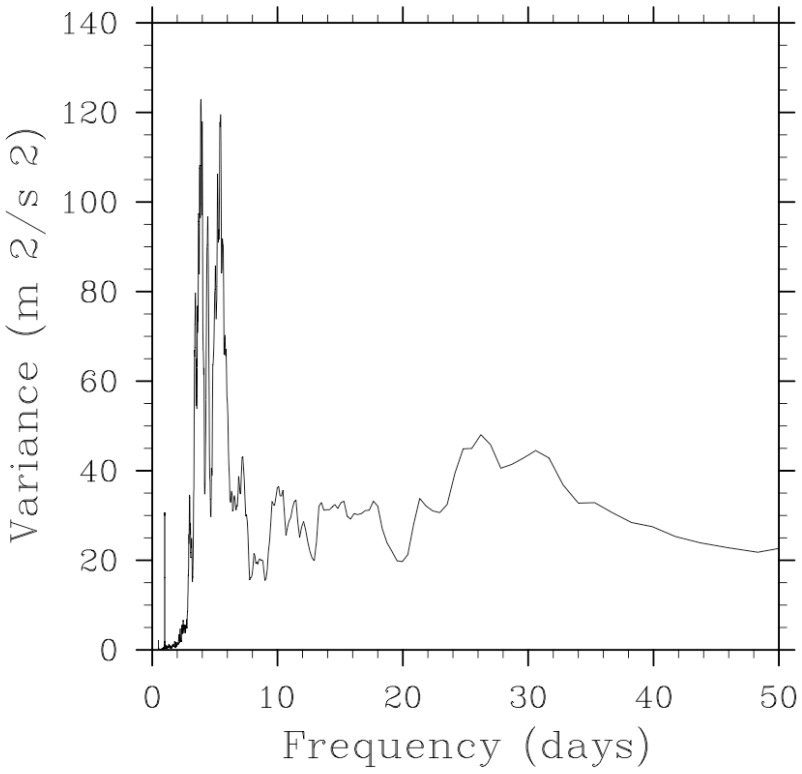

Figure 3.10: Time spectrum of 700hPa meridional wind averaged over 10-20ºW and 10-20ºN from June to October, 2000-2005 from the NRCM.

maximum. The spatial distribution of 2-6 day filtered meridional wind is in a good agreement with observations (Figure 3.11), except for the NRCM underestimating the variance over the MDR, which suggests that AEWs in the NRCM quickly dissipate as they move over the ocean. Further, a spectral analysis of precipitation reveals that the variance of westward propagating convective clusters is markedly underestimated in this region (Tulich et al. 2009). This finding is intriguing as the NRCM has high biases in low-tropospheric moisture content and moist static instability (Figures 3.5 and 3.6). This implies that a mechanism for effectively using these thermodynamical conditions in the maintenance of convective systems embedded in AEWs appears to be lacking in the

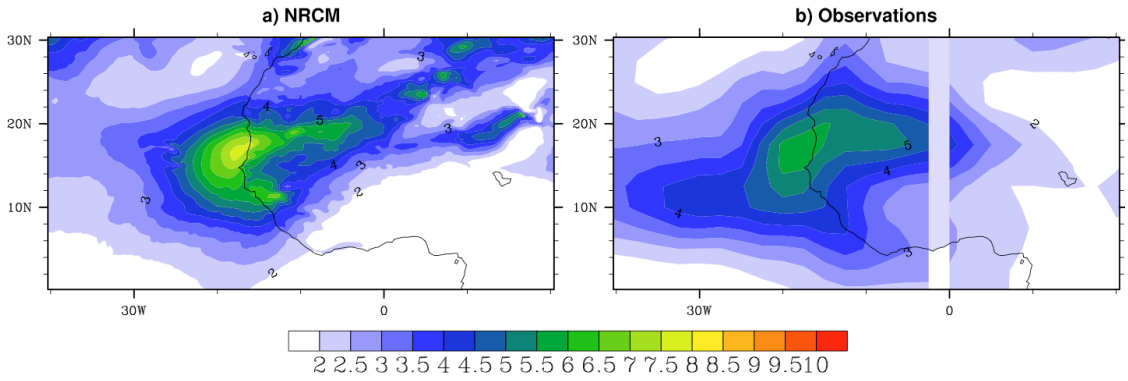

Figure 3.11: Variance of the 2-6 day filtered meridional wind (m s^{-1}) at 700hPa for June-October, averaged over 2000-2005 from a) the NRCM and b) observations.

NRCM. The underestimation of TC genesis in the North Atlantic cannot be attributed to the vertical wind shear, which is sufficiently low. Thus, it appears that the underestimation of TC genesis in the North Atlantic is associated with the poor development and maintenance of moist and convective AEWs over the ocean.

Interestingly, however, the simulated interannual variability of TC frequency is well correlated (r=0.84, Figure 3.3a) with observations in the North Atlantic. There is no statistical significance to this correlation due to the limited 6-year period of the simulation. But the high correlation in the North Atlantic stands out compared to other basins (Figure 3.3). Hopsh et al. (2007) found that the interannual variability of TC genesis in the MDR is more strongly correlated with the dry, large-scale components of AEWs, rather than the mesoscale convections that are embedded within AEWs. Our simulation results from the NRCM appear to be in agreement with these findings.

Figure 3.12 compares PDFs of lifetime maximum intensities from the model and observations. The observed curve is skewed with a maximum near tropical cyclone

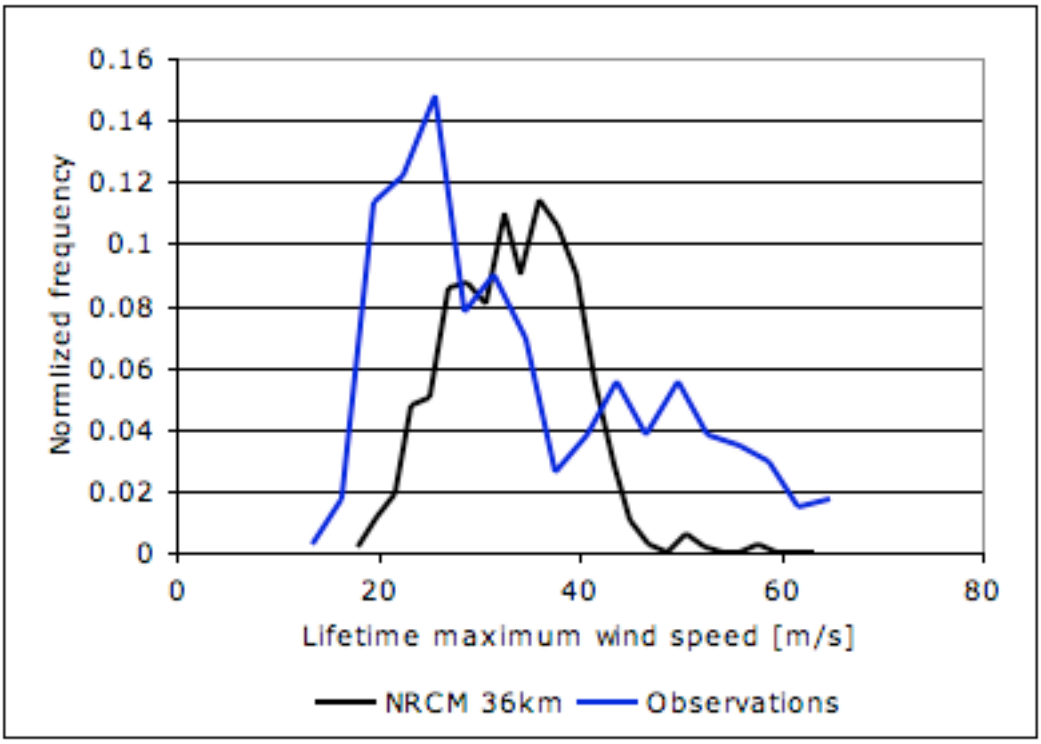

Figure 3.12: Probability distribution functions of TC lifetime maximum wind speed (m s^{-1}) for the NRCM non-nested simulation (black) and observations (blue).

(17-32 m s^{-1}) strength. However, the simulated curve is more Normal-shaped, and maximized at Category 1 (33-42 m s^{-1}) strength. The wind-pressure relationship (Figure 3.13) shows that the simulated wind speed is underestimated when compared to observations for a given pressure under ~970hPa, implying that the resolution of the NRCM (36km) is not sufficient to resolve the steep pressure gradient observed in intense storms. These are well-known issues with other comparable regional models (e.g. Bender et al 2010, Walsh et al 2004, Oouchi et al. 2006). Meanwhile, the occurrence of weaker storms is also underestimated. This is partly due to the 17 m s^{-1} cut-off in TC tracking criteria (Chapter II Section 4). There is also a tendency to overestimate the intensity of

weak storms by the model (Dudhia et al. 2008, Davis et al. 2010), but it is not known how much of this tendency is contributing to the intensity distribution bias seen here.

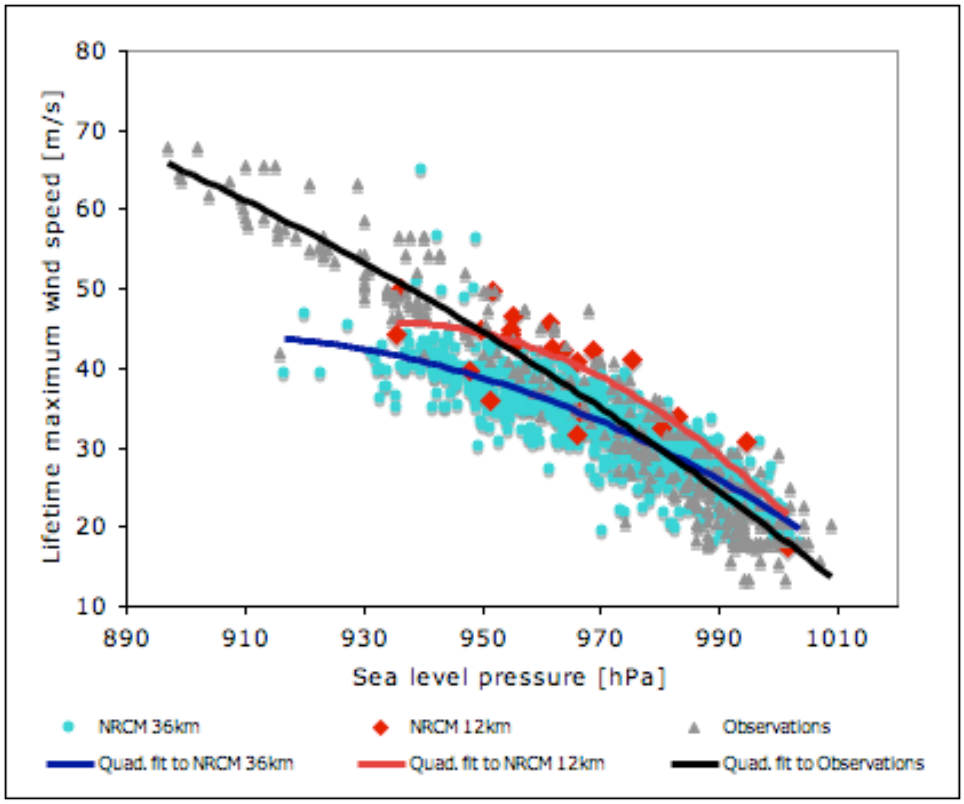

Figure 3.13: Scatter plots of TC maximum wind speed (m s^{-1}) and minimum sea level pressure (hPa) for all TCs at their lifetime maximum intensity, from the NRCM non-nested 6-year simulation at 36km resolution (blue dots), the NRCM two-way nested 12km domain (red dots), and from observations (black dots). Quadratic fit for each is also shown.

3.3.2 High-resolution two-way nested simulation for the North Atlantic (May-November 2005)

The two-way nesting simulation utilizes two domains with different horizontal resolutions: a larger *parent* domain with coarser horizontal resolution, and a smaller *child* domain nested within the parent domain with finer horizontal resolution. The two domains integrate in a sequence. The parent domain integrates to the next time step first and provides boundary conditions for the child domain. Next, the child domain integrates with a finer time step that is proportional to the horizontal resolution ratio of the parent and child domains. Then, the solution of the child domain replaces that of the parent domain. In our case, the parent domain is the 36km resolution tropical channel domain, and the child domain is the 12km domain covering the North Atlantic (Figure 3.1).

We will present (1) the *upscale* (from child to parent) impact of two-way nesting in the general simulated climatology of TCs by comparing the results from the parent domain to the original 6-yr tropical channel 36km simulation (hereafter referred to as *non-nested run*), as well as (2) the impact of an increased resolution to the simulated TC intensities comparing the child domain with the non-nested run.

Figure 3.14 compares the simulated TC tracks from the parent and child domains of the two-way nested run (panels b and c, respectively), as well as from the 6-year non-nested run (panel a). The same tracking criteria are used to detect simulated TCs in all cases.

Comparing the parent domain and the non-nested run reveals the upscale impact of the high-resolution two-way nesting (Figure 3.15 a and b). The addition of a high-resolution nest (the child domain) improved the overall TC climatology with an increase

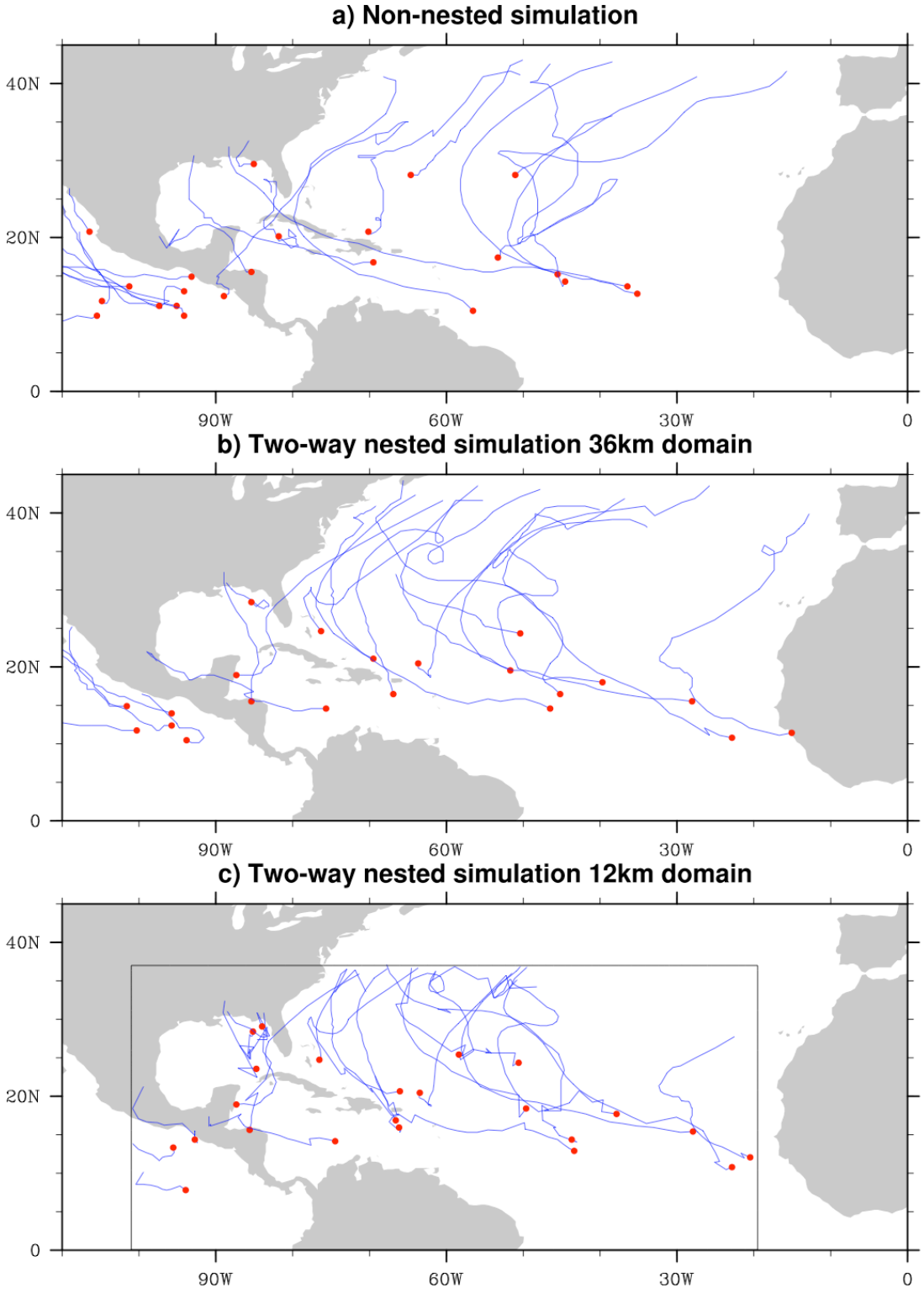

Figure 3.14: TC tracks (blue line) and their genesis locations (red dots) from a) non-nested simulation (shown tracks originated in 2005 May-November only), b) two-way nested simulation 36km parent domain, and c) two-way nested simulation 12km child domain. Think black lines in c) denote the 12km child domain boundaries.

in TC frequency from 13 (non-nesting) to 16 (two-way nesting), although this was still less than the observed number of 25 for the period of May-November 2005 (excluding tropical depressions to be consistent with the TC tracking).

A remarkable difference is that the high-resolution nesting produced three TCs east of 30°W in the parent domain. This is significant as there was no TC genesis simulated east of 30°W in the entire 6-year non-nested run (Figure 3.2).

The non-nested run had a marked dry bias in mesoscale convective systems embedded in AEWs, which was intriguing as the simulated thermodynamic conditions were biased more favorable towards moist convective activities (Figure 3.6). These seemingly contradicting findings hinted for a lack of mechanism that takes advantage of thermodynamic conditions in maintenance of convective systems in the non-nested run. Comparing the Hovmöller diagrams of 2-6 days filtered precipitation indicates that there are more precipitating, moist convective systems embedded in AEW in the two-way nested run when compared to the non-nested run (Figure 3.15). Here, mesoscale convective systems are better resolved in the child domain, owing to the increased resolution (Figure 3.16). Better resolved precipitating convection in the child domain is forced to the parent domain, resulting in more precipitation for the parent domain in mesoscale convective systems embedded in AEW. The latent heat release from these convections allows for a better organization of convections and leads to an increased chance of TC genesis. This finding suggests that model resolution is a key factor in realizing the mechanism to maintain moist convective systems in AEW from favorable thermodynamic conditions. But it is not the sole factor, as will be shown in Chapter IV.

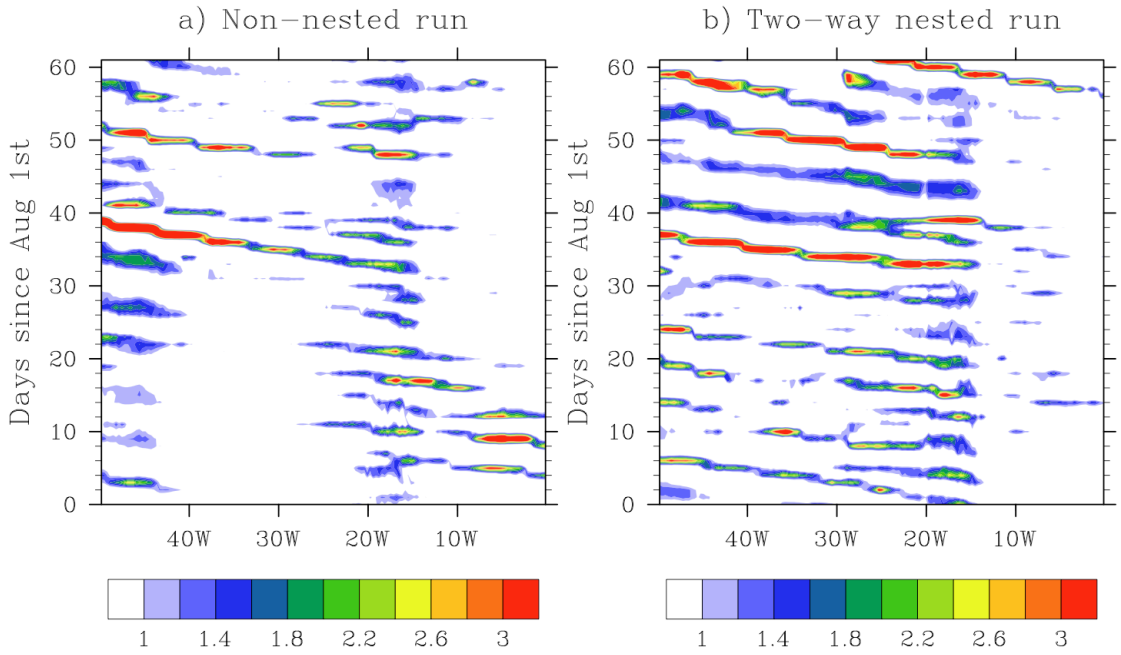

Figure 3.15: Hovmöller diagrams of precipitation (mm per 6-hours) averaged over 10-20ºN for 1 August through 30 September of 2005 from a) the NRCM 6-year non-nested simulation at 36km resolution, and b) two-way nested simulation 36km parent domain.

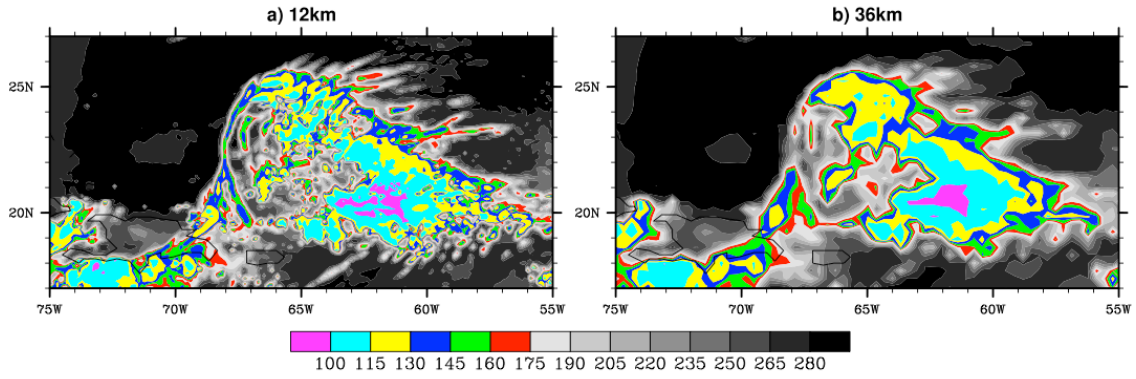

Figure 3.16: A snapshot of the simulated outgoing logwave radiation (W m^{-2}) of a pre-TC disturbance on 06Z 11 October 2005 in the NRCM two-way nested simulation, comparing a) 12km child domain, and b) 36km parent domain.

Figure 3.14c shows the simulated TC tracks in the 12km child domain (the boundary locations are denoted with dotted lines). The child domain developed 20 TCs within its boundaries. It is still less than observed but is an increase from the 16 TCs found in the 36km parent domain. Of the 16 storms that are present in both domains, three are detected earlier in the 12km child domain with higher wind speed resolved in the finer resolution. Four storms that are not present in the 36km parent domain are short-lived storms that did not reach sufficient intensity to pass the TC tracking criteria in the 36km parent domain. The difference of intensities is also evident in the SLP-wind relationship (Figure 3.13). Clearly, storms in the 12km child domain have higher wind speeds for a given minimum SLP when compared to the 36km resolution. However, the 12km child domain still has difficulty producing Category 3+ intensities.

There are indications of upscale impacts outside the nested domain. In the North Indian Ocean, the number of simulated TCs increased from 3 to 6 after two-way nesting was introduced. Also, an anomalous blocking pattern developed over southeastern Australia, which leads to enhanced drought conditions. This may be due in part to the internal model variability rather than arising directly from the addition of the North Atlantic nest. This is the subject of ongoing research.

The foregoing leads to an important remark. Simulated synoptic behaviors in a regional climate model have high sensitivity to boundary location (Seth and Giorgi 1998) and initial conditions (Lucas-Picher et al. 2008). For the year of 2000, an additional NRCM tropical channel simulation was made with exactly same configurations as the current simulation presented here, but with the southern boundary location shifted to 35°S (as opposed to 45°S in the current simulation). In the additional simulation with the

southern boundary at 35°S, simulated TC frequency in the Southern Indian Ocean increased by 34% compared to the simulation with the 45°S boundary location. Also, as will be discussed in Chapter IV, the simulated TC frequency for a fixed time period can change by altering initial conditions. These uncertainties, combined with those associated with the TC tracking, suggest that care must be taken in interpreting regional climate simulations of TC activity.

3.4 Summary

This chapter investigated the capability of the NRCM in simulating TCs in two simulations. The first is a non-nested, single-domain simulation covering the global tropics, and the second is a two-way nested simulation with a nested, finer-resolution domain over the North Atlantic. Both simulations were forced with the NCEP/NCAR reanalysis at northern and southern boundaries.

The NRCM is shown to be capable of producing realistic spatial and temporal characteristics of the observed TC climatology, but it also tends to over produce TCs overall. This finding is sensitive to the TC tracking method. However, the over prediction of TCs is outside of a reasonable level of uncertainty associated with TC tracking method (as defined in Chapter II). Further, there are some dynamical reasons to support this being a real difference. First, the NRCM tends to be more convective than observations, as indicated by the analysis of simulated precipitation and OLR patterns. Second, westerly flow associated with the East Asian summer monsoon is anomalously high in the simulation, creating more favorable TC genesis conditions in the Northwest Pacific, where much of the global overestimation in simulated TC frequency takes place. In the

North Atlantic, however, the simulated TC frequency is underestimated due to the lack of moist AEWs in the model. Meanwhile, it is also shown that the simulated TC frequency can be altered by changing the lateral boundary location.

The implementation of a two-way nested, finer-resolution domain in the North Atlantic improved the simulated TC climatology by generating more TCs, especially in the MDR. Better-resolved mesoscale convective systems in the finer-resolution domain helped moisten the AEWs, leading to an improved organization of convections and to more TC genesis in the MDR. That two-way nesting led to an improvement in the simulated TC climatology in our series of simulations implies that the interactive nesting is yet another source of uncertainty in simulating TC activity. In addition, we noted some possible upscale impacts associated with two-way nesting, with more frequent North Indian Ocean cyclogenesis and an increased blocking pattern in southeastern Australia. However, it is not clear whether these changes are indeed as a result of upscale impact from two-way nesting, or simply reflecting the model's sensitivity to initial conditions.

The simulated TC wind-pressure relation is close to observations for weaker storms, but the coarse model resolution results in a low wind speed bias for stronger storms and major hurricane intensities do not occur. This is a well-known inability for 36km resolution models to resolve the steep pressure gradients observed in intense TCs. The simulated wind-pressure relation is improved with the 12km resolution, but still has difficulty resolving major hurricane intensities.

Despite the tendency of overestimating the TC frequency, the NRCM is shown to be capable of simulating the general spatiotemporal characteristics of the current

observed TC activity. This result gives a confidence to proceed to the climate change experiment, which will be presented in Chapter IV.

CHAPTER IV

NORTH ATLANTIC HURRICANE CLIMATE CHANGE EXPERIMENT

4.1 Introduction

The recent increase of North Atlantic TC activity has attracted considerable attention especially since the exceptional hurricane season of 2005. Causes for this increase have been hotly debated in an attempt to determine whether it is within a range of natural variability, the result of global warming, or merely a byproduct of an inhomogeneous TC record.

A number of modeling studies have considered the impact of increased greenhouse gases on global and/or regional TC activities, using course-resolution global climate models (GCMs) (e.g., Broccoli and Manabe 1990 and Tsutsui 2000), high-resolution atmospheric general circulation models (AGCMs) (Oouchi et al. 2006, Zhao et al. 2009, and Murakami and Wang 2010) and regional models (Walsh et al. 2004, Knutson et al. 2007). There is an emerging consensus in the projected reduction in global TC frequency from these studies. This global reduction is generally attributed to the stabilization of the atmosphere due to warming of the upper troposphere from the greenhouse gas effect (e.g., Knutson and Manabe 1995). A general consensus for an increase in TC intensities has also surfaced among these studies as well. But there is no consensus in the projected changes in regional TC frequency. For the North Atlantic, in particular, some studies report a projected increase (Oouchi et al. 2006, Sugi et al. 2009), while others projected a decrease (Knutson et al. 2007).

The disagreement in projections of regional TC frequency changes may arise from many factors, such as model resolution, forcing data, model physics and parameterizations. In AGCM and regional model simulations, the outcome appears to depend strongly on their forcing data, which is usually a combination of current climate observations and future projections from GCM outputs. Sugi et al. (2009) and Zhao et al. (2009) showed that future projections of regional TC frequency differ according to which GCM is used to create future boundary forcing. An increase of the global mean SST is projected by all of the GCM predictions submitted to the 4th assessment report of the Intergovernmental Panel on Climate Change (IPCC AR4). However, the spatial variations of SST increase vary from model to model, and may be contributing to inconsistent projections of future TC frequency by AGCM and regional model simulations (Sugi et al. 2009 and Zhao et al. 2009). Also, the method of constructing future boundary forcing varies. The majority of modeling studies have adopted a pseudo-global warming approach, whereby future boundary forcing is constructed as the sum of global warming signals (or trends) from GCMs and the time-variation obtained from current observations. The pseudo-global warming approach conserves current climate variability on all timescales (from diurnal to interdecadal), and does not allow for the possibility that this variability may change with global warming. Capturing these variability changes is particularly important in modeling the future change of TC activities since there is a strong relationship between TC genesis and processes across the wide range of spatial and temporal scales (e.g., Marks 2003).

In this study, the full output of a GCM simulation is used to drive the Nested Regional Climate Model (NRCM, Holland et al. 2010) to project future changes of TC

activity in the North Atlantic with increasing greenhouse gases. First, limitations of this approach are identified and discussed. Then, the simulated changes of TC activity are presented. Here, attention is given to the sensitivity of the simulated TC activity change to TC tracking criteria. The simulated large-scale changes from the NRCM are also assessed with respect to changes in explicit TC count. Finally, a comparison of the projected large-scale changes from the NRCM and its forcing GCM is presented to show the deviation of model climate in the NRCM from its forcing data.

4.2 Experimental design and data description

The NRCM is configured in a similar manner to the tropical channel simulation (Chapter III); it has 36km horizontal resolution and 51 vertical levels with the top of the model atmosphere at 10hPa. All physics options are kept the same. The major differences from the tropical channel experiment are the forcing data and the domain setting, which are described in detail below.

The boundary and initial conditions are derived from 6-hourly outputs from the Community Climate System Model version 3 (CCSM, Collins et al. 2006). Three 11-year time slices are chosen for the NRCM simulation: a representation of current climate and two representations of future climate (nominally 2020-2030 and 2045-2055). Boundary forcing for the current climate simulation is derived from the twentieth century realization of CCSM for IPCC AR4. An 11-year time slice was chosen as being sufficiently long to represent the mean state for that period. However, the difference in future and current climate simulation means may reflect natural multidecadal oscillations (such as Atlantic Multidecadal Oscillation) instead of, or as well as, forced climate

change signal. To offset this possibility, three ensembles are made for each of the future simulations. One of the ensembles is forced by A1B scenario, and the other two are forced by the two independent realizations of A2 scenario from the IPCC AR4. The selection of these scenarios is based on the similarity in the greenhouse gas concentration for the time period of study, and the availability of the CCSM data archive at 6-hourly frequency.

The domain extends from the central Pacific (160°W) to the western edge of the Middle East (50°E) in order to allow the NRCM to develop African Easterly Waves (AEWs) (Figure 4.1). There is little AEW forcing to the NRCM at the eastern boundary, because the version of CCSM used in this experiment does not produce waves that are comparable to observed AEW characteristics. Consequently, it is important to allow the NRCM to spin up AEWs internally.

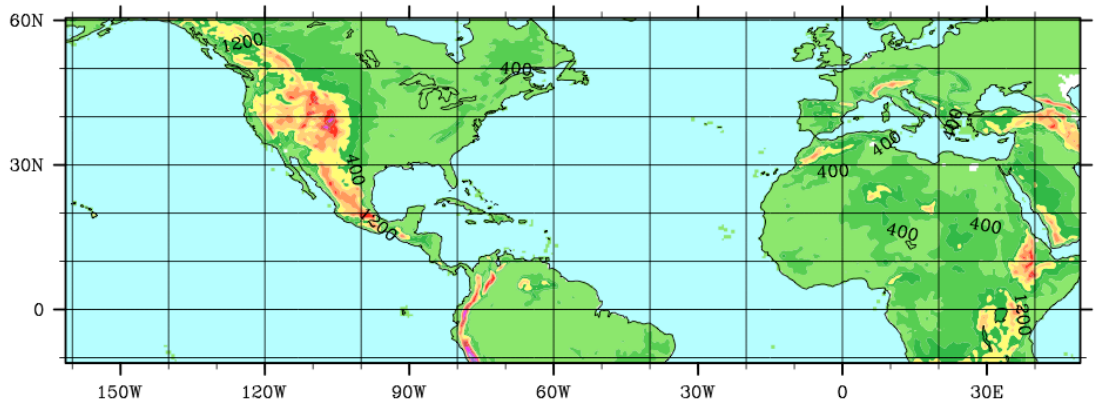

Figure 4.1: Terrain height (in meters) of the NRCM domain for North Atlantic climate change experiment.

Simulated TCs are detected and tracked using the objective TC tracking scheme described in Chapter II. Observed current TC climatology statistics are derived from

International Best Track Archive for Climate Stewardship (IBTrACS, Knapp et al. 2010). To be consistent with the TC tracking criteria, only storms with maximum lifetime intensity of 17 m s^{-1} or greater are considered. Observed current TC climatology comprises of storms from 1975 through 1994 for reasons described in the following section. The current climate large-scale atmospheric statistics are derived from the NCEP/NCAR reanalysis (Kalnay et al. 1996).

4.3 Bias issues

During the course of the simulations, it was found that the NRCM failed to produce a realistic North Atlantic TC climatology due to a high bias in vertical wind shear (Figure 4.2a, also as discussed by Holland et al. 2010 and Bruyere et al. 2010). The high shear bias extends from Caribbean Sea to the Main Development Region (MDR, tropical Atlantic between Caribbean Sea and Africa) with a magnitude exceeding 40 m s^{-1} in the seasonal mean, which is an overestimate of nearly 400% when compared to the current observations (Figure 4.2d). The bias is consistent throughout the simulation periods and evident in all of the ensemble members (not shown). It has been found that the bias originated from the CCSM forcing (Bruyere et al. 2010, Holland et al. 2010) as explained below.

The CCSM exhibits a similar spatial pattern in the seasonal mean vertical wind shear as in the NRCM simulations (Figure 4.2c). The maximum value in the eastern Caribbean Sea is approximately 25 m s^{-1} in the CCSM. This is much less than the NRCM, but still an overestimate when compared to observations. This anomaly high vertical shear is the result of anomalous easterlies in upper troposphere and anomalous

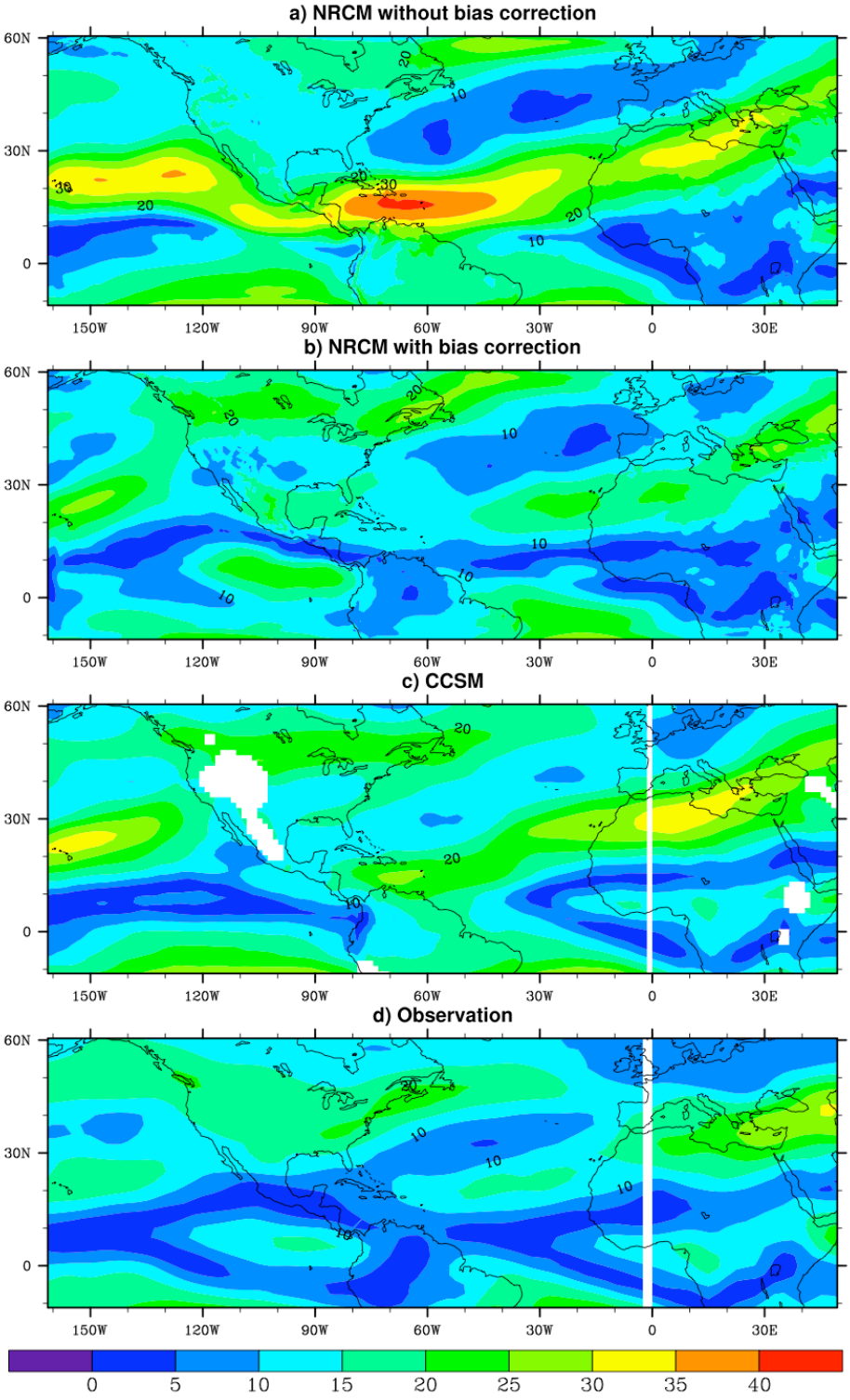

Figure 4.2: Vertical wind shear (vertical difference of winds in m s^{-1} between 850 and 200hPa) averaged for August-October 1996 from a) NRCM simulation with the original CCSM forcing, b) NRCM simulation with bias corrected CCSM forcing, c) original CCSM, and d) observations.

westerlies in lower troposphere (Figure 4.3). This anomalous flow pattern does not appear when the atmospheric component of the CCSM is run with observed SST forcing (not shown), hence ocean coupling seems to play a significant role in producing the biased flow. When the CCSM is run fully coupled with atmosphere and ocean components, the SST exhibits an El Nino-like bias with anomalously high SST in the eastern tropical Pacific, and cold anomaly in the tropical North Atlantic (Figure 4.4), which may be responsible for the biased flow pattern via establishment of stationary Rossby waves in the upper troposphere (Shaman et al. 2009). This SST bias is not unique to the CCSM, but it is a common problem in many of the global coupled climate models (Randall et al. 2007).

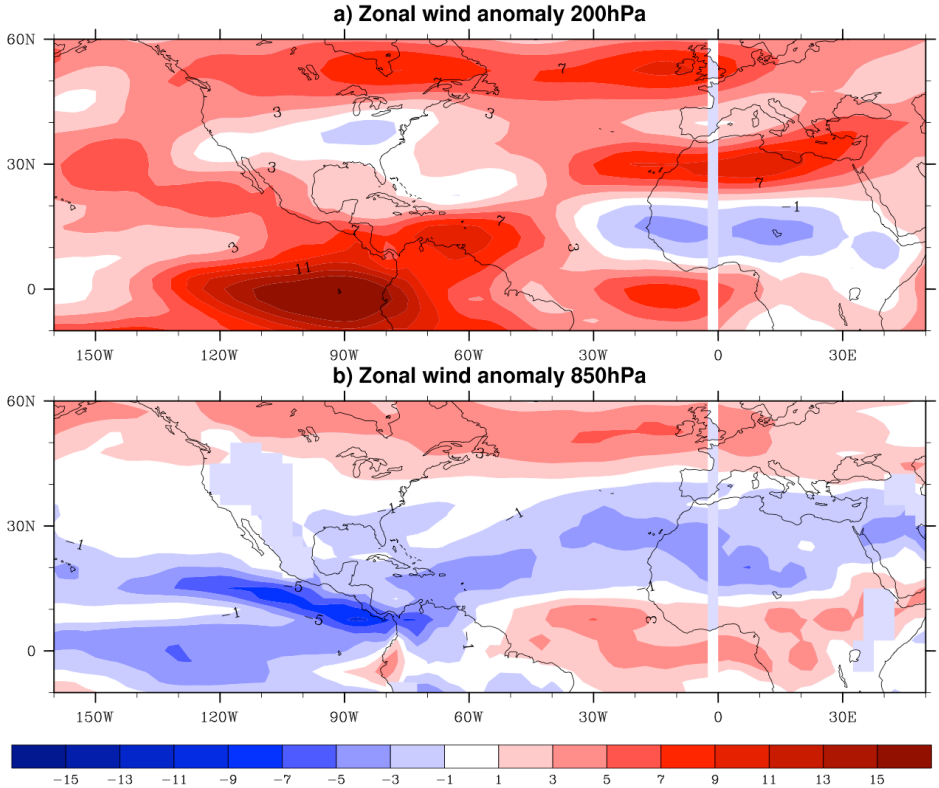

Figure 4.3: Differences (original CCSM minus observations) of zonal winds (in m s^{-1}) averaged for August-October of current climate years (50-year average) at a) 200hPa, and b) 850hPa.

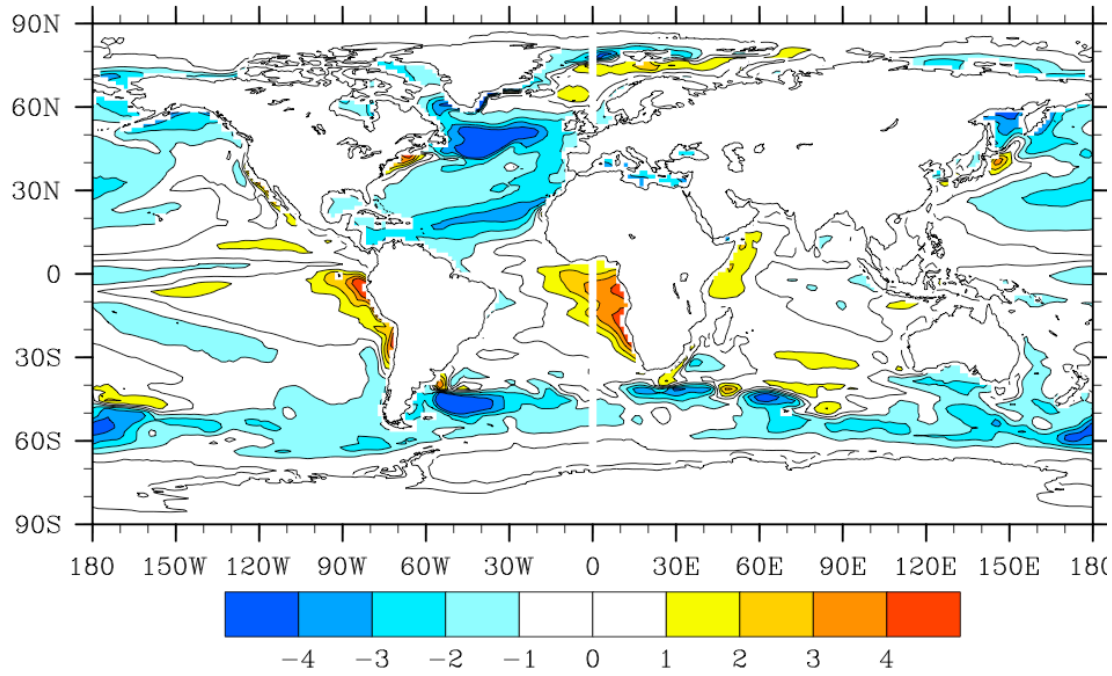

Figure 4.4: Differences (original CCSM minus observations) of SST (K) averaged for August-October of current climate years (50-year average).

Given this result, a simple bias correction method is adopted to remove the biased mean state from CCSM data and replace it with the observed mean state (Bruyere et al 2010, Holland et al 2010). The specific steps of bias correction method are described below:

1) The original 6 hourly CCSM data is separated into the mean seasonal cycle and the residual;

$$CCSM_t = \overline{CCSM_{75-94}} + CCSM'_t$$

where $CCSM_t$ is the original 6 hourly CCSM output at time t, $\overline{CCSM_{75-94}}$ is the mean seasonal cycle derived from 1975-1994 CCSM monthly data linearly interpolated to 6 hourly, and $CCSM'_t$ is the residual. This procedure is

done for time steps in future climate (e.g., 0Z, 1 January 2045). As we are taking out the seasonal cycle derived from 1975-1994 mean, the signal of climate change remains in $CCSM_t'$.

2) 6-hourly NCEP/NCAR reanalysis is separated in the same manner;

$$NNRP_t = \overline{NNRM_{75-94}} + NNRP_t'$$

3) Bias corrected CCSM data are constructed as the sum of the observed seasonal cycle and the residual from CCSM;

$$CCSM_{t,corrected} = \overline{NNRP_{75-94}} + CCSM_t'$$

Note that this procedure simply removes the bias in the CCSM hindcast of seasonally varying mean state relative to observations. This procedure conserves all other variability from the CCSM including diurnal cycle, interannual variability, and climate trends. Climate trends are conserved in that the future mean difference fields calculated from the original and bias corrected data are identical. Bias correction is applied to all atmospheric and oceanic fields in the CCSM data. With this, the El Nino-like anomalous signature is removed from both wind patterns and SST.

The original and bias corrected SSTs are presented in order to provide a visualization of the effect of bias correction. Figure 4.5 shows the annual time series of the original and bias corrected SST at 2.5°S and 85°W, where El Nino-like SST bias is prominent in the original CCSM data. Comparing the two time series, the bias corrected time series is simply shifted down to the observed level for current climate era, and tracks upward in the future climate era with the same rate as in the original CCSM time series.

The NRCM simulations are repeated with the bias corrected CCSM forcing data. The current climate simulation with the bias corrected CCSM forcing shows that the

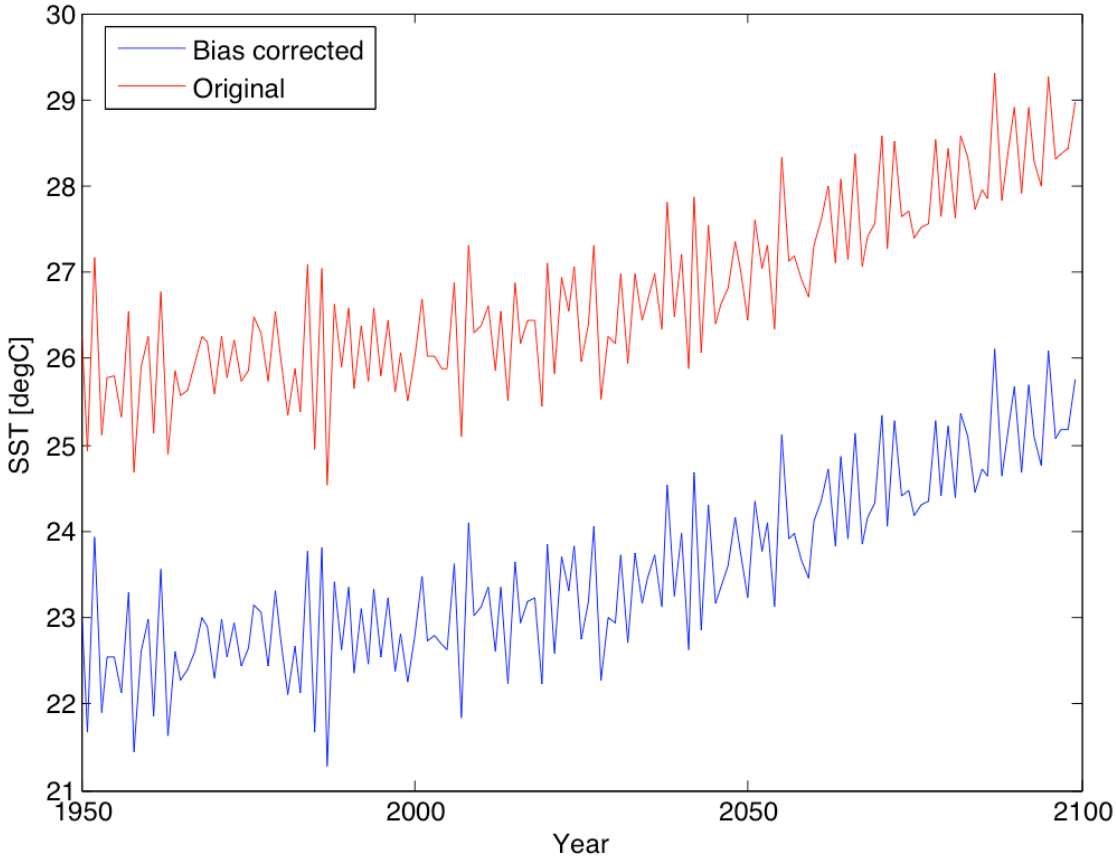

Figure 4.5: Annual time series of the original CCSM (red line) and bias corrected SSTs (blue line) at 2.5ºS, 85ºW.

vertical wind shear bias is significantly reduced (Figure 4.2b) and the TC climatology is simulated realistically in the North Atlantic (Figure 4.6a, b). Note that the time period 1975-1994 represents as the base state for the current climate. Therefore the simulated TC climatology from the current climate simulation will be compared to observations derived from 1975-1994 TC statistics. Owing to computational constraints, only one ensemble is made for each of the future simulations using A2 scenario.

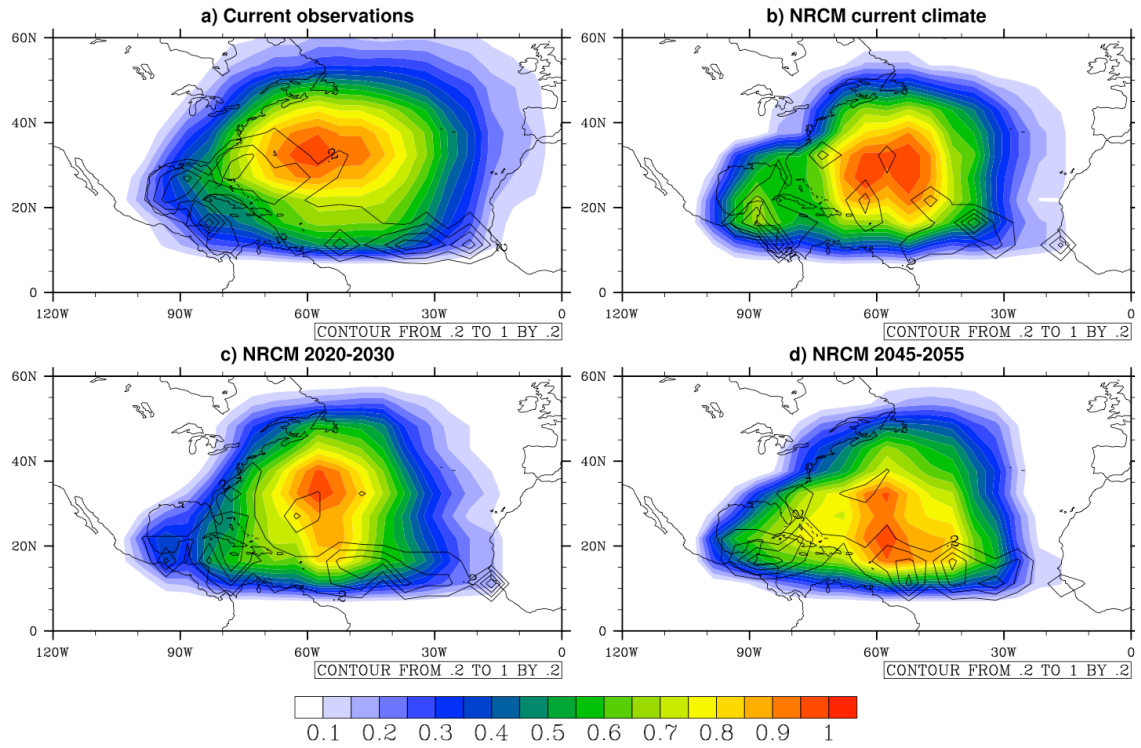

Figure 4.6: Density plots of TC tracks (color contours) and genesis locations (black contours) normalized by the maximum population for a) current climate observations, b) NRCM current climate simulation, c) 2020-2030 simulation, and d) 2045-2055 simulation. Densities are calculated for every 5 degree boxes.

4.4 Simulated TC climatology and future changes

Table 4.1 summarizes various statistics of simulated TC climatology in the NRCM. Average annual frequency for the current climate simulation is 7.6, which is an underestimation when compared to the observed current climate mean of 9.3. Current climate spatial distributions of genesis location and track trajectory are well simulated in the NRCM (Figure 4.6a, b). Seasonality is also well captured with an annual maximum in August through October (Figure 4.7).

Table 4.1: Summary of simulated TC statistics from NRCM. Here STD denotes standard deviation, and Sig.level is statistical significance level of changes from current climate simulation using Student's T-test.

		NRCM current climate	2020-2030	2045-2055
Annual frequency	Mean	7.6	8.5	10.4
	STD	4.1	1.2	4.1
	Sig. level		90%	99%
TC duration (days)	Mean	3.69	4.12	4.14
	STD	5.69	6.43	5.59
	Sig. level		NA	NA
Lifetime max. intensity (m/s)	Mean	29.66	30.37	31.00
	STD	5.04	5.10	5.30
	Sig. level		NA	99%
Radius of max. wind (km)	Mean	122.24	117.25	110.24
	STD	104.64	109.25	104.15
	Sig. level		99%	99%

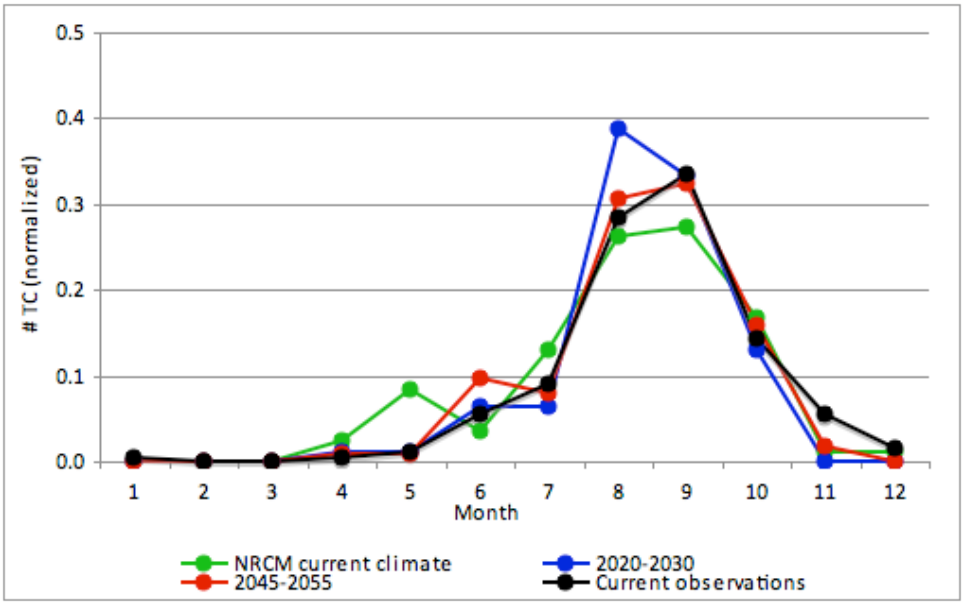

Figure 4.7: Monthly average TC frequency for current climate observation (black), NRCM current climate simulation (green), 2020-2030 simulation (blue), and 2045-2055 simulation (red).

Going into the future, the mean annual TC frequency increases to 8.5 in 2020-2030, and 10.4 in 2045-2055 (Table 4.1). This change is significant at the 90% significance level for 2020-2030, and 99% for 2045-2055. To ensure the robustness of simulated TC frequency increase, two additional sets of simulated TC statistics are constructed using different TC tracking criteria. The intensity and duration criteria are perturbed by observed TC track data resolution (5 knots and 6 hourly, respectively) from the standard 17 m s^{-1}, 48-hours criteria set (see section 2.5). The simulated TC frequency increases in the future for each of these criteria (Figure 4.8). A more detailed examination on interannual time scales is shown in Figure 4.9. The three time series track one another quite well and the interannual variability does not change with tracking criteria, only the net frequency.

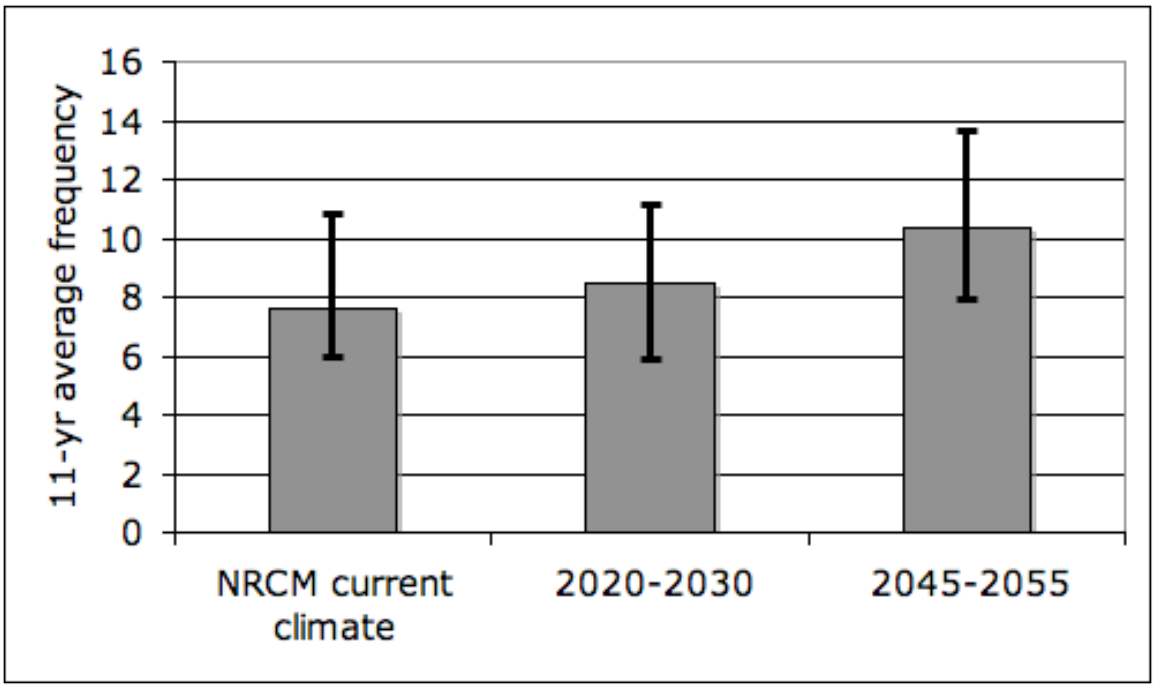

Figure 4.8: Simulated 11-year averaged annual TC frequency from the NRCM using the standard (wind speed = 17 m s^{-1}, duration = 48 hours) TC tracking criteria (gray bars), and their perturbations by altering the wind speed threshold by 2.5 m s^{-1} and the duration by 6 hours in the TC tracking criteria (error bars).

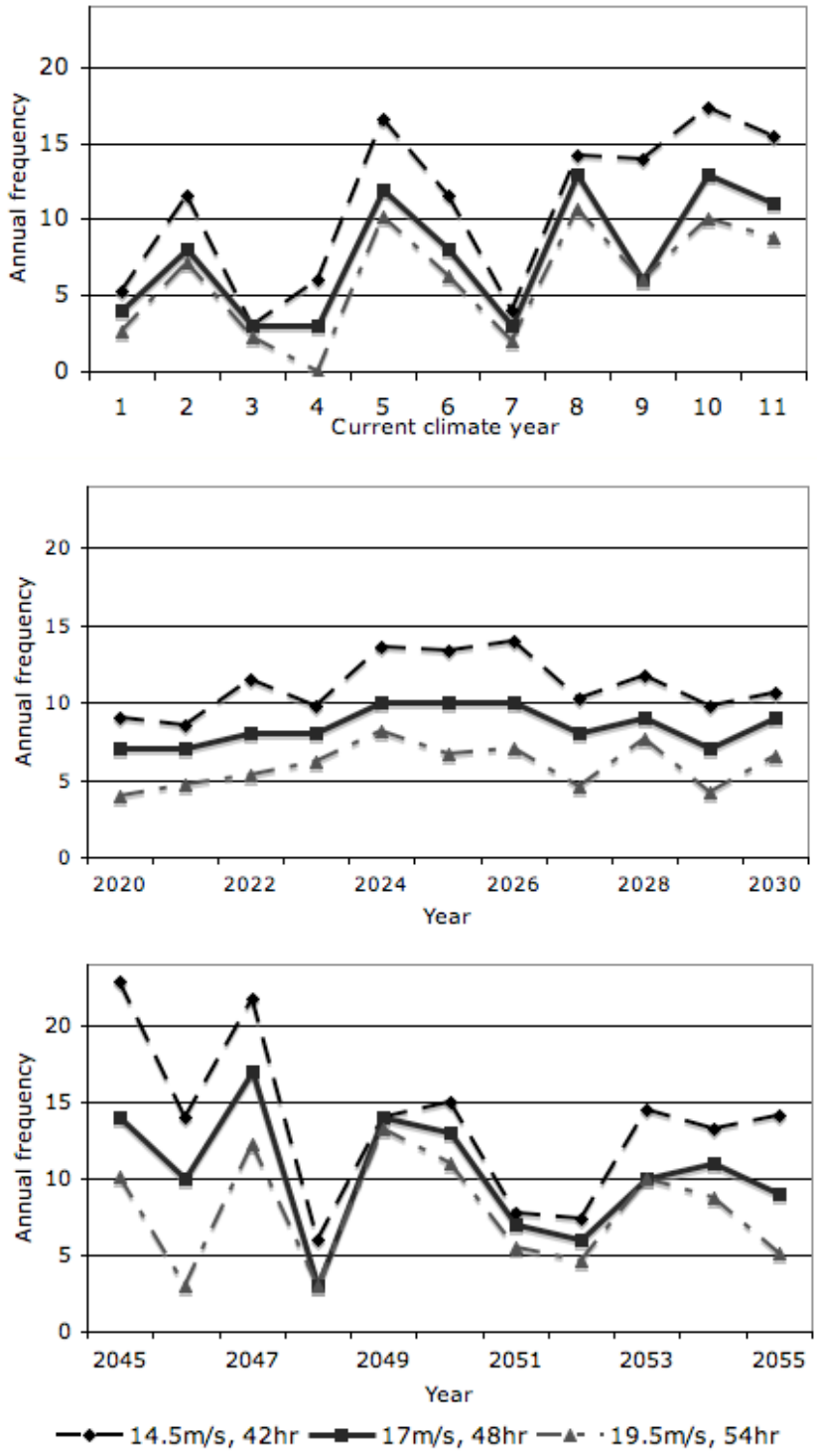

Figure 4.9: Time series of annual TC frequency from three NRCM simulation period using three different TC criteria combinations: standard (wind speed = 17 m s^{-1}, duration = 48 hours) (solid black line), and their puturbasions (dashed black and gray lines) by altering the wind speed threshold by 2.5 m s^{-1} and the duration by 6 hours in the TC tracking criteria.

This analysis suggests that the simulated climate change signal is independent of variations in the tracking criteria. Thus subsequent analysis will focus on TC behavior changes derived from the standard 17 m s^{-1}, 48-hours TC tracking criteria.

Much of the simulated TC frequency increase arises from increases of TC genesis in the MDR, where 11-year average annual TC genesis frequency increases from 2.36 to 5.82, and 6.45 by 2020-2030 and 2045-2055 simulation periods, respectively (Figure 4.10). TC genesis frequency is also increased in Caribbean region, but to a much lesser degree. By 2045-2055 simulation period, TC genesis frequency increases by 173% and 66% in the MDR and the Caribbean, respectively. As proportionally more TC genesis occurs in the MDR in future simulation periods, the mean track duration and lifetime

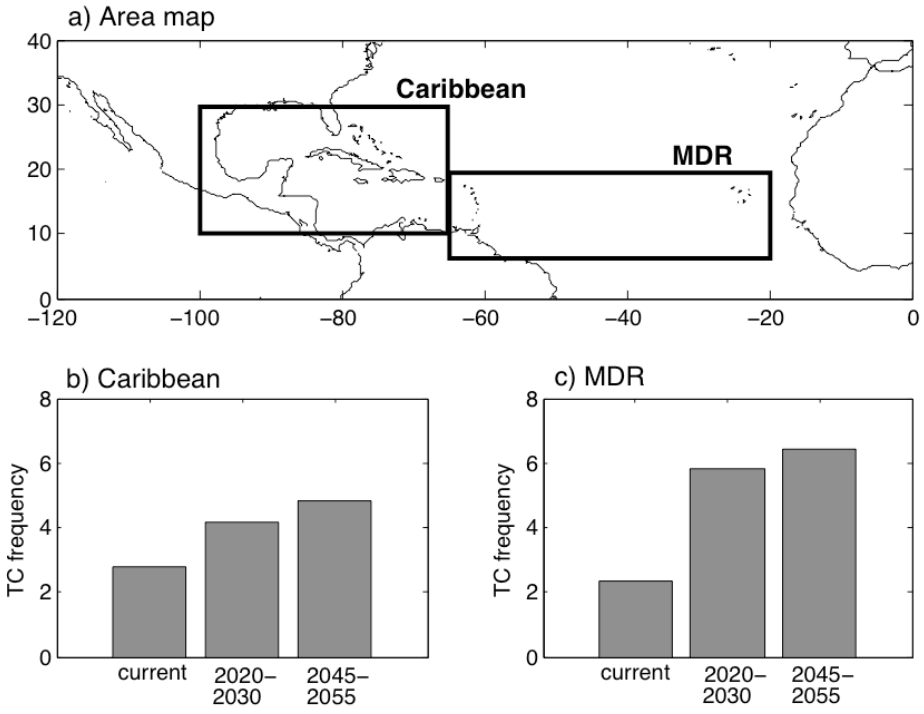

Figure 4.10: Simulated 11-year mean TC genesis frequency for b) Caribbean and c) MDR. Thick black boxes in a) indicate boundaries for each regions.

maximum intensities also increase (Table 4.1). The duration increase is not statistically significant, but the increase of lifetime maximum intensity from 29.7 m s^{-1} in current climate to 31.0 m s^{-1} in 2045-2055 is significant at 99%. The boxplots of the simulated TC lifetime intensity indicate that the most intense storms are projected to become more intense in the future climate (Figure 4.11). The median values are also projected to increase, indicating a shift of the intensity probability distributions to higher intensities. However, the simulated intensity is capped at approximately 40 m s^{-1} owing to the limited resolution. Changes to intense storms will be assessed in Chapter V by utilizing extreme value theory.

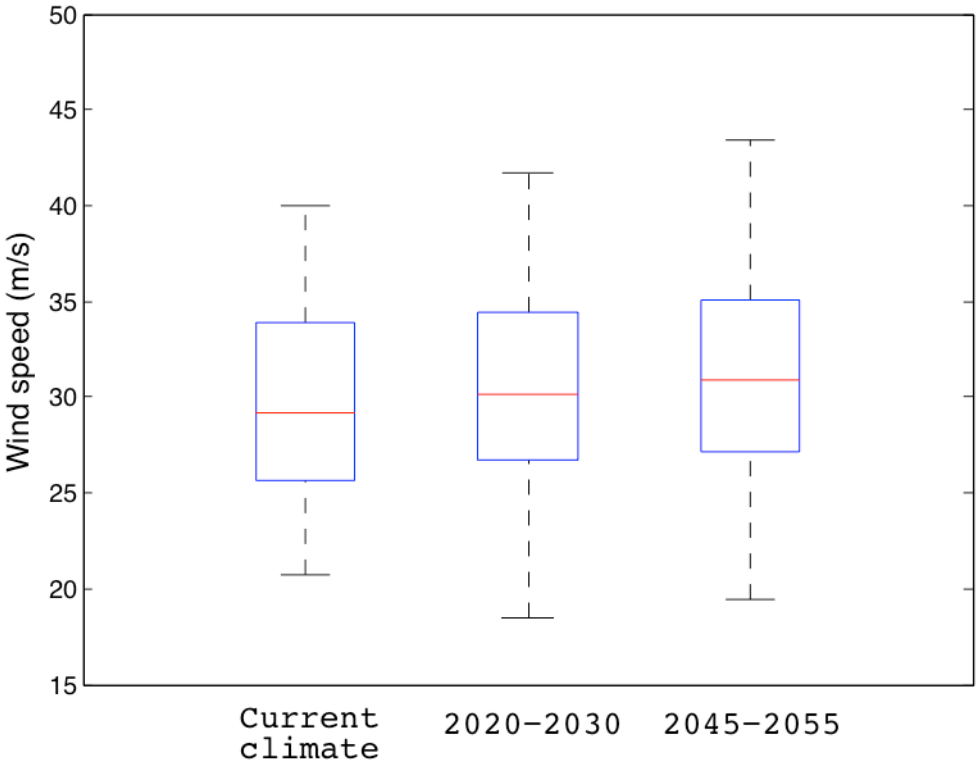

Figure 4.11: Boxplots of TC lifetime maximum intensity for thre three NRCM simulation periods. Red line is median, edges of box are 25th and 75th percentiles. Whiskers indicate the extent of the most extreme data points.

The mean storm size (measured as the radius of maximum wind) decreases for both future runs and is statistically significant at 99% (Table 4.1). There is no significant change in seasonality (Figure 4.7). The mean location of storms reaching their lifetime maximum intensity occurs in the Gulf of Mexico in the current climate simulation, consistent with observations (Figure 4.12). The mean location moves to the east of Florida in 2020-2030 simulation, and returns to the Gulf in the 2045-2055 simulation, implying a multi-decadal oscillation. A similar multi-decadal signature is also seen in the variance of TC frequency (Table 4.1). The source of these decadal variations is not known.

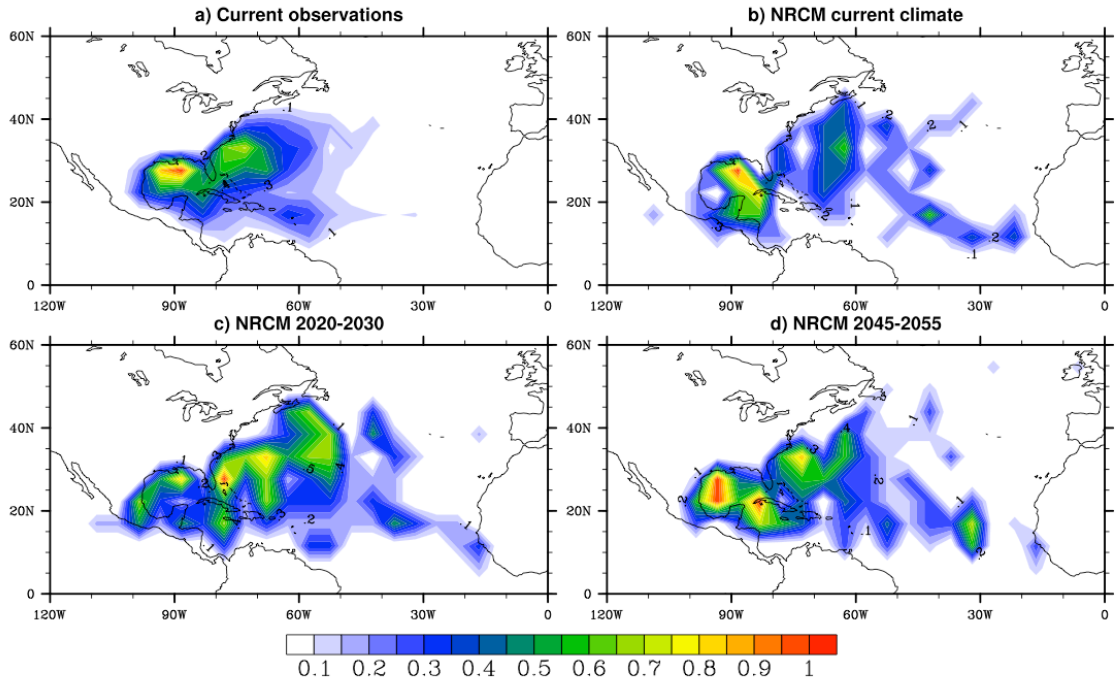

Figure 4.12: Density plots of locations of TCs reaching their lifetime maximum intensity for a) current observations, b) NRCM current climate, c) 2020-2030, and d) 2045-2055 simulations. Densities are calculated for every 5 degree boxes, and are normalized by the maximum population.

Another source of uncertainty is the model's internal variability (or sensitivity to initial conditions). Using the same model configurations and bias corrected CCSM data, an estimate of NRCM's model internal variability was made by a 10-member ensemble generated by varying the model start date between 1st January 2047 and 1st April 2047, and running each member through 1st December 2047(data provided by James Done, personal communication). The standard (17 m s^{-1}, 48-hours) TC tracking criteria are used to extract number of simulated TCs for hurricane season from each of the ensemble members. The resulting simulated TC frequency ranges from 13 to 20 storms per year, similar to that from varying the tracking criteria (Figure 4.9c). This shows a stochastic nature of TC formation, and that a single realization of a hurricane season by the model is not deterministic. What this implies to the future projection of TC activity is not known, and is being investigated further in a separate study.

4.5 Large-scale environment assessment

The simulated changes in large-scale environment by the NRCM are assessed in a search of reasons behind the simulated TC activity changes. A focus will be given to changes in the MDR because TC genesis increase in this region is responsible for much of the overall increase of North Atlantic TC frequency in the NRCM.

After Gray (1968), five environmental factors that are known to modulate TC climatology are assessed: SST; vertical wind shear measured as the total wind difference (using both zonal and meridional winds) between 200 and 850hPa; 700hPa relative humidity; moist inertial stability (measured as the difference of equivalent potential temperature from the surface to 600hPa, positive change indicates destabilization); and

850hPa zonal wind fields as representative of the large-scale circulation. Only mean changes of 2045-2055 from current climate simulation are presented in the subsequent assessment, as general characteristics of changes for 2020-2030 are similar except that the magnitude of the changes are smaller.

SST forcing is fixed to those from CCSM as a one-way coupled boundary forcing. Therefore, we examine future SST changes predicted by CCSM. The August-October averaged SST is increased everywhere in the North Atlantic (Figure 4.13a) by a minimum of 0.5K. The SST increase is particularly elevated in the MDR. The collocation of elevated SST and TC genesis frequency increase is in agreement with the observed relationship of increasing trends between local SST and TC genesis (Emanuel 2005, Hoyos et al. 2005, Webster et al. 2005, Holland and Webster 2006, Saunders and Lea 2008). Meanwhile, the North Atlantic SST changes relative to the global tropical mean has been suggested as important for the general activity of North Atlantic TCs. A relative warming of the MDR SST may modulate TC genesis by two distinctive forms of teleconnection patterns; in longitudinal direction via El Nino Southern Oscillation (ENSO) like pattern (Gray 1984, Vecchi and Solden 2007, Swanson 2008, Wu et al. 2010), and in meridional direction via Atlantic Meridional Mode (AMM) like pattern (Gu and Adler 2009, Kossin and Vimont 2007). The ENSO-like teleconnection pattern stems from an increase of the tropical Atlantic SST relative to the tropical Pacific Ocean, which induces a shift in Walker circulation creating more favorable large-scale environment in the MDR for TC genesis by reducing wind shear, enhancing upward motion, and destabilizing troposphere (Gray 1984, Shapiro 1987). The AMM-like teleconnection is induced by inhomogeneous SST changes in meridional direction, which creates TC-

favoring environment in the MDR by a northward shift of the Atlantic Inter-Tropical Convergence Zone (ITCZ) during the positive phase of AMM (Nobre and Shukla 1996, Kossin and Vimont 2007, Gu and Adler 2009). In our simulations, the SST gradient change is more prominent in meridional direction compared to longitudinal direction (Figure 4.13b). Therefore the AMM-like teleconnection pattern may have contributed to the simulated increase of TC genesis in the MDR more than the ENSO-like pattern.

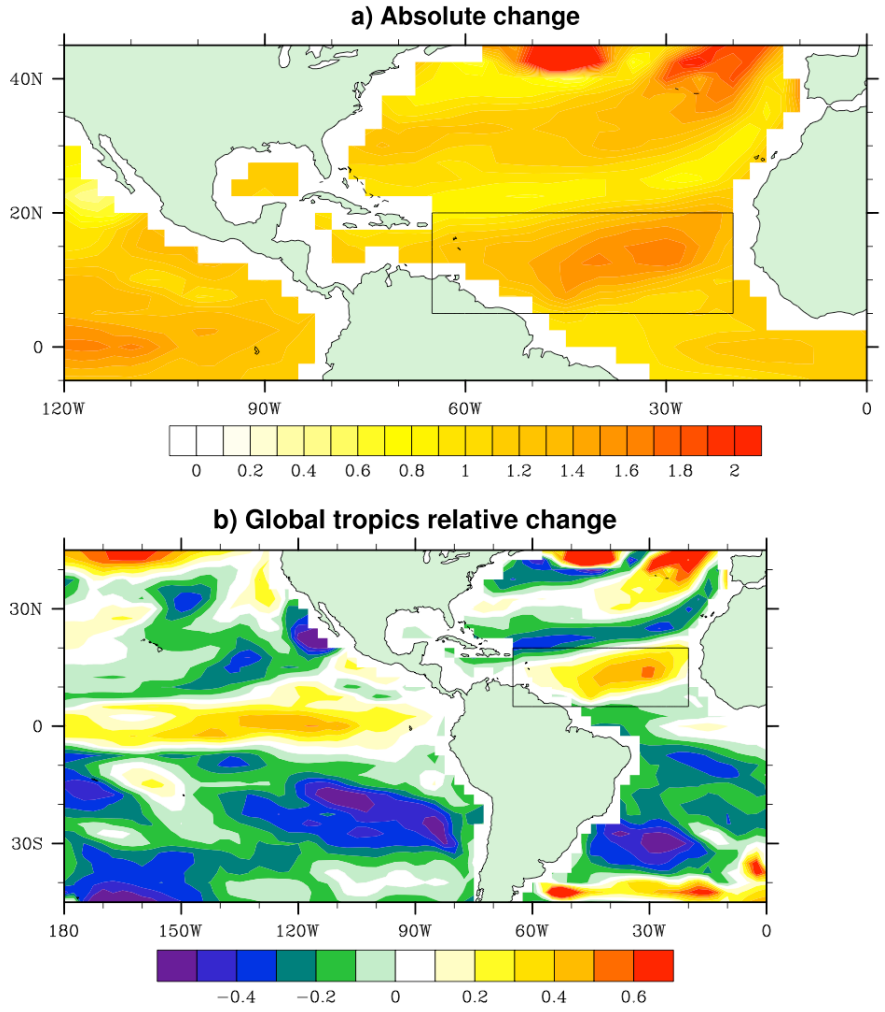

Figure 4.13: Future SST as projected by the CCSM for 2045-2055 period compared to the current climate mean; a) mean absolute change (K), and b) relative to global tropical (20˚S-20˚N) mean change (K). Black box indicates the area where TC genesis increased in the NRCM simulation.

The previous conclusion is further assessed by examining the simulated mean changes in the large-scale atmospheric conditions from the NRCM (Figure 4.14). Precipitation change indicates a northward shift of ITCZ with the longitudinally elongated area of decreased precipitation along 5°N latitude line and increased precipitation in 10-20°N latitudes in the tropical Atlantic. Anomalous southerly to southwesterly winds in this area are also a characteristic anomaly seen during the positive phase of AMM, favoring a northward shift of ITCZ. Simulated changes in other environmental variables are also towards more favorable for TC genesis in MDR: Vertical shear reduced by approximately 5 m s^{-1}, relative humidity increased by ~5%, and moist inertial stability decreased. These changes, combined with the meridionally inhomogeneous SST changes noted earlier, hint at an association with the simulated environmental changes to the AMM-like teleconnection pattern.

A free-running regional climate model develops its own internal climatology (Giorgi and Mearns 1999, and Miguiez-Macho et al. 2005). Therefore, a comparison of simulated changes of large-scale environment from the NRCM and the CCSM is also presented. This comparison will allow us to examine the consistency between two forms of downscale techniques to infer TC activity from a coarse resolution GCM results; a statistical downscale whereby TC activity and large-scale environmental factors are statistically related (e.g., Camargo et al 2007, Zhang et al. 2010), and a dynamical downscale using a numerical model such as the one presented in this study.

Figure 4.15, together with Figure 4.14, compares the simulated large-scale environmental changes from the NRCM and the CCSM, respectively. In the CCSM, large-scale changes also favor TC genesis in the MDR. Therefore, the statistical

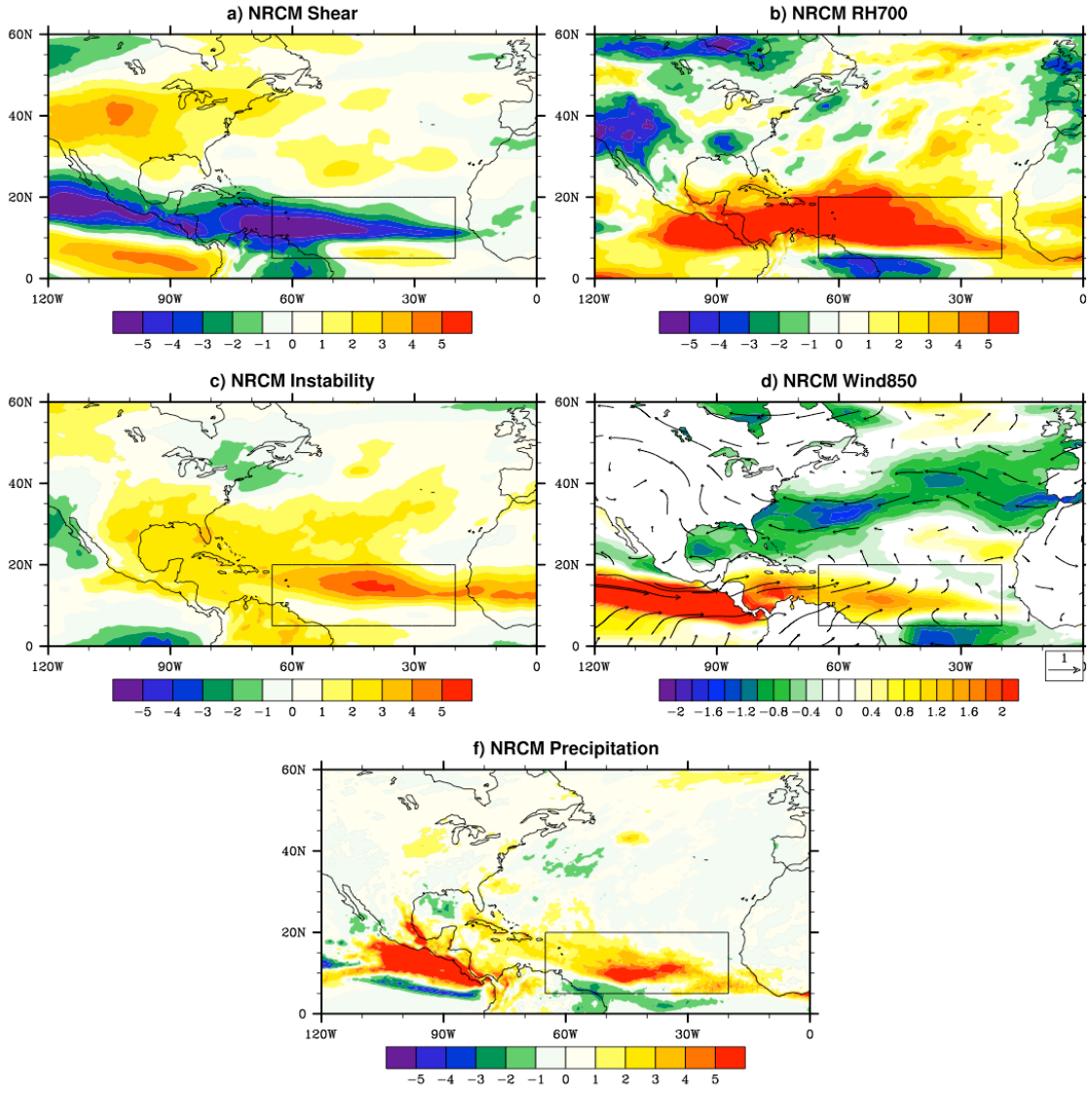

Figure 4.14: Simulated future mean changes for 2045-2055 simulation period compared to current climate simulation by the NRCM: a) vertical wind shear (m s^{-1}), b) relative humidity at 700hPa (percent), c) moist inertial stability (K), d) zonal wind speed (color contours, m s^{-1}) and wind vector, and d) precipitation (mm per month). Black box indicates the area where TC genesis increased in the NRCM simulation.

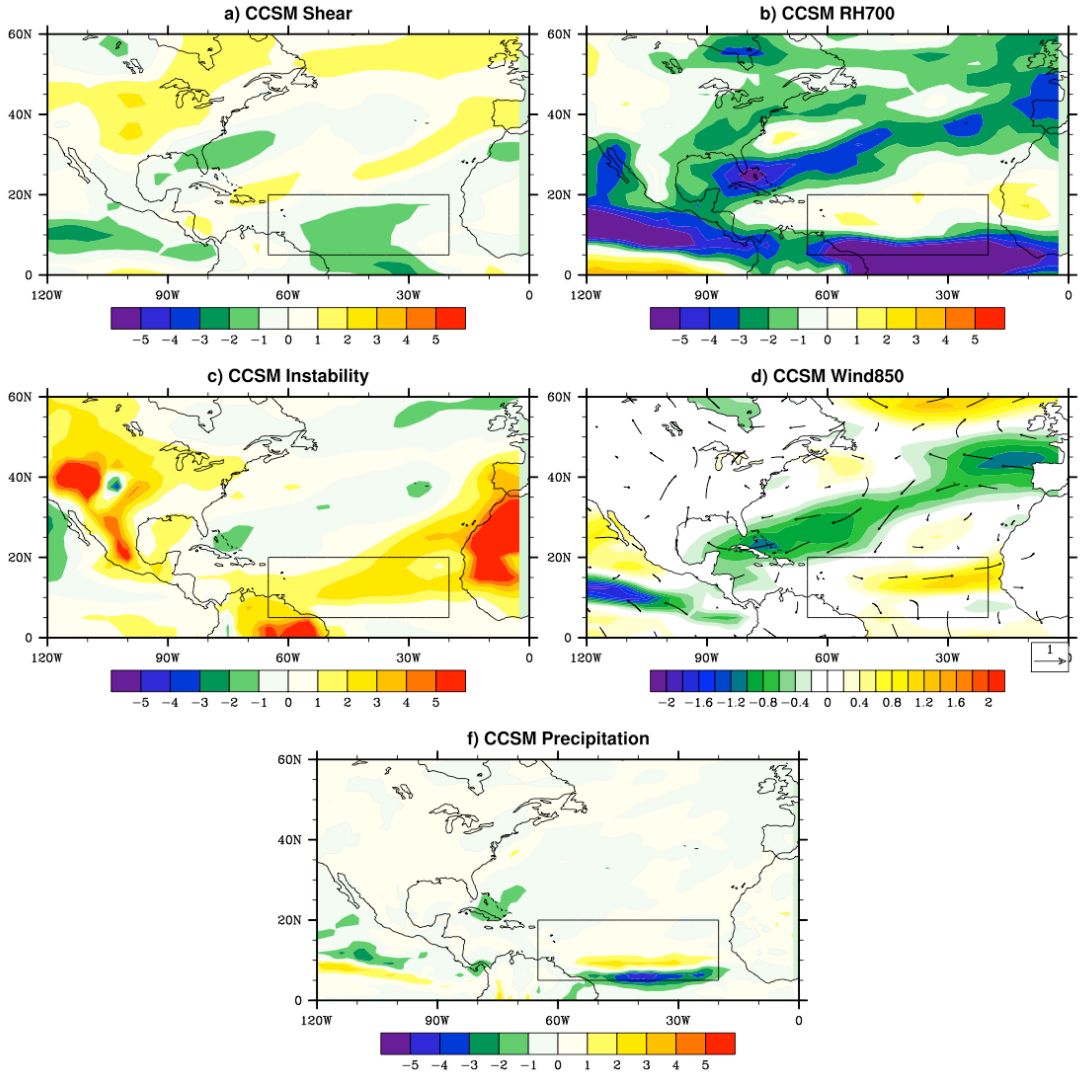

Figure 4.15: Similar to Figure 4.14, but for the CCSM.

downscaling would also indicate an increases in the MDR TC genesis, and would be consistent with the results from dynamical downscaling. However, the magnitudes and the spatial patterns of the changes are vastly different from the NRCM. In both of the models, a northward shift of the ITCZ is indicated by the spatial pattern of precipitation changes, yet the magnitude the precipitation changes is substantially less in the CCSM. In

the NRCM, the area of TC-favoring changes extends to the Caribbean region in the NRCM. In contrast, the area of TC-favoring changes is largely confined within the deep tropical Atlantic in the CCSM. The difference in such spatial patterns between the two models suggests that the driving factors behind the simulated large-scale environment may be different in the two models.

4.6 Summary and discussion

Potential future changes of North Atlantic TC activity with increasing greenhouse gases are simulated by the NRCM, a one-way interactive system model of the ARW and the CCSM. Three 11-year simulations are completed; one for current climate and two future periods (2020-2030 and 2045-2055) using the IPCC AR4 A2 scenario. In contrast with the pseudo-global warming experimental design adopted by many past studies, the CCSM output is used directly as the forcing for the ARW conserving all variabilities and trends from the CCSM.

An El Nino-like SST bias in the CCSM induced anomalously high vertical wind shear over the tropical North Atlantic with marked impact on cyclone development in the NRCM. A bias correction method was applied to remove the seasonally varying base state from the CCSM data for both current and future climates, and the base state was replaced with that of observations. With this approach, all variabilities are conserved from the CCSM.

The simulation results indicate that North Atlantic TC frequency, intensity, and duration will increase under IPCC AR4 A2 scenario. The frequency increase is robust to the use of different TC tracking criteria and is dominated by a large increase in TC

genesis in the MDR. This also leads to a longer mean TC duration and intensity increase as TCs spend more time over the warm ocean. These simulated changes in TC activity are robust in both future runs (2020-2030 and 2045-2055). There is a sign of multi-decadal oscillation in the location of TCs reaching their lifetime maximum intensities, and standard deviation of annual TC frequency over the three 11-year simulation periods. Such signs of decadal variations make it difficult to be explicit on the future changes. It is not yet known how the decadal variations arise. We also presented the stochastic response of TC formations to the model's internal variability, though its pertinence to the future projections has yet to be explored.

Consistent with the simulated TC frequency change, environmental conditions known to modulate TC activity to the NRCM predicts a movement towards more favorable conditions in the NRCM. These include: reduced vertical wind, increased low-tropospheric moisture and increased moist instability over the MDR. It is suggested these large-scale changes are a response to the simulated spatially inhomogeneous SST increase. The simulated future change of SST also resembles that of the positive phase of AMM, which shifts Atlantic ITCZ northward and makes the large-scale environment more favorable for TC genesis in the MDR. Increasing favorability in the large-scale environment of the MDR is also seen in the CCSM. But the magnitude and spatial patterns are different from the NRCM. This provides an insight to the merit of using dynamical downscaling over large domains not only in the explicit prediction of TC activity changes but also in changes to the large scales.

CHAPTER V

STATISTICAL MODELING OF TROPICAL CYCLONE INTENSITY

5.1 Background

In the North Atlantic climate change experiment (Chapter IV), the Nested Regional Climate Model (NRCM) projected an increase of mean TC intensity under increasing greenhouse gas concentrations (Table 5.1 and Figure 5.1). However, explicit projection of changes in intense storms (Category 3+, maximum lifetime wind speed greater than 50 m s^{-1}) was not possible due to the limited horizontal resolution.

The inability of simulating intense storms is a universal limitation in what are commonly referred to as "high-resolution" (horizontal grid resolution less than 50 km) models. Bender et al. (2010) rendered this limitation by further downscaling each of the simulated TCs in their regional model with a very high-resolution hurricane model and extrapolated the TC intensity projection to Category 5. However, this approach is computationally expensive. Alternatively, one may extrapolate the TC intensity

Table 5.1: Mean and variance of maximum lifetime TC wind speed (m s^{-1}) from current climate observation (using 1985-2008 data), and from NRCM simulations. Also shown is the simulated future % change of mean and variance of TC wind speed calculated as difference between future NRCM runs (2020-2030 and 2045-2055) and current climate run.

	Original		% change from 1995-2005	
	mean	variance	mean	variance
Current climate observations	37.00	158.32		
NRCM current climate	29.62	25.43		
NRCM 2020-2030	30.37	26.01	2.54	2.31
NRCM 2045-2055	31.00	28.12	4.67	10.59

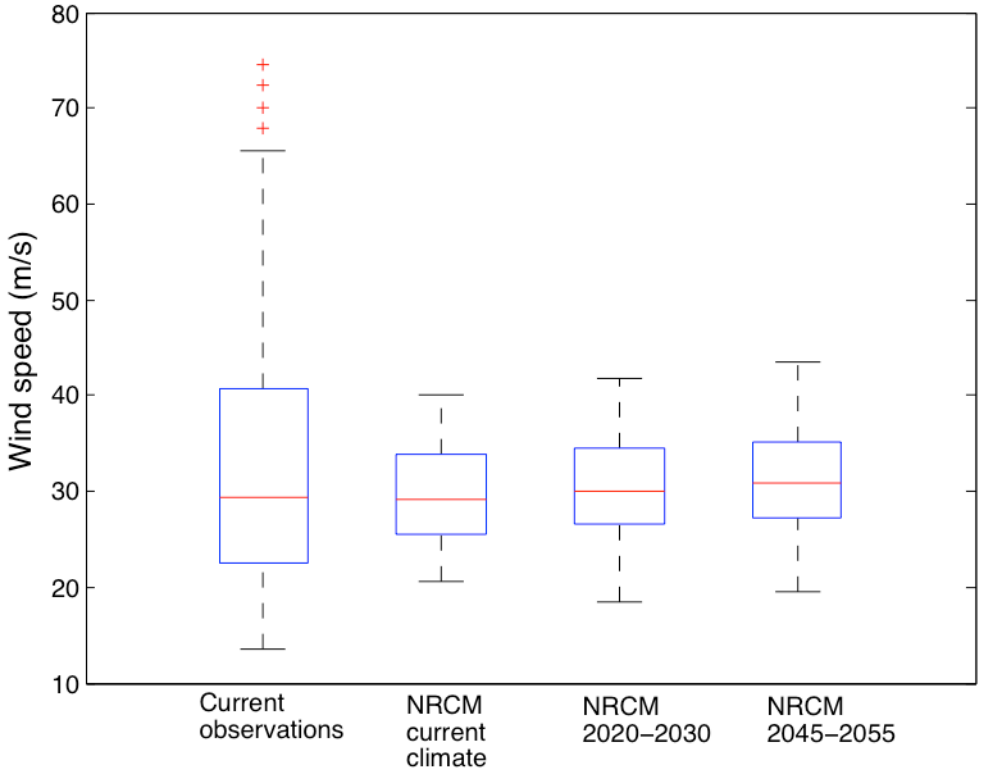

Figure 5.1: Boxplots of TC maximum lifetime wind speed (m s^{-1}) from the NRCM simulations and the current climate observations. Red line is median, edges of box are 25th and 75th percentiles. Whiskers indicate the extent of data range, and red plus signs are outliers.

projection from a limited resolution model statistically, which is the approach presented here.

The inability of simulating intense storms by the NRCM cannot be treatable with commonly used bias correction methods (such as rank order swapping or quantile-to-quantile mapping) for reasons described below. As shown in Figure 5.1, the shape of the probability distribution of the simulated TC intensity from the NRCM is normal-like (i.e., symmetric about the mean), whereas the observed distribution is skewed. The difference in the distribution shapes stem from the truncation of TC intensity in the NRCM. This

truncation occurs at both extremities: the TC tracking method does not locate low-intensity systems below tropical cyclone strength (Chapter II), and the higher intensities are prevented by the course-resolution not being able to develop the strong associated gradients. The model also has a tendency to overestimate the intensities of weak storms (maximum wind speed < 33 m s^{-1}, Chapter III). Intense storms are *truncated* rather than *missing* because the simulated annual frequency of TCs in the NRCM is comparable to observations. That is, those storms that are in environments supportive of Category 3+ storms were restricted to weaker intensities because at 36km grid spacing the NRCM was incapable of resolving the necessary sharp gradients for more intense storms. Thus in order to assess the future changes in intense storms, we need to estimate the proportion of simulated storms that would have become Category 3+ intensity given sufficient resolution. However, such an estimate is not readily attainable. A simple bias correction method that involves rank order swapping would conserve the original distribution shape and does not extract the truncated intensities.

An alternative approach is to reflect the simulated changes in mean and variance of TC intensity to the observed current climate TC intensity (e.g., Holland 2010) and this is the approach adopted here. This approach requires a statistical model of the observed current climate TC intensity. To this end, we use extreme value theory and model the TC intensity probability distribution function (PDF) using the generalized Pareto distribution (GPD). A brief description of extreme value theory will be given followed by the definition of GPD and an explanation of why GPD is chosen as a statistical model of TC intensity in this study. Then, the simulated overall TC intensity changes from the NRCM

are applied to the GPD-modeled TC intensity to project the future changes in intense storms. A discussion of underlying assumptions in our approach is also given.

5.2 Data description

For simplicity, TC lifetime maximum wind speed is used as the measure of TC intensity. Six-hourly wind measurements could be used instead but here the interest is in changes to lifetime maxima. Simulated TC intensities come from the NRCM North Atlantic climate change experiment (Chapter IV). For convenience, these are referred to as "simulated" intensity, while those obtained by statistical modeling are referred to as "statistically modeled" intensity. The observed current climate TC intensity is derived from the International Best Track Archive for Climate Stewardship (IBTrACs, Knapp et al. 2010) over the period 1975-2005. All North Atlantic tracks archived in the IBTrACs are used, which includes subtropical storms, tropical storms and hurricanes. This yields 375 tracks, and their maximum lifetime intensities range from 13.6 to 74.6 m s^{-1}.

5.3 Extreme value theory and its application to modeling TC intensities

Statistical modeling provides a means of obtaining a continuous distribution of a particular object of study whose dynamically derived theoretical distribution is not known. In many cases, a statistical model is chosen based on the nature of a particular object of study using its discrete data, such as the mean and shape of the PDF. Once a model is fitted to the discrete data, the "goodness-of-fit" is tested to confirm that the selected model is indeed an appropriate choice.

In addition to the goodness-of-fit assessment, there are theories that can be used to help decide which distribution family may be an appropriate statistical model for a particular object of study. For example, the central limit theory states that if mean values from sets of random variables having a common distribution function are collected, then the behavior of these collected data can be modeled by a normal distribution. Similarly, extreme value theory states that a collection of extreme values from sets of random variables having a common distribution function follow one of a small number of extreme-value type distributions. Such distributions include the generalized extreme value (GEV) distribution, and the generalized Pareto distribution (GPD). Maximum lifetime intensity of TC can be viewed as the extreme end of wind speed measurements of all tropical convective disturbances, which includes a large number of systems weaker than tropical cyclone strength (Figure 5.2). In this framework, it is relevant to adopt extreme value theory in modeling of TC intensity. Past studies have adopted extreme value theory to model TC intensities but in a different framework (Simiu et al. 1996, Coles and Casson 1998, Jagger and Elsner 2006), in that only annual maximum intensities are modeled. In their framework, the parent sample is the annual record of TC intensities. The originality of the current study is to treat intensities of all tropical convective disturbances as the parent sample. Either frameworks are valid in adopting extreme value theory as the basis to model TC intensities, as explained further below.

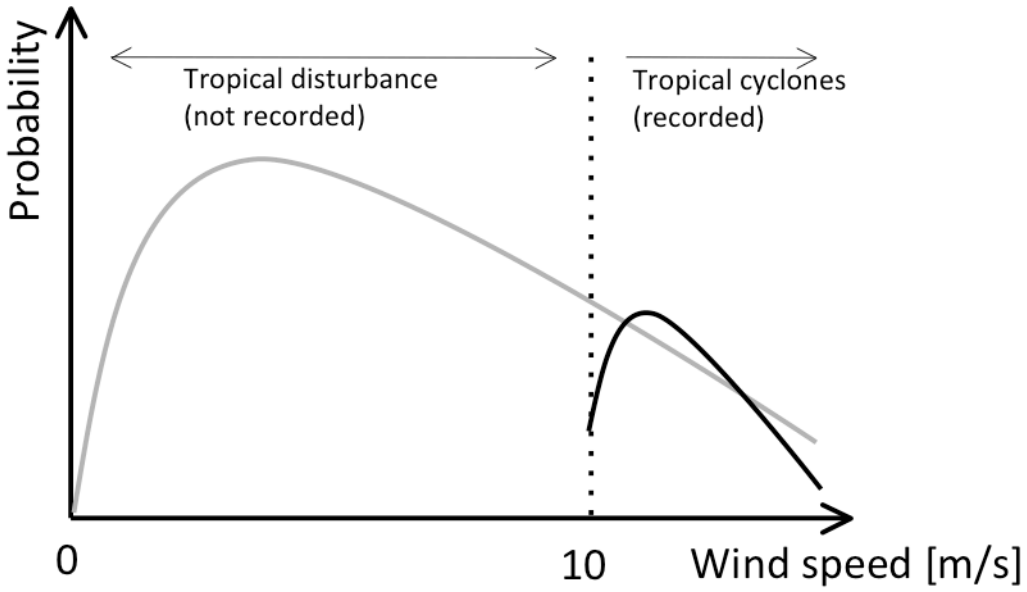

Figure 5.2: Hypothetical probability functions of lifetime maximum wind speed of tropical disturbances (gray line) and tropical cyclones (black).

Here we present a brief description of extreme value theory attained to GEV and GPD adopted from Coles (2001);

Let $x_n = \{X_1, X_2, ..., X_n\}$, be a sample of independent identically distributed (iid) variables with size n from a common distribution function F, and let $M_n = \max(x_n)$. Then,

$$\Pr\{M_n \leq z\} \rightarrow G(z) \text{ as } n \rightarrow \infty.$$

where

$$G(z) = \exp\left\{-\left[1 + \xi\left(\frac{z-\mu}{\sigma}\right)\right]^{-1/\xi}\right\} \qquad \text{- (1)}$$

for some $\mu, \sigma > 0$ and ξ. Here $G(z)$ is the cumulative distribution function of GEV family of distributions. GEV has three parameters: scale parameter σ, shape parameter ξ, and

location parameter μ. Further, for large enough u, the distribution function of threshold excess $(X - u)$, is approximated as

$$H(y) = 1 - \left(1 + \frac{\xi y}{\sigma'}\right)^{-1/\xi} \qquad \text{- (2)}$$

conditional on $X > u$ and defined on $\{y : y > 0 \ \ and \ \ (1 + \xi y / \sigma') > 0\}$, where

$$\sigma' = \sigma + \xi(u - \mu) \qquad \text{- (3)}$$

Here $H(y)$ is the cumulative distribution function of the GPD.

Note that GEV is a model for describing maximum values, whereas GPD is a model for describing threshold excess and individual extreme events. GEV is useful in cases where only maximum values are available (e.g., annual maximum). GPD is appropriate in instances where available data exceed a certain threshold. The measurements of TC intensity fit the latter category, as they are recorded only when they exceed tropical storm strength.

A notable advantage of GPD is that the mean and variance of GPD are direct functions of GPD parameters;

$$mean = u + \frac{\sigma'}{1 - \xi} \qquad \text{- (4)}$$

$$\text{var} = \frac{\sigma'^2}{(1 - \xi)^2 (1 - 2\xi)} \qquad \text{- (5)}$$

and this enables explicit calculation of the future GPD parameters based on the simulated mean and variance changes from the NRCM and the GPD parameters of current climate observations.

5.4 Modeling procedure and results

The specific procedure for assessing the future TC intensity using GPD is as follows. First a GPD is fitted to the current climate observed TC data for the North Atlantic 1975-2005 period. GPD parameters are estimated using the Maximum Likelihood Estimate (MLE). The GPD mean and variance for current climate observations are calculated using eq. (4) and (5) from the MLE of GPD parameters. Then the percentage changes of the simulated TC intensity mean and variance changes from the NRCM (Table 5.1) are multiplied by the GPD mean and variance to yield the projected future GPD mean and variance. From the resulting GPD mean and variance, the future GPD parameters are calculated from eq. (4) and (5). Then future TC intensity distribution is reconstructed with these future GPD parameters.

Fitting of the GPD requires the selection of threshold u that it is sufficiently high to ensure the extreme value assumption is not violated, but it also minimizes the sensitivity to the estimates of shape and scale parameters (Cole 2001). If the GPD is a good fit to the data, then there exists a threshold u_o such that for any $u < u_o$ the MLE of shape and scale parameters remains constant. An optimal value for u_o can therefore be determined by plotting u against the MLE of either shape or scale parameter. Here we examine the sensitivity of the shape parameter MLE, ξ, by varying u (Figure 5.3). The MLE of ξ is relatively constant for u <25 m s^{-1}, implying that the sensitivity of u to the MLE of ξ grows rapidly after this point. To pinpoint the optimum value of u further, quantile-quantile (Q-Q) plots of the observed and modeled TC intensities are made for $17 \leq u \leq 25$ (Figure 5.4). Here, the linearity in a Q-Q plot suggests that the discrete raw data is well modeled with GPD. In all cases the linearity in Q-Q plot is quite strong, which

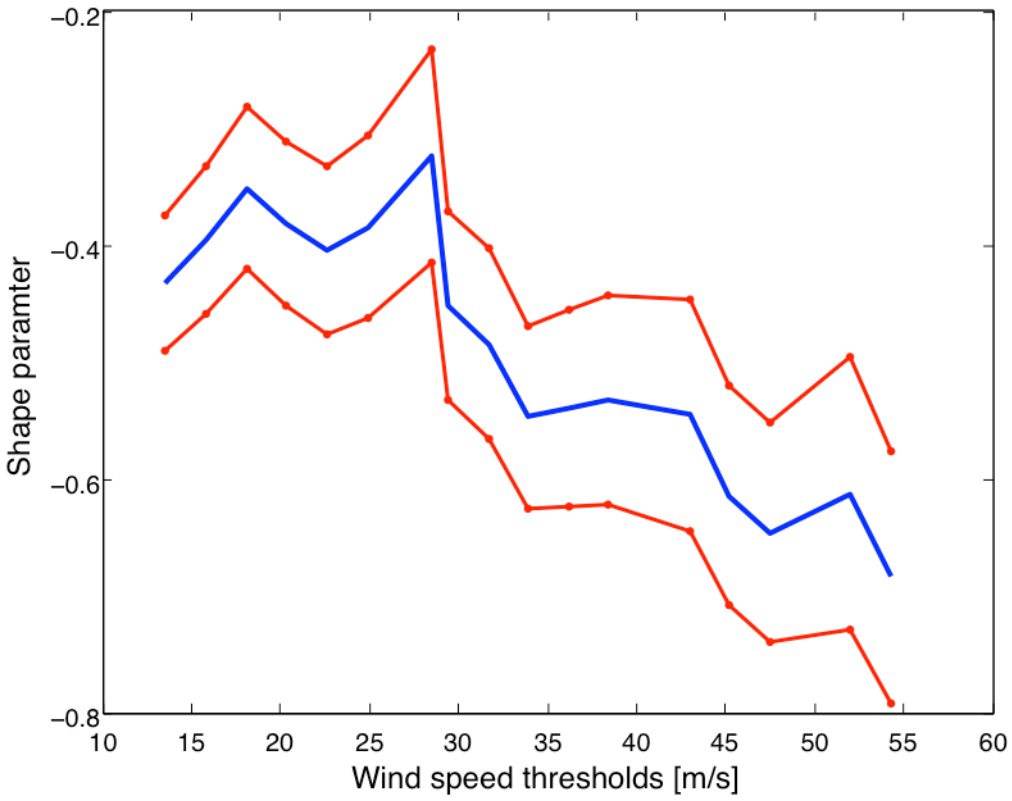

Figure 5.3: Maximum-likelihood estimate of GPD shape parameter as a function of threshold value (blue line) with 95% confidence level (red lines).

gives confidence in the choice of GPD as the statistical model of TC intensity. In most cases, however, GPD appears to slightly underestimate the higher intensity. Differences in the linearity are minimal and there is no value of u that gives a particularly strong linearity. However, by a slight difference, u = 18 and 22 give better estimate in the higher intensity. We choose u = 22 as the threshold in order to fit best with the extreme value assumption. Choosing u = 22 yields a MLE of shape and scale parameters as (ξ, σ) = (-0.30, 19.61). Here the upper bound of the estimated shape parameter is dominantly $\xi < 0$ (Figure 5.3), so the mean and variance of GPD can be calculated using equations (4) and

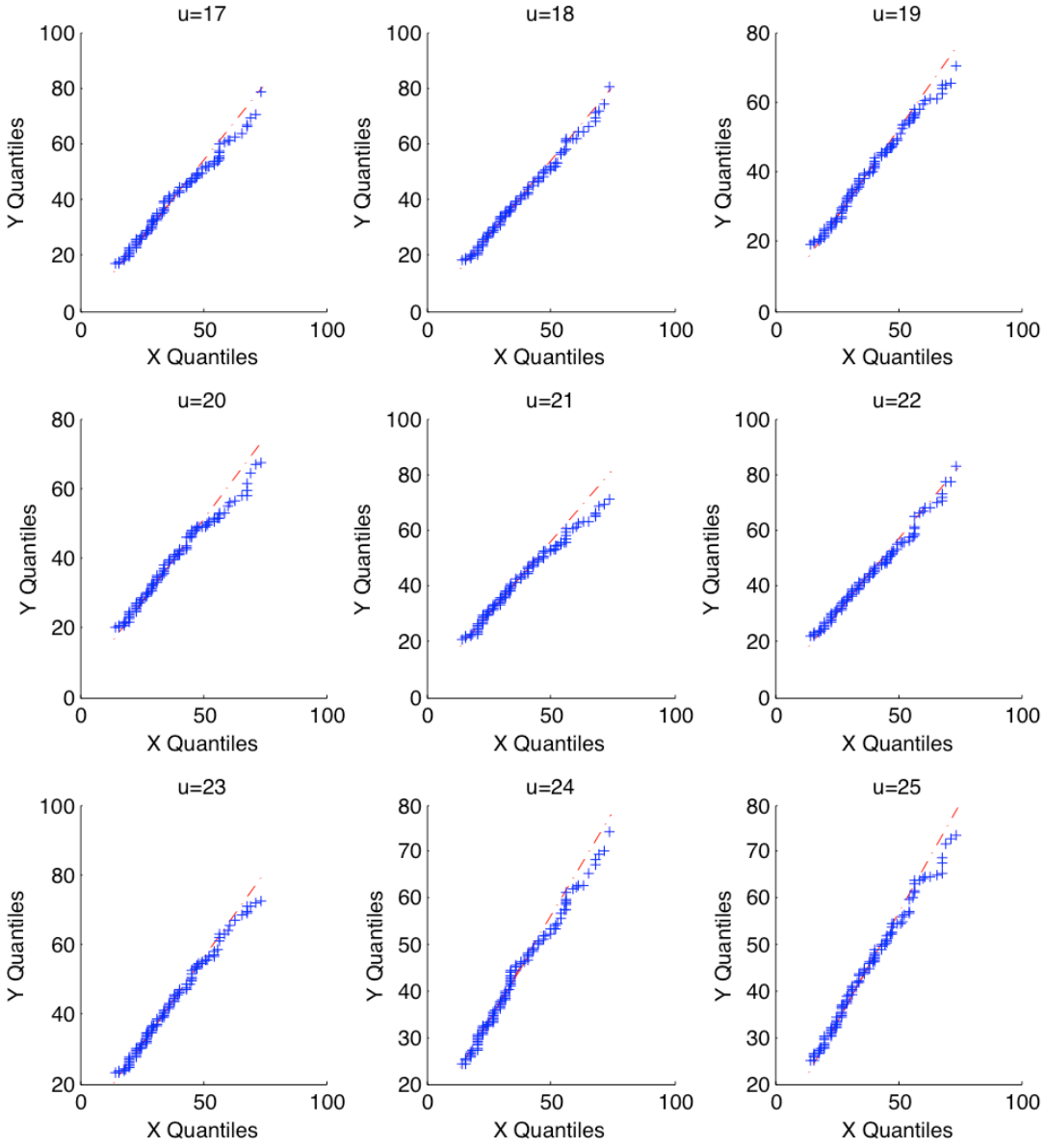

Figure 5.4: Q-Q plots of observed (x-axis) and modeled current climate intensity by GPD (y-axis) with threshold values ranging from 17 to 25 m s^{-1}.

(5) to give 37.14 and 144.26, respectively. These compare well with the mean and variance from the discrete observed data (37.0 and 158.32) when measurements less than 22 m s^{-1} are excluded (note that the GPD is fitted only for TC intensities greater than the

threshold value). This provides us with additional confidence in the selection of the GPD as a statistical model of the observed TC intensity.

The simulated percentage changes between the future (2020-2030 and 2045-2055) and current (1995-2005) NRCM simulations (Table 5.1) are applied to the GPD mean and variance obtained above. From these altered mean and variances, future GPD parameters are calculated using equation (4) and (5) with u kept at 22, with the resulting values summarized in Table 5.2.

Table 5.2: General Pareto distribution (GPD) parameters for current climate observed North Atlantic TC maximum lifetime intensity, and for modeled future TC intensity distribution derived by mean/variance alteration of GPD-modeled current climate TC intensity according to the simulated changes from NRCM (see text).

	ξ	σ
Current climate observations	-0.30	19.61
Modeled 2020-2030	-0.37	22.00
Modeled 2045-2055	-0.39	23.35

Figure 5.5 shows the probability density functions (PDFs) of the fitted GPD for current climate TC intensity, and the GPD reconstruction of future TC intensity for 2020-2030 and 2045-2055 periods. Future PDFs reflect the increase of mean TC intensities from the NRCM with a reduced probability of weaker TCs and an increased probability of intense TCs. These changes appear small from the PDF alone, but applying the exceedance probability reveals marked changes (Figure 5.6). The probability of Category 1+ hurricanes is projected to increase by roughly 9% for both of the future periods. For Category 5 hurricanes, exceedance probability increases by 57% and 29% for 2020-2030 and 2045-2055, respectively.

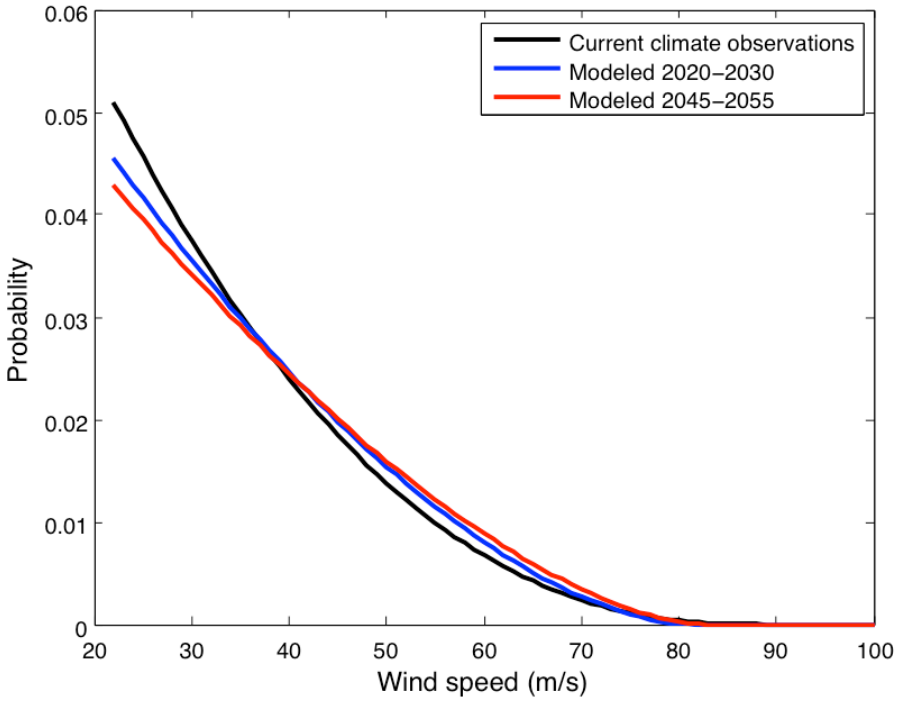

Figure 5.5: PDF of GPD fitted to current climate observed TC intensity (black), and of modeled future intensity distributions (blue for 2020-2030, and red for 2045-2055) after mean/variance alteration procedure.

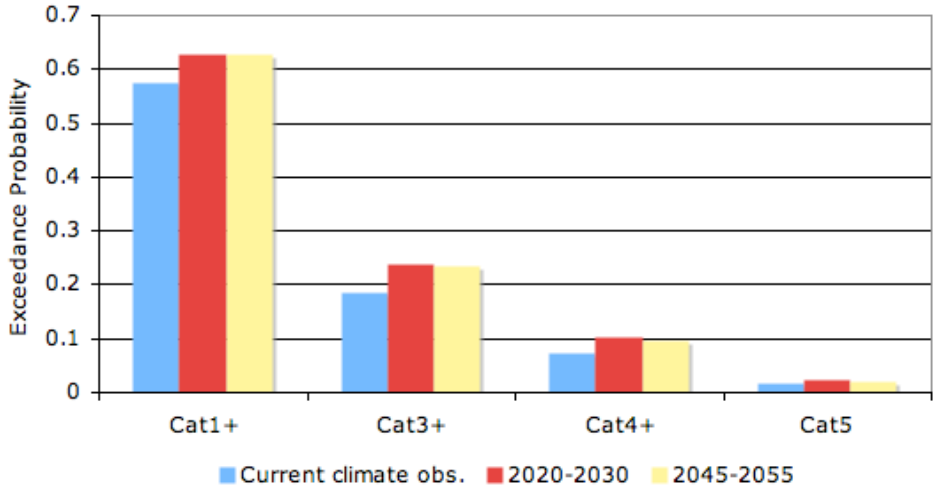

Figure 5.6: Exceedance probability of each hurricane categories for current climate observation (blue), 2020-2030 (red), and 2045-2055 (yellow) time periods.

Another way of representing the exceedance probability is to convert it to a return period. Return period T is defined as the number of years in between each of Category 5 storm occurrence;

$$T = \frac{1}{(TC \quad frequency) \times (Cat5 \quad exceedance)} \quad \text{- (6)}$$

where TC frequency is the average annual frequency of TCs with intensity exceeding 22 m s^{-1}. Note that exclusion of storms with intensity less than 22 m s^{-1} is required due to the GPD threshold selection. The observed average annual frequency of storms with intensities greater than 22 m s^{-1} is 9.9 per year. Assuming stationarity in the TC frequency at 9.9 per year, a change of exceedance probability from 0.0156 (current climate) to 0.0201 (2045-2055) would result in the reduction of return period of Category 5 storms from 6.5 years to 4.7 years. This is longer than for current observations, the implications for which are discussed below. The NRCM predicts an increase in the TC frequency by 11.8% for 2020-2030, and 36.8% for 2045-2055 periods (Chapter IV). With these TC frequency changes in consideration, the change in Category 5 return period can be estimated as going from 6.7 years for current climate to roughly 3.7 years in both of the future periods, which is an approximately 43% reduction.

The reduction in the return period is sensitive to the threshold selection for GPD. As indicated by the linearity of Q-Q plots (Figure 5.4), GPD is a reasonable fit to the observed TC intensity as long as $u < 25$. From this reason, it is helpful to see the range of uncertainty associated with the threshold selection for $u < 25$. To this end, the above exercise is repeated for $17 \leq u \leq 25$ to see its impact on the resulting reduction rate of the Category 5 storm return period. The results are shown in Figure 5.7. The reduction rate is in the range of 35 to 50% for all cases with the 2020-2030 period having a higher

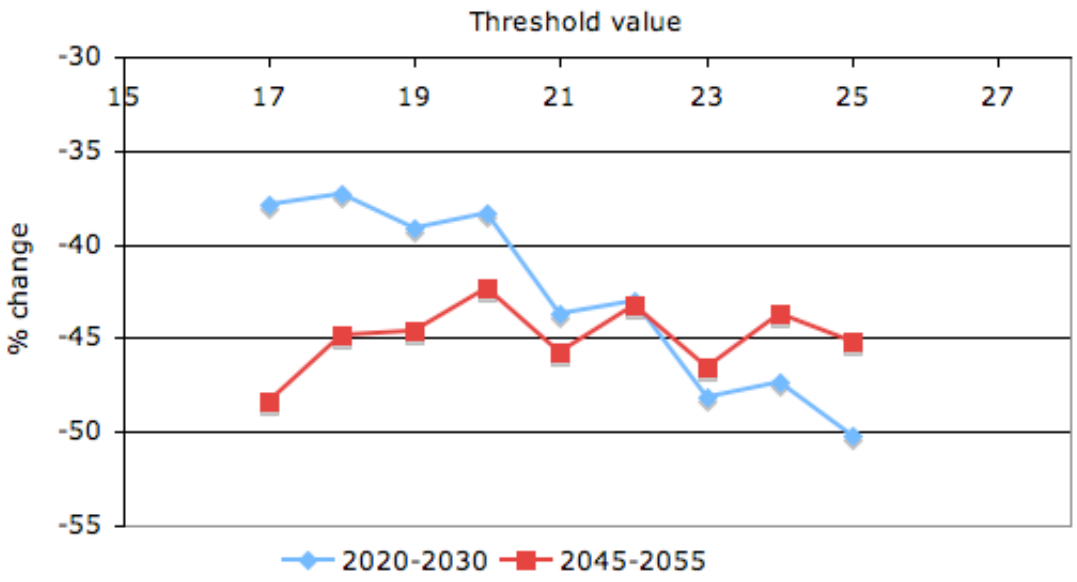

Figure 5.7: Sensitivity of threshold value to % change in Category 5 storm return period compared to the current climate observation with the simulated change of TC frequency in consideration.

sensitivity to the threshold selection compared to the 2045-2055 period. This is because the future change of TC intensity variance from the NRCM is smaller for 2020-2030 period (Table 5.1). For 2045-2055, the simulated variance change is large and dominates sensitivity to the threshold selection. Here we take the mean return period change (-45%) for 2045-2055 for further implications outlined below.

Note that the Category 5 return period from GPD is overestimated for the current climate: The observed Category 5 return period is 3 years for 1975 to 2005, but the GPD-modeled return period is 6.7 years. If the 45% reduction of Category 5 return period is applied to the observed value of 3 years, as indicated by the GPD for 2045-2055, then it results in a return period of 1.65 year.

The underestimation of Category 5 return period with GPD implies that the approach used here may not be able to capture the recently observed increase in frequency of Category 5 storms (especially the four Category 5 storms that occurred in 2005). We also note that MLE of the shape parameter ξ is dominantly negative. From eq. (2), GPD is upper-bounded when $\xi < 0$. This is also evident from the PDF of fitted GPD, which goes to zero at approximately 80 m s^{-1} (Figure 5.5). This is a statistical indication that there is a theoretical limit to which a TC can intensify. But how this compares to that of a thermodynamically derived limit (e.g., Emanuel 1988, Holland 1997) is not known.

We also assume that the NRCM is able to capture the mean and variance changes of TC intensity. This assumption may be questionable as the simulated TC intensity is upper-bounded due to the NRCM's horizontal resolution, which necessarily limits the variance in particular. Since the real variance and its changes are likely to be higher, the GDP application will likely underestimate the change. In any case, the approach presented here can be a "case in point" to extrapolate the simulated TC intensity prediction to the higher intensities while the horizontal resolution limit is still in place.

5.5 Summary

This chapter presented an approach to assessing future changes in intense TCs by combining the simulated results from the NRCM with a statistical model. The combination was motivated by the inability of the NRCM to produce intense storms explicitly due to the limited horizontal resolution. The observed TC intensity PDF is approximated by a GPD then the simulated changes of mean and variance of TC intensity from the NRCM are applied to this to reconstruct the future TC intensity PDF.

Calculation of excedance values from the GDP then provides a basis for assessing the changes in hurricanes of various categories. The selection of GPD as the statistical model of TC intensity is based on extreme value theory and the nature of the intensity PDF, with its decay to small probabilities for intense systems.

GPD is shown to be a good fit to the observed TC intensity as long as the fitting threshold < 25 m s^{-1}. From visual examination of Q-Q plots, a threshold value of 22 m s^{-1} is chosen. With this threshold value, GPD provides a reasonable representation of the observed intensity PDF, as evaluated by the visual examination of Q-Q plots and comparison of GPD and observed means and variances. However, there is a tendency to underestimate the frequency of very intense storms. This tendency is reflected in the overestimation of Category 5 storm return period; the GDP return period is 6.7 years, but the empirical value is about 3 years.

GPD assessments of future TC intensity distributions show a reduction in weak storms and increases when compared to current climate. Assuming stationarity in the overall TC frequency, analysis of exceedance probability indicates that the return period of Category 5 storms will be reduced by approximately 27% in the future climate. However, when the predicted changes of TC frequency determined from the NRCM are applied, the Category 5 return period is reduced by approximately 43%. Applying a range of thresholds, the results in reduction rate ranges from 35-50%. Applying these reduced return period changes to empirical estimates of current climate return periods results in one Category 5 storm every 1.5 to 2 years in the future climate.

It is noteworthy that the MLE of shape parameter for the current climate observed TC intensity is dominantly negative, implying that there is a theoretical limit to which

TCs can intensify. That there is a limit for TC intensity is in agreement with previous thermodynamic predictions (e.g., Emanuel 1988, Holland 1997). On the negative side, this approach assumes that the NRCM is able to capture the changes in TC intensity and variance associated with climate variability and change. This assumption is questionable due to the artificial capping of the simulated TC intensity caused by the NRCM resolution. However, this is most likely to provide a conservative estimate of future changes, as the changes to the mean and variance are also likely to be reduced by the resolution cut-off. Thus, the approach presented in this study can provide a conservative estimate for future changes to the more intense hurricanes for which explicit predictions are limited due to the horizontal resolution in numerical models.

CHAPTER VI

CONCLUDING REMARKS

The impact of increasing greenhouse gases on TC activity is one of the most pressing issues for both the scientific and industrial/governmental communities. The current debate can largely be divided into two parts. First, has there been a shift in TC activity associated with increasing greenhouse gases? And second, how will TC activity change in the future? While the answer to the first question remains somewhat inconclusive (Knutson et al. 2010), the answer to the second question is in strong demand among the industrial and governmental communities. Dynamical modeling can be used to project the future TC activity with increasing greenhouse gases, and this is the topic of investigation in this study.

Current global climate models (GCMs) are not capable of simulating TCs explicitly owing to their coarse horizontal resolutions. High-resolution atmospheric global circulation models (AGCMs) and regional climate models (RCMs) have great advantages as they can resolve the core characteristics of TCs better than GCMs. However, their usage is still in its infancy and requires careful evaluation of their capacity in simulating TC activity. This study analyzed a series of the Nested Regional Climate Model (NRCM, Holland et al. 2010) simulations. A number of sources of uncertainty and limitations were identified, and approaches to reduce some of the uncertainty and limitations were also proposed.

This study paid particular attention to the sensitivity of the simulated TC activity to the choice of TC tracking parameters and their thresholds. It was demonstrated that TC

tracking methodology is a large source of uncertainty in simulating the TC activity. In fact, the uncertainty is sufficiently large enough that one may tune the TC detection and tracking scheme to attain a desired "simulated" TC frequency. We have also demonstrated that the commonly used warm-core definition may not be sufficient to distinguish clearly between the tropical systems and other low-pressure systems. The distinction can be improved by incorporating the Cyclone Phase technique (Hart 2004). Furthermore, it was shown that the wind speed and duration parameters have a dominant role in determining the number of detected storm tracks. Based on this result, we proposed a procedure to objectively select the TC tracking parameters. First, TC tracking parameters are selected so that the resulting number of detected storm tracks best matches the TC counts from visual inspection of animated loops from the model output. Second, the range of uncertainty in the detected number of storm tracks is assessed by perturbing the wind speed and duration thresholds by 5 knots and 6-hours. The perturbation range is based on the intensity and duration record resolution of the best track data.

In order to reduce the subjectivity in the TC tracking method further, we compared the simulated large-scale environment with the TC tracking results. This comparison led to a more objective assessment of the NRCM tropical channel experiment, which is the first set of the NRCM simulations presented in this study. In the tropical channel simulation, the NRCM was nested within a reanalysis data to evaluate its capacity to simulate the observed TC activity. The TC tracking results indicated an overestimation of TC frequency well outside of the range of uncertainty associated with the TC tracking method. We identified two reasons for the overestimation of TCs using the simulated large-scale environment. First, the model produced excessive convection

and convectively coupled waves. And second, the biased monsoon flow in western North Pacific, plus the excessive convection, led to enhanced regional TC formations. On the other hand, the simulated TC frequency in the North Atlantic was underestimated in the model, which was found to be due to the lack of moist African Easterly Waves in the model.

Furthermore, some uncertainties and limitations were identified in the tropical channel experiment. First, it was shown that simulated TC frequency in the Southern Indian Ocean is highly sensitive to the location of southern boundary. Second, a two-way nesting simulation revealed both downscale (from the parent domain to the child domain) and upscale impacts. For downscaling, TC structure and intensity were better represented owing to the increased horizontal resolution. Potential upscaling impacts included an induced a blocking pattern over Australia in the parent domain resulting from high-resolution simulation over the North Atlantic. And this contributed to an increase of TC genesis in Northern Indian Ocean. However, it is not clear whether these upscale impacts are due entirely to the two-way nesting, or were the result of different initial conditions.

In the second set of simulations, the NRCM was nested within the Community Climate System Model (CCSM) to project future North Atlantic TC activity out to 2055. An El Nino-like SST bias in the CCSM induced anomalously high vertical wind shear in the tropical North Atlantic, inhibiting TCs from forming in this region. Such bias is not unique to the CCSM, but is a common issue in many of the GCMs submitted to the IPCC-AR4. Past studies avoided the bias issue by taking only the future trends from GCMs and added them to current observations to construct the future boundary forcing. Here we adopted a different approach: a bias adjustment was made to CCSM fields for

current climate to make them consistent with the observed seasonal mean state, and this correction was assumed to not change in future climate. These adjustments were made to the NRCM at the ocean surface and horizontal boundaries. For current climate simulation, this bias correction enabled the NRCM to develop a TC climatology consistent with the current climate. For future climate the bias may vary and our assumption of constancy introduces unknown uncertainties in the projections.

The NRCM projected an increase of TC frequency and the mean intensities under increased greenhouse gases. This result is independent of the range of uncertainty associated with TC tracking. There is an increase of TC genesis in the MDR, where TC formation environment was projected to become more favorable with a northward shift of ITCZ, associated with an increase of meridional SST gradient in the region. It was also shown that the simulated TC frequency is sensitive to initial conditions. Other concurrent work has also shown that this sensitivity can even extend to changing the computer architecture (James Done and Cindy Bruyere, personal communication 2010).

The NRCM was not able to project the future changes in intense (Category 3+) storms explicitly owing to its horizontal resolution. We utilized Extreme Value Theory to extrapolate the intensity projection to the intense storm range. The General Pareto Distribution (GPD) was selected as a statistical model of TC intensity to enable a focus on the extreme intensities being assessed. GPD was used to statistically model the current observed TC intensity distribution, and the projected changes in the mean and standard deviation of TC intensity from the NRCM were applied to the GPD-modeled TC intensity. The result was a 27% increase in the probability of Cat 5 hurricane occurrence, assuming stationarity in the overall TC frequency. However, when the projected change

in TC frequency by the NRCM was taken into the consideration, the probability of Cat 5 hurricane occurrence was projected to increase by 43%. The result implies, for example, that there may by at least one Cat 5 hurricane every 1.5 to 2 years in the future climate, as opposed to the current observed rate of one in every 3 years. The extreme value theory approach presented here can serve as a useful tool to extrapolate the intensity projection of intense storms that cannot be resolved explicitly due to horizontal resolutions in dynamical models.

We conclude with a summary of uncertainties and limitations in simulating TC activity that have been identified or examined in this study.

Items tested and analyzed in this study:

1. TC tracking method
   - Subjectivity in the TC tracking method can be decreased by mirroring the tracking results with the simulated large-scale environment, and by presenting a range of uncertainty in the tracking results
2. Horizontal resolution
   - Resolutions tested in this study (36- and 12km) are not sufficient for simulating intense storms. We demonstrated a statistical approach to extrapolate the model intensity projections to intense storms.

Items identified in this study

1. Influence of the following in TC frequency: lateral boundary location; nesting; and initial conditions.
2. A method for correcting biases in GCMs for application to regional climate modeling.

Additional items noted by other studies include parameterizations and nudging. Ongoing work using the NRCM has shown recently that simulated TC frequency can vary by computer architectures as well.

In our experiments, North Atlantic TCs were projected to increase in both intensity and frequency. The projected increase of intensity is in agreement with the consensus made by past studies (Knutson et al. 2010). That there is a clear tendency among downscale experiments, despite the differences in their model configurations, implies that the projected increase of TC intensity with global warming may be above the range of uncertainties associated with downscale experimental design. However, projection of North Atlantic TC frequency remains divided. Out of 23 downscale experiments summarized in a review article by Knutson et al. (2010), 10 experiments resulted in an increase, and 13 resulted in a decrease of North Atlantic TC frequency with global warming. Our result adds to the 10 experiments that indicated an increase. It remains unclear how each sources of uncertainties contributes to the disagreement in the projection of TC frequency.

This study has added knew knowledge on a range of methods for analyzing tropical cyclones in regional climate models, and identified several areas of bias and uncertainty along with their impacts and recommended approaches to reducing these. Regional climate modeling of high-impact weather is very much a growth area as computing resources of sufficient capacity become available. These results, while developed for tropical cyclones, are generally applicable to these other severe weather studies.

REFERENCES

Avila, L. A., and R. J. Pacsh, 1992: Atlantic tropical systems of 1991. *Mon. Wea. Rev.*, **1 20**, 2688-2696.

Bender, M. A., T. R. Tknutson, R. E. Tuleya, J. J. Sirutis, G. A. Vecchi, S. T. garner, and I. M. Held, 2010: Modeled impact of anthropogenic warming on the frequency of intense Atlantic hurricanes. *Science*, **327**, 454-458.

Bengtsson, L., H. Böttger, and M. Kanamitsu, 1982: Simulation of hurricane-type vortices in a general circulation model. *Tellus A,* **34**, 440-457.

Bengtsson, L., M. Botzest, and M, Esch, 1995: Hurricane-type vortices in a general circulation model. *Tellus*, **47A**, 175-196.

Bengtsson, L., K. Hodges, M. Esch, N Keenlyside, L. Kornblueh, J-.J. Luo, and T. Yamagata, 2007: How may tropical cyclones change in a warmer climate? *Tellus A*, **59**, 539-561.

Bessafi, M., and M. Wheeler, 2006: Modulation of South Indian Ocean tropical cyclones by the Madden-Julian Oscillation and convectively coupled equatorial waves. *Mon. Wea. Rev.*, **134**, 638-656.

Broccoli, A., and S. Manabe, 1990: Can existing climate models be used to study anthropogenic changes in tropical cyclone climate? *Geophys. Res. Lett.*, **17**, 1917-1920.

Bruyere, C., G.J. Holland, A. Suzuki-Parker and J. Done, 2010: Lessons learned from North American Regional Climate Model (NRCM) Experiments. Preprints, *29th Conf. on Hurricanes and Tropical Meteorology,* Amer. Meteor. Soc.

Camargo, S., A . Sobel, G. Anthony, and K. Emanuel, 2007: Tropical cyclone genesis potential index in climate models. *Tellus A,* **59**, 428-443.

Caron, J. M., 2011: Madden Julian Oscillation in the nested regional climate model. *Clim. Dyn.,* submitted.

Chan, J. C. L., 1985: Tropical cyclone activity in the Northwest Pacific in relation to the El Nino/Southern Oscillation phenomenon. *Mon. Wea. Rev.*, **113**, 599-606.

Chan, J. C. L., 2006: Comment on "Changes in tropical cyclone number, duration, and intensity in a warming environment." *Science*, **311**, 1713b-1713b.

Chan, J. C. L., 2008: Decadal variations of intense typhoon occurrence in the western North Pacific. *Proc. R. Soc. A*, **464**, 249-272.

Chan, J. C. L., and M. Xu, 2009: Inter-annual and inter-decadal variations of landfalling tropical cyclones in East Asia. Part I: time series analysis. *Int. J. Climatol.*, **29**, 1285-1293.

Chang, E., and Y. Guo, 2007: Is the number of North Atlantic tropical cyclones significantly underestimated prior to the availability of satellite observations? *Geophys. Res. Lett.*, **34**, L14801.

Chauvin, F., J-.F. Royer, and M. Déqué, 2006: Response of hurricane-type vortices to global warming as simulated by ARPEGE-Climate at high resolution. *Clim. Dyn.*, **27**, 377-399.

Coles, S., 2001: *An Introduction to Statistical Modeling of Extreme Values*. Springer Series in Statistics, 208pp., Springer, London; New York.

Coles, S., and E. Casson, 1998: Extreme value modeling of hurricane wind speeds. *Str. Safe.*, **20**, 283-296.

Collins, W.D., and Coauthors, 2004: Description of the NCAR Community Atmosphere Model (CAM 3.0), *NCAR Technical Note*, NCAR/TN-464+STR, 226pp.

Collins, W. D., and Coauthors, 2006: The Community Climate System Model version 3 (CCSM3). *J. Climate,* **19**, 2122-2143.

Davis, C., W. Wang, J. Dudhia, and R. Torn, 2010: Does increased horizontal resolution improve hurricane wind forecasts? *Wea. Forcast.* **25**, 1826-1841.

Done, J. M., L. R. Leung, C. A. Davis, and Y-. H. Kuo, 2005: Simulation of warm season rainfall using WRF regional climate model. Preprints, *Sixth WRF workshop,* Boulder, CO.

Done. J., G. Holland, and P. Webster, 2010: The role of wave energy accumulation in tropical cyclogenesis over the tropical North Atlantic, *Clim. Dyn*., **36**, 753-767.

Dudhia, J., J. Done, W. Wang, Y. Chen, Q, Xiao, C. Davis, G. Holland, R. Rotunno, and R. Torn, 2008: Prediction of Atlantic tropical cyclones with the Advanced Hurricane WRF (AHW) model. *Preprint.* 28th Conference on hurricanes and tropical meteorology. Orlando, FL.

Dvorak, V., 1984: Tropical cyclone intensity analysis using satellite data. *NOAA Tech. Report NESDIS*, **11**, 47pp.

Ek, M. B., K. E. Mitchell, Y. Lin, P. Grunmann, E. Rogers, G. Gayno, and V. Koren, 2003: Implementation of the upgraded Noah land-surface model in the NCEP operational mesoscale Eta model. *J. Geophys. Res.*, **108**, 8851, doi:10.1029/2002JD003296.

Elsner, J., J. Kossin, and T. Jagger, 2008: The increasing intensity of the strongest tropical cyclones. *Nature*, **455**, 92-95.

Emanuel, K., 1988: The maximum intensity of hurricanes. *J. Atm. Sci.*, **45**, 1143-1155.

Emanuel, K., 2005: Increasing destructiveness of tropical cyclones over the past 30 years. *Nature*, **436**, 686-688.

Evans, J. E. and R. Hart, 2003: Objective indicators of the life cycle evaluation of extratropical transition of Atlantic tropical cyclones. *Mon. Wea. Rev.*, **131**, 909-925.

Frank, N. L., 1969: The "inverted V" cloud pattern – An easterly wave? *Mon. Wea. Rev.*, **97** (2), 130-140.

Franklin, J. L., S. J. Lord, S. E. Feuer, and F. D. Marks, Jr., 1993: The kinematic structure of hurricane Gloria (1985) determined from nested analysis of dropwindsonde and doppler radar data. *Mon. Wea. Rev.*, **121**, 2433-2451.

Franklin, J. L., M. L. Black, and K. Valde, 2003: GPS dropwindsode wind profiles in hurricanes and their operational implications. *Wea. Forecasting,* **18**, 32-44.

Gillet, N., P. Scott, and B. Santer, 2008: Attribution of cyclogenesis region sea surface temperature change to anthropogenic influence. *Geophys. Res. Lett.*, **35**, L09707.

Giorgi, F. and L. Mearns, 1999: Introduction to special section: Regional climate modeling revisited. *J. Geophys. Res.*, **104** (D6), 6335-6352.

Goldenberg, S., C. Landsea, A. Mestas-Nuñez, W. Gray, 2001: The recent increase in Atlantic hurricane activity: Causes and Implications. *Science*. **293**, 474-479.

Gray, W., 1968: Global view of the origin of tropical disturbances and storms. *Mon. Wea. Rev.*, **96** (10), 669-700.

Gray, W., 1984: Atlantic seasonal hurricane frequency. Part I: El Nino and 30 mb quasi-biennial oscillation influences. *Mon. Wea. Rev.*, **112**, 1649-1668.

Gu, G. and R. F. Adler, 2009: Interannual variability of boreal summer rainfall in the equatorial Atlantic. *Int. J. Climatol.*, **29** (2), 175-184.

Hall, J., A. Matthews, and D. Karoly, 2001: The modulation of tropical cyclone activity in the Australian region by the Madden-Julian oscillation. *Mon. Wea. Rev.*, **129**, 2970-2982.

Hart, R. E., 2001: The extratropical transition of Atlantic tropical cyclones: climatology,

lifecycle definition, and a case study. Ph.D thesis, The Pennsylvania State university, 176 pp.

Hart, R. E., 2004: A cyclone phase space derived from thermal wind and thermal asymmetry. *Mon. Wea. Rev.*, **131**, 585-616.

Holland, G. J., 1995: Scale interaction in the western Pacific monsoon. *Meteor. Atmos. Phys.*, **56**, 57-79.

Holland, G., 1997: The maximum potential intensity of tropical cyclones. *J. Atm. Sci.*, **54**, 2519-2541.

Holland, G., 2007: Misuse of landfall as a proxy for Atlantic tropical cyclone activity. *EOS Trans*., **88**, 349-350.

Holland, G., and P. Webster, 2007: Heightened tropical cyclone activity in the North Atlantic: Natural variability or climate trend? *Phil. Trans. A*, **365**, 2695-2716.

Holland, G., 2008: A Revised Hurricane Pressure–Wind Model. *Mon. Wea. Rev.*, ***136***, 3432–3445

Holland, G., 2010: Impact of climate variability and change on hurricane extremes. *Preprint*. 29th Conference on Hurricanes and Tropical Meteorology, 10 – 14 May 2010, Tucson, AZ.

Holland, G., J. Done, C. Bruyere, C. Cooper, and A. Suzuki-Parker, 2010: Model investigation of the effects of climate variability and change on future Gulf of Mexico tropical cyclone activity. *OTC Metocean 2010*, 13pp.

Hong, S. –Y., and J. –O. J. Lim, 2006: The WRF single-moment 6-class microphysics scheme (WSM6), *J. Korean Meteor. Soc.,* **42**, 129-151.

Hong, S. –Y., Y. Noh, and J. Dudhia, 2006: A new vertical diffusion package with an explicit treatment of entrainment processes. *Mon. Wea. Rev.*, **134**, 2318-2141.

Hopsch, S. B., C. D. Thorncroft, K. Hodges, and A. Aiyyer, 2007: West African Storm Tracks and Their Relationship to Atlantic Tropical Cyclones. *J. of Climate*, **20** (11), 2468-2483.

Hoyos, C., P. Agudelo, P. Webster, and J. Curry, 2005: Deconvolution of the factors contributing to the increase in global hurricane intensity. *Science*, **312**, 94-97.

Huffman, G. J., R. F. Adler, D. T. Bolvin, G. Gu, E. J. Nelkin, K. P. Bowman, Y. Hong, E. F. Stocker, and D. B. Wolef, 2007: The TRMM multisatellite precipitation analysis (TMPA): quasi-globl, multiyear, combined-sensor precipitation estimates at fine scale. J. Hydrometeorol., **8**, 38-55.

Hurrell, J., J. J. Hack, D. Shea, J. M. Caron, and J. Rosinski, 2008: A New Sea Surface Temperature and Sea Ice Boundary Dataset for the Community Atmosphere Model. *J. of Climate,* **21**, 5145-5153.

Jagger, T., and J. Elsner, 2006: Climatology models for extreme hurricane winds near the United States. *J. of Climate.*, **19**, 3220-3236.

Kain, J. S., and J. M. Fritsch, 1993: Convective parameterization for mesoscale models: The Kain-Fritsch scheme. *The representation of cumulus convection in numerical models*. K. A. Emanuel and D. J. Raymond, Eds., Amer. Meteor. Soc., 246pp.

Kalnay, E., M. Kanamitsu, R. Kistler, W. Collins, D. Deaven, L. Gandin, M. Iredell, S. Saha, G. White, and J. Woollen, 1996: The NCEP/NCAR 40-year reanalysis project. *Bull. Amer. Met. Soc.,* **77** (3), 437-471.

Kim, H-. M., P. Webster, and J. Curry, 2009: Impact of shifting patterns of Pacific Ocean warming on North Atlantic tropical cyclones. *Science*, **325** (5936), 77-80.

Knapp, K., and M. Kruk, 2009: Quantifying inter-agency differences in tropical cyclone best track wind speed estimates. *Mon. Wea. Rev.*, **138**, 1459-1473.

Knapp, K., M. Kruk, D. hevinson, H. Diamond, and C. Neumann, 2010: The international best track archive for climate stewardship (IBTrACS). *Bull. Amer. Met. Soc.*, **91**, 363-376.

Knutson, T., and S. Manabe, 1995: Time-mean response over the tropical Pacific to increased CO2 in a coupled ocean-atmosphere model. *J. Climate.*, **8**, 2181-2199.

Knutson, R. Tuleya, and Y. Kurihara, 1998: Simulated increase of hurricane intensities in a CO2-warmed climate. *Science*, **279**, 1018-1020.

Knutson, T, J. Sirutis, S. Garner, and I. Held, 2007: Simulation of the recent multidecadal increase of Atlantic hurricane activity using an 18-km-grid regional model. *Bull. Amer. Soc.*, **88**, 1549-1565.

Knutson, T., J. Sirutis, S. Garner, and G. Vecchi, and I. Held, 2008: Simulated reduction in Atlantic hurricane frequency under twenty-first-century warming conditions. *Nature Geoscience*, **1**, 359-364.

Knutson, T., and Coauthors, 2010: Tropical cyclones and climate change. *Nat. Geosci*., **3** (3), 157-163.

Kossin, J., and C. Valden, 2004: A pronounced bias in tropical cyclone minimum sea level pressure estimation based on the Dvorak technique. *Mon. Wea. Rev.*, **132** (1), 165-173.

Kossin, J., and J. Vimont, 2007: A more general framework for understanding Atlantic hurricane variability and trends. *Bull. Amer. Met. Soc.*, **88** (11), 1767-1781.

Krishnamurti, T., R. Correa-Torres, M. Latif, and G. Daughenbaugh, 1998: The impact of current and possibly future sea surface temperature anomalies on the frequency of Atlantic hurricanes. *Tellus A*, **50** (2), 186-210.

Landman, W., A. Seth, and S. Camargo, 2005: The effect of regional climate model domain choice on the simulation of tropical cyclone-like vortices in the Southwestern Indian Ocean. *J. Climate.*, **18** (8), 1263-1274.

Landsea, C., 2007: Counting Atlantic tropical cyclones back to 1900. *EOS Trans.*, **88** (18), 197-208.

Leung, L., Y-.H. Kuo, and J. Tribbia, 2006: Research Needs and Directions of Regional Climate Modeling Using WRF and CCSM. *Bull. Amer. Met. Soc.*, **87** (12), 1747-1751.

Liebmann, B., H. Hendon, and J. Glick, 1994: The relationship between tropical cyclones of the western Pacific and Indian Oceans and the Madden-Julian oscillation. *J. Meteor. Soc. Japan*, **72** (41), 401-412.

Lighthill, J. G. Holland, W. Gray, C. Landsea, G. Craig, J. Evans, Y. Kurihara, and C. Guard, 1994: Global climate change and tropical cyclones. *Bull. Amer. Met. Soc.*, **75** (11), 2147-2157.

Lin, J-. L., and Coauthors, 2006: Tropical intraseasonal variability in 14 IPCC AR4 climate models. Part I: Convective signals. *J. Climate*, **19**, 2665-2690.

Liu, K., and J. C. L. Chan, 2008: Interdecadal variability of western North Pacific tropical cyclone tracks. *J. Climate*, **21** (17), 4464-4476.

Lucas-Picher, P., D. Caya, R. de Elia, and R. Laprise, 2008: Investigation of regional climate models' internal variability with a ten-member ensemble of 10-year simulations over a large domain. *Clim. Dyn.*, **31** (7), 927-940.

Madden, R., and P. Julian, 1972: Description of global-scale circulation cells in the tropics with a 40-50 day period. *J. Atm. Sci.*, **29** (6), 1109-1123.

Maloney, E. D., and D. L. Hartmann, 2000a: Modulation of eastern north Pacific hurricanes by the Madden-Julian Oscillation. *J. Climate*, **13**, 1451-1460.

Maloney, E. D., and D. L. Hartmann, 2000b: Modulation of hurricane activity in the Gulf of Mexico by the Madden-Julian Oscillation. *Science*, **287** (5460), 2002-2004.

Manabe, S., Holloway Jr., J. and H. Stone, 1970: Tropical circulation in a time-integration of a global model of the atmosphere. *J. Atm. Sci.*, **27**, 580-612.

Mann, M., and K. Emanuel, 2006: Atlantic hurricane trends linked to climate change. *EOS Trans.*, **87** (24), 233-244.

Marks, F. D., 2003: Hurricanes. *Encyclopedia of Atmospheric Sciences*. Elsevier Science Ltd., London, UK, 942-966.

McBride, J., 1984: Comments on "Simulation of hurricane-type vortices in a general circulation model". *Tellus A*, **36** (1), 92-93.

Miguez-Macho, G., G. L. Stenchikov, and A. Robock, 2005: Regional climate simulations over North America: Interaction of local processes with improved large-scale flow. *J. Climate*, **18**, 1227-1246.

Murakami, H., and M. Sugi, 2010: Effect of model resolution on tropical cyclone climate projections. *SOLA*, **6**, 73-76.

Murakami, H., and B. Wang, 2010: Future change of North Atlantic tropical cyclone tracks: Projection by a 20-km-mesh global atmospheric model. *J. Climate.*, **23**, 1699-2721.

Oouchi, K., J. Yoshimura, H. Yoshimura, R. Mizuta, S. Kusunoki, and A. Noda, 2006: Tropical cyclone climatology in a global-warming climate as simulated in a 20 km-mesh global atmosphere model: Frequency and wind intensity analysis. *J. Met. Soc. Japan*, **84** (2), 259-276.

Pielke Jr., R., J. Gratz, C. Landsea, D. Collins, M. Saunders, and R. Musulin, 2008: Normalized hurricane damage in the United States: 1900-2005. *Nat. Haz. Rev.*, **9** (1), 29-42.

Randall, D. and R. A. Wood, 2007: Climate Change 2007: The physical science basics, Chapter 8 Climate Models and Their Evaluation. *IPCC AR-4 assessment report*, 591-648.

Ritchie, E., and G. Holland, 1997: Scale interactions during the formation of typhoon Irving. *Mon. Wea. Rev.,* **125**, 1377-1396.

Saunders, M., and A. Lea, 2008: Large contribution of sea surface warming to recent increase in Atlantic hurricane activity. *Nature*, **451** (7178), 557-560.

Seth, A., and F. Giorgi, 1998: The effects of domain choice on summer precipitation simulation and sensitivity in a regional climate model. *J. Climate*, **11**, 2698-2712.

Shaman, J., S. Esbensen, and E. Maloney, 2009: The dynamics of the ENSO-Atlantic

hurricane teleconnection: ENSO-related changes to the North African-Asian jet affect Atlantic basin tropical cyclogenesis. *J. Climate*, **22**, 2458-2482.

Shapiro, L. J., 1987: Month-to-month variability of the Atlantic tropical circulation and its relationship to tropical storm formation. *Mon. Wea. Rev.*, **115** (11), 2598-2614.

Simiu, E., N. A. Heckert, and T.Whalen, 1996: Estimates of hurricane wind speeds by the 'Peaks over threshold' method. *NIST Technical Note*, **1416**, 46pp.

Skamarock, W. C., J. B. Klemp, J. Dudhia, D. O. Gill, D. m. Barker, M. G. Duda, X. –Y. Huang, W. Wang, and J. G. Powers, 2008: A description of the Advanced Research WRF version 3. *NCAR Technical Note,* NCAR/TN-475+STR, 113pp.

Stowasser, M, Y. Wang, and K. Hamilton, 2007: Tropical cyclone changes in the Western North Pacific in a global warming scenario. *J. Clim.*, **20**, 2378-2396.

Sugi, M., H. Murakami, and J. Yoshimura, 2009: A reduction in global tropical cyclone frequency due to global warming. *SOLA*, **5**, 164-167.

Swanson, K., 2008: Nonlocality of Atlantic tropical cyclone intensities. *Geochem. Geophys. Geosyst.*, **9**, doi:10.1029/2007GC001844.

Tsutsui, J., 2002: Implication of anthropogenic climate change for tropical cyclone activity: A case study with the NCAR CCM2. *J. Met. Soc. Japan*, **80** (1), 45-65.

Tulich, S., G. Kiladis, and A. Suzuki-Parker, 2009: Convectively coupled Kelvin and easterly waves in a regional climate simulation of the tropics. *Clim. Dyn.,* doi 10.1007/s00382-009-0697-2.

Vecchi, G., and B. Solden, 2007: Effect of remote sea surface temperature change on tropical cyclone potential intensity. *Nature*, **450** (7172), 1066-1070.

Vecchi, G., K. Swanson, and B. Soden, 2008: Whither hurricane activity. *Science*, **322** (5902), 687-689.

Vecchi, G., and T. Knutson, 2008: On estimates of historical North Atlantic tropical cyclone activity. *J. Climate.*, **21** (14), 3580-3600.

Villarini, G., G. Vecchi, T. Knutson, M. Zhao, and J. Smith, 2011: North Atlantic tropical storm frequency response to anthropogenic forcing: Projections and sources of uncertainty. *J. Climate.*, doi:10.1175/2011JCL13853.1.

Walsh, K., K. –C. Nguyen, J. McGregor, 2004: Fine-resolution regional climate model simulations of the impact of climate change on tropical cyclones near Australia. *Clim. Dynm.*, **22** (1), 47-56.

Walsh, K., M. Fiorino, C. Landsea, and K. McInnes, 2007: Objectively determined resolution-dependent threshold criteria for the detection of tropical cyclones in climate models and reanalysis. *J. Climate.*, **20** (10), 2307-2314.

Webster, P. J. and H-. R. Chang, 1997: Atmospheric wave propagation in heterogeneous flow: basic flow controls on tropical-extratropical interaction and equatorial wave modification. *Dyn. of Atm. and Oceans*, **27** (1997), 91-134.

Webster, P., G. Holland, J. Curry, and H. Chang, 2005: Changes in tropical cyclone number, duration, and intensity in a warming environment. *Science*, **309**, 1844-1846.

Wu, M-. C., K-. H. Yeung, and W-. L. Chang, 2006: Trends in western North Pacific tropical cyclone intensity. *EOS Trans*., **87** (48), 537-548.

Wu, L., L. Tao, and Q. Ding, 2010: Influence of sea surface warming on environmental factors affecting long-term changes of Atlantic tropical cyclone formation. *J. Climate.*, **23** (22), 5978-5989.

Zhang, R., and T. Delworth, 2009: A new method for attributing climate variations over the Atlantic hurricane basin's main development region. *Geophys. Res. Lett.*, **36**, L06701.

Zhang, Y., H. Wang, J. Sun, and H. Drange, 2010: Changes in the tropical cyclone genesis potential index over north pacific in the SRES A2 scenario. *Adv. Atmos. Sci.*, **27**, 1246-1258.

Zhao, M., I. Held, S-. L. Lin, and G. Vecchi, 2009: Simulations of global hurricane climatology, interannual variability, and response to global warming using a 50-km resolution GCM. *J. Climate.*, **22** (24), 6653-6678.